STUDY OF THE FEASIBILITY AND ENERGY SAVINGS OF PRODUCING AND PRE-COOLING HYDROGEN WITH A 5-KW AMMONIA BASED COMBINED POWER/COOLING CYCLE

By

ROBERT JOSEPH REED

A THESIS PRESENTED TO THE GRADUATE SCHOOL
OF THE UNIVERSITY OF FLORIDA IN PARTIAL FULFILLMENT
OF THE REQUIREMENTS FOR THE DEGREE OF
MASTER OF SCIENCE

UNIVERSITY OF FLORIDA

2004

ACKNOWLEDGMENTS

First and foremost, I would like to thank my wife for her constant love and support during the pursuit of my degree. Her patience and understanding while I completed this thesis will be forever appreciated. I would also like to thank my fellow graduate students for making our office an enjoyable work environment and a place I looked forward going to everyday.

I would like to thank my advisor, Dr. Herbert (Skip) Ingley, for his guidance during my research efforts. Always willing to help, he provided much needed advice and knowledge; but he also allowed me to develop my own ideas and solutions, providing a wonderful learning experience. I thank my committee members Sherif A. Sherif, D. Yogi Goswami, and Herbert (Skip) Ingley for all of their support.

Finally, I would like to thank my parents for believing in me from the beginning and always encouraging me that I could accomplish anything I put my mind to.

TABLE OF CONTENTS

page

LIST OF TABLES

Table page

LIST OF FIGURES

Figure page

NOMENCLATURE

A	ampere [A]
AC	alternating current
CHWS	chilled water source
CHWR	chilled water return
CWS	cooling water source
CWR	cooling water return
CO_2	carbon dioxide
COP	coefficient of performance
DC	direct current
E	voltage [V] or energy transfer rate[Btu/hr or kW]
F	Faraday's constant
FOM	figure of merit
G	Gibbs energy [Btu/lbm]
GFR	Gibbs free energy of reaction [Btu/lbm]
H	enthalpy [Btu/lbm]
HHV	higher heating value [Btu/lbm]
HHWS	heating hot water source
HHWR	heating hot water return
HX	heat exchanger
IC	internal combustion

I.D.	Inner diameter [in.]
KOH	potassium hydroxide
L	liquid
LH_2	liquid hydrogen
LHV	lower heating value [Btu/lbm]
LN_2	liquid nitrogen
P	pressure [psia]
PV	photovoltaic
Q	heat transfer rate [Btu/hr or kW]
R	mass specific gas constant [Btu/lbm-R]
S	entropy [Btu/lbm-R]
SMR	steam/methane reformation
STP	standard temperature and pressure
T	temperature [°R or °F]
V	volts [V] or volumetric flow rate [cfm]
$\forall$	volumetric flow rate [ft^3/min or cfm]
W	work transfer rate [kW]
X	ammonia mass fraction
c_p	isobaric heat capacity [Btu/R]
d	displacement [cm^3/rev]
e^-	electron
g	vapor
h	enthalpy [Btu/lbm] or hour [hr]

m	mass flow rate [lbm/hr]
n	number of electrons
v	specific volume [ft^3/lbm]
w	specific work [kW/lbm]
x	mass flow ratio
y	liquid yield ratio
z	nitrogen requirement ratio

Greek

β	coefficient of thermal expansion
ε	heat exchanger effectiveness
η	efficiency
μ_{JT}	Joule-Thompson expansion coefficient
μ_s	isentropic expansion coefficient
ρ	density [lbm/ft^3]
ϖ	rotational speed [rad/s]

Subscripts

C	ortho/para conversion process
CW	cooling water
Elec	electrolyzer
FW	feed water
H_2	hydrogen
N_2	nitrogen
NH_3	ammonia vapor

P	isobaric or pump
T	isothermal
ab	absorber
act	actual
ad	adiabatic
c	compressor
cool	cooling load
e	expander
f	liquid
g	electric generator
h	isenthalpic
in	expander gas inlet
max	maximum
min	minimum
o	standard conditions
opt	optimum
out	expander gas outlet
rect	rectifier
s	isentropic
shaft	expander pulley shaft
strong	high ammonia concentration stream
th	thermoneutral
v	volumetric

vg	vapor generator
weak	low ammonia concentration stream
wf	working fluid

Abstract of Thesis Presented to the Graduate School
of the University of Florida in Partial Fulfillment of the
Requirements for the Degree of Master of Science

STUDY OF THE FEASIBILITY AND ENERGY SAVINGS OF PRODUCING AND PRE-COOLING HYDROGEN WITH A 5-KW AMMONIA BASED COMBINED POWER/COOLING CYCLE

By

Robert Joseph Reed

May 2005

Chair: H. A. (Skip) Ingley
Major Department: Mechanical and Aerospace Engineering

This thesis presents the results of a study on hydrogen production and liquefaction and the feasibility of the 5-kW ammonia based combined power/cooling cycle to energize these processes. Analytical models of the electrolysis, Claude liquefaction, and combined cycle processes are developed to study the effects of variable boundary conditions and component efficiencies on the hydrogen production rate and to determine the optimum operating conditions. Additionally, a performance study is implemented to gauge the applicability of a scroll expander with the 5-kW combined cycle. This research is motivated by the current energy crisis and recent research efforts in the development of renewable energy-based hydrogen production methods.

Analytical models are adapted to computer simulations that calculate the thermodynamic properties, heat and work interactions, and efficiencies of each system for variable boundary conditions and component efficiencies. Data from these simulations are used to deduce the optimum configuration that results in the maximum

hydrogen production rate. The scroll expander performance test was carried out with a common automotive air-conditioning scroll compressor arranged in an open-cycle configuration using air at variable inlet pressures. Predictions on its performance with ammonia were made based on the observed trends and by contrasting the properties of the two working fluids.

The minimum specific energy required for electrolysis and liquefaction is 24.839 kW-h/lbm-H_2 (54.76 kW-h/kg-H_2) and 3.817 kW-h/lbm-H_2 (8.41 kW-h/kg-H_2), respectively, for a total of 28.656 kW-h/lbm-H_2 (63.18 kW-h/kg-H_2). With a 5-kW output from the combined cycle, the maximum liquid hydrogen production rate is 7.21 gallons (27.3 liters) per day. Experimental measurements of the scroll expander's performance show isentropic efficiencies of 15 to 20 percent with maximum power output of 0.368 Hp (0.274 kW) at 1460 RPM with an inlet pressure of 80 psig (653 kPa).

Simulation results show pre-cooling the hydrogen prior to liquefaction does not reduce the specific energy consumption and, in fact, is detrimental to the thermal efficiency. Furthermore, pressurized electrolysis is found to be the most effective means of reducing the specific energy of liquefaction. The heat and work interactions of the combined cycle scale with the inverse of the expander efficiency. Additionally, isentropic expander efficiencies above 60% are required to extract any cooling from the cycle. The performance test proved that scroll tip leakage is the major cause of poor expander performance. Improvements of the scroll design such as increasing the scroll wrap and introducing low-friction materials would significantly increase its efficiency and make it a suitable design for low-output applications.

CHAPTER 1
MOTIVATION

Current energy consumption and forecasted demand with regard to limited fossil fuel reserves is presented in this chapter to demonstrate the necessity for the conversion to a renewable resources-based global energy market. Economical, environmental, and political factors are addressed as further motivation. The remainder of the discussion introduces hydrogen as a potential energy carrier for a renewable energy market.

Current Energy Trends

Approximately 85.7% of the world's energy is currently supplied by fossil fuels, with crude oil making up 38.8% of that total. Global energy consumption is projected to increase 54% over the next 25 years (Energy Information Administration, 2004).

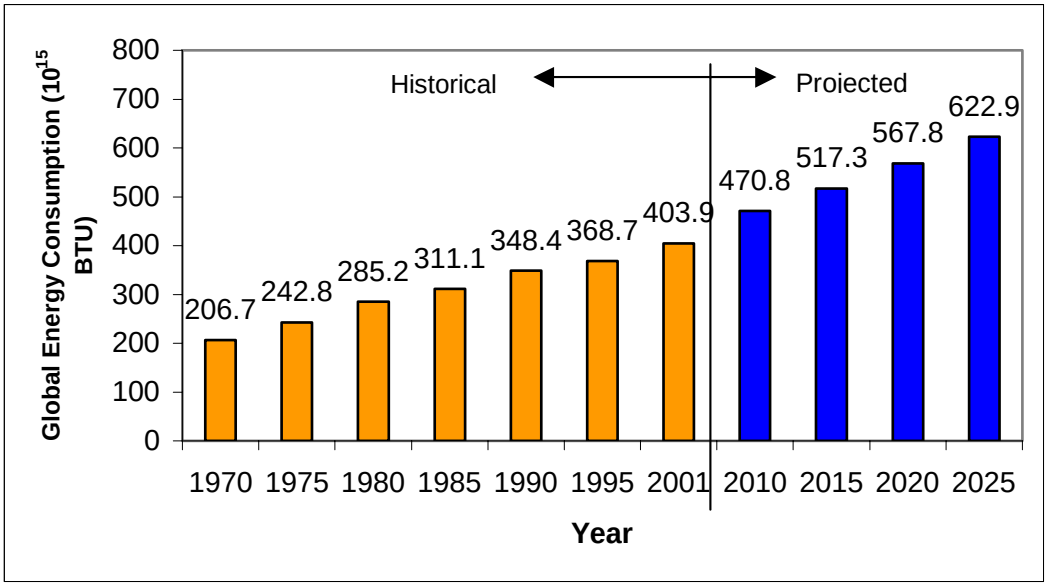

Figure 1.1. World energy consumption since 1970 with projections to 2025 (Energy Information Administration, 2004)

This increased demand is being fed primarily from countries with rapidly industrializing and emerging economies such as India and China. Proven oil reserves are sufficient to satisfy this demand over the next 20 years, after which there is debate as to whether oil production will peak before 2030 or that continued technological progress and new oil discoveries will satisfy the demand well into this century (Ramsay, 2003).

The economic effects of increasing energy demand on a limited supply are apparent today with peak 2004 oil prices near $50/barrel and average gas prices in the US near $2.00/gallon. As fossil fuel production peaks and inevitably begins to decline, and without other viable energy sources, prices will continue to escalate.

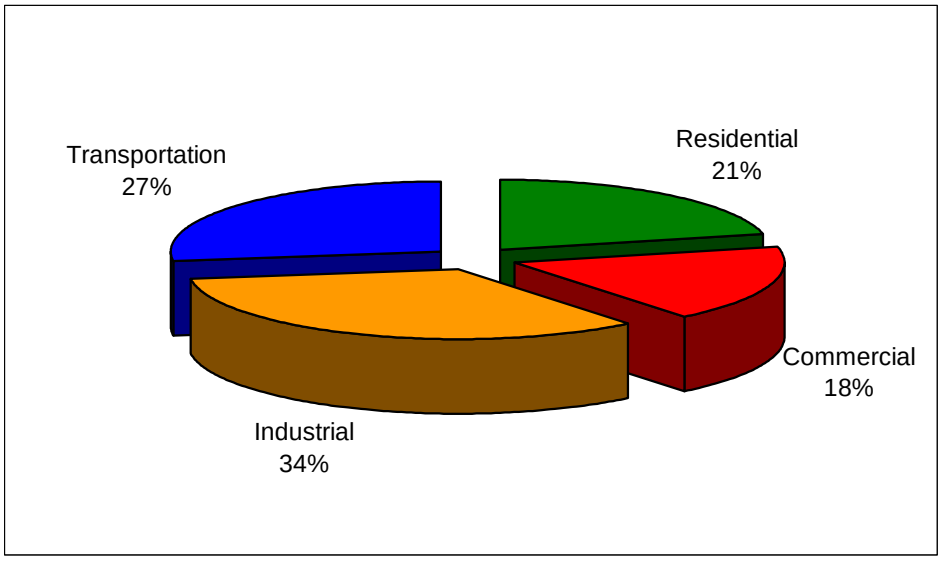

Figure 1.2. US energy consumption by sector in 2002 (Energy Information Administration, 2003)

Figure 1.2 gives an overview of how energy is consumed in the US economy. Industry is affected directly and indirectly by the cost of energy. The direct effect is to increase the cost of processing raw materials and production. Fuel costs involved with transporting finished goods is the indirect effect. The natural response of industry to increasing cost is to slow production and/or reduce labor forces, thus slowing the entire economy.

A number of adverse environmental phenomena such as the greenhouse effect, air pollution, acid rain, and oil spills are attributed to the use of fossil fuels. The burning of all fossil fuels produces carbon dioxide, a greenhouse gas. The Energy Information Administration reports that carbon dioxide contributes over 84% to the total of greenhouse gases emitted (Mirabal, 2003). Global warming is widely debated as an on-going occurance, but if it were found to be so, carbon dioxide emissions would be the main cause. Another by-product of fossil fuel combustion in air is the formation of nitrogen oxides (NOx) that contribute to ozone depletion as well as smog formation. Complex fossil fuels, such as petroleum and coal may also contain sulfur, which form sulfides that can cause acid rain. These environmental factors and others mentioned contaminate water supplies, damage ecosystems, and are related to the occurrence of many respiratory illnesses in humans.

In 1985, the US imported 27.3% of the oil it consumed. Over the past 18 years, as shown in Figure 1.3, the U.S. dependence on foreign oil has steadily increased to 56.1% and is projected to be 69.6% of that consumed by 2025 (Energy Information Administration, 2003).

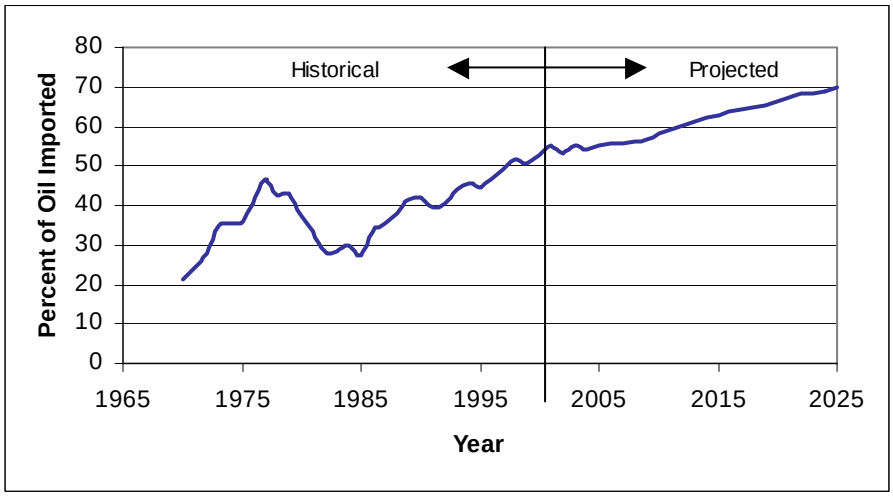

Figure 1.3. Foreign oil imported as a percentage of the total oil consumed in the U.S.

With greater dependence on foreign oil, the U.S. will be reliant on a stable Middle East, Russia, and South America. International crises such as those recently in Iraq and Venezuela will have a more significant impact on oil prices as they do today.

It is important that alternative energy sources are developed today to deal with the issues of tomorrow. Current research initiatives around the world are focused on hydrogen as the fuel of the future. With the development of a hydrogen economy based on renewable resources, greenhouse gas emissions will be reduced, the economy will be more independent of oil prices, and foreign policy will be less influenced by oil reserves.

Hydrogen as a Future Energy Carrier

In 2001, 20.4% of global energy consumption supported transportation; of which 96% was supplied by crude oil (Energy Information Administration, 2003). By developing an alternative fuel for transportation, world oil consumption could be reduced by as much as 19.6%. Reducing oil consumption likewise reduces greenhouse emissions and ozone depletion. Hydrogen holds promise as the fuel to achieve these goals because it can be produced from water using renewable energy sources and it burns clean; with water and heat as the only combustion products (NOx emissions are possible when burned in air).

One of the barriers to the widespread use of renewable resources is the geographical limitation. For example, hydropower can only be utilized in areas where damns can be built and solar power is dependent on incident sunlight, which varies from region to region. Renewable energy technologies can be utilized more efficiently and on a broader scale by constructing large capacity plants in regions with prominent sources of energy. The energy can subsequently be converted to chemical energy by producing hydrogen, enabling delivery to a larger market.

Governments around the world realize the potential of hydrogen as an alternative fuel. Many countries have adopted research initiatives in the production, storage, and utilization of hydrogen. The U.S. Department of Energy has recently announced plans to advance toward a hydrogen-based energy system making fuel-cell-powered vehicles available by 2010. Industry is following suit as most major automobile manufactures have significant programs in place to develop fuel cell powered vehicles (Ramsay, 2003).

Hydrogen is a safe and clean fuel that when produced using renewable energy is virtually pollution free. Hydrogen also provides a means to convert from a fixed source of energy to one compatible with the needs of transportation. With further development of production and storage technology, hydrogen can become the primary source of fuel for the transportation sector and can help usher in the renewable energy era.

CHAPTER 2
BACKGROUND AND THEORY

This chapter introduces hydrogen as a potential fuel and presents a brief overview of hydrogen storage and production systems. An emphasis is placed on the transportation sector and renewable technologies to develop the importance of electrolysis and liquefaction in a hydrogen economy. Following the theory of electrolysis and hydrogen liquefaction, the ammonia-water combined cycle is introduced as a means of converting low-temperature energy sources into usable electricity to power both systems; and refrigeration to pre-cool hydrogen prior to liquefaction. The scroll compressor is introduced as a potential high-efficiency expander for use with the combined cycle as motivation for the current study.

Hydrogen as an Energy Carrier

Hydrogen is the simplest, most abundant element in the universe comprising 75% of all visible matter by mass (Flynn, 1997). Currently, the majority of the hydrogen produced in the U.S. is used as a chemical in a variety of commercial applications including ammonia production, hydrogenation of fats and oils, and methanol production (National Hydrogen Association, 2004). With the continuing depletion and increasing cost of fossil fuels, however, greater consideration is being given to hydrogen as an alternative fuel.

Characteristics

Hydrogen has several characteristics that make it a desirable alternative fuel for transportation:

- Highest energy content per unit mass of any known fuel (51,574 Btu/lbm) – hydrogen produces 2.7 times more energy per unit mass than gasoline when burned.

Table 2.1. Heating values of hydrogen and other common fuels at STP

Fuel	Higher Heating Value		Lower Heating Value	
	Btu/lbm	kJ/g	Btu/lbm	kJ/g
Hydrogen	60954	141.78	51574	119.96
Methane	23861	55.5	21500	50.01
Propane	21651	50.36	19772	45.99
Gasoline	20464	47.6	19003	44.2
Diesel	20249	47.1	18831	43.8
Methanol	9746	22.67	8564	19.92

(Gater, 2001)

- Clean – combustion of hydrogen produces no carbon dioxide or sulfur emissions. When burned with oxygen, the only byproducts are water and heat. If burned in air, nitrogen oxides may be produced.

- Renewable – hydrogen can be produced by a variety of methods using renewable energy sources for a virtually limitless and pollution free fuel supply.

- Technologically compatible – in the 1920s, German engineer Rudolf Erren successfully converted IC engines to hydrogen burning engines (National Hydrogen Association, 2004). Hydrogen can also be reacted with oxygen in a fuel cell to produce electricity to drive a motor.

- Efficient utilization – hydrogen IC engines are about 25% efficient, fuel cells are 45-60% efficient; typical gasoline IC engines are 18-20% efficient (National Hydrogen Association, 2004). Hydrogen fuel cell powered vehicles can be up to three times more efficient than today's gasoline engines.

Production Technologies

The U.S. currently produces 9 million tons or 3.2 trillion cubic feet (90 billion Nm^3) of hydrogen per year. Of this amount, 95% is produced by steam/methane reformation (SMR) (National Hydrogen Association, 2004). SMR operates by reacting a natural gas feedstock with steam at high temperatures (700 – 925 °C) to produce carbon monoxide and hydrogen. The carbon monoxide is then consumed in a water/gas shift reaction to create CO_2 and additional hydrogen. Other hydrogen production methods are

outlined in Figure 2.1. Detailed descriptions of each fossil fuel based production technology are given by Mirabal (2003). Renewable energy systems are outlined by the U.S. Department of Energy (2003).

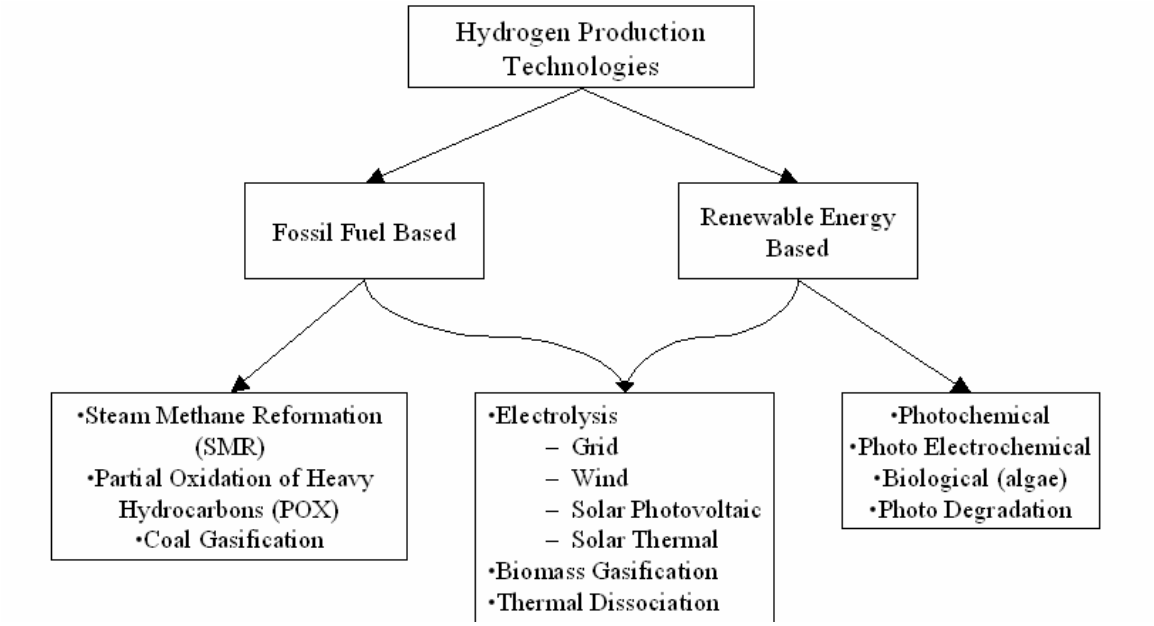

Figure 2.1. Hydrogen production technologies by energy source

SMR is currently the most cost effective method of producing hydrogen; however, because of increasing fossil fuel cost due to diminishing supplies and reduced capital cost of renewable energy due to technological improvements, wind and ammonia-water combined power/refrigeration cycle solar power based electrolysis are projected to become the most cost competitive by 2020 (Mirabal, 2003).

Table 2.2. Projected hydrogen costs of various production methods[1]

	Hydrogen Production Costs ($/lb)			
Year	**2003**	**2010**	**2030**	**2050**
Steam Methane Reformation	0.66	0.90	2.75	9.88
Partial Oxidation	0.80	0.90	1.44	2.89
Coal Gasification	1.12	1.20	1.65	2.83
Electrolysis - Grid Power (fossil fuel based)	1.53	1.63	2.42	4.12
Electrolysis - PV / Antenna Power	3.47	2.40	0.91	0.65
Electrolysis - Wind Power	1.33	1.14	0.78	0.60
Electrolysis - Ammonia Water Combined Cycle	2.50	1.37	0.89	0.63

[1] Original data converted from $/GJ using the HHV of hydrogen (Mirabal, 2003)

Although there are other methods available to produce hydrogen from renewable resources, electrolysis is the most versatile and technologically developed. Electrolyzers do not require high temperature for operation as do thermal decomposition, dissociation, or chemical processes nor are they dependent exclusively on sunlight. For these reasons, electrolysis is expected to be the predominate method of hydrogen production in a future hydrogen economy.

Storage Technologies

One of the barriers preventing the wide use of hydrogen as a fuel is its storage. This issue centers on hydrogen's low density and correspondingly low energy density. Table 2.3 displays these characteristics for hydrogen under several conditions as well as for other common fuels.

Table 2.3. Mass and energy density of select fuels

Fuel	Density		Energy density	
	lb/ft^3	kg/m^3	Btu/ft^3	MJ/m^3
Hydrogen				
gas (STP)	0.005309	0.085044	323.60	12.06
gas (3,000 psig, 60 F)	0.9631	15.428	58,705	2,187
gas (10,000 psig, 60 F)	2.484	39.797	151,434	5,643
liquid	4.4197	70.798	269,398	10,038
Methane				
gas (STP)	0.042358	0.6785	1010.70	37.66
gas (3,000 psig, 60 F)	10.778	172.650	257,174	9,583
liquid	26.367	422.367	629,143	23,442
Propane				
gas (STP)	0.1183	1.895	2561.75	95.45
liquid	36.298	581.450	785,888	29,283
Gasoline (liquid)	45.884	735.010	938,976	34,987
Diesel (liquid)	53.064	850.012	1,074,483	40,036
Methanol (liquid)	49.380	791.012	481,260	17,932

(National Institute of Standards and Technology 2003, Chevron 1998)

Because of its low density, hydrogen requires a large volume for an equivalent amount of stored energy as compared to other common fuels. To illustrate this fact, the energy

equivalent of 10 gallons (37.85 liters) of gasoline would require a tank size of 175 gallons (662.4 liters) for gaseous hydrogen at 3000 psig and 37.6 gallons (142.3 liters) for liquid hydrogen. Another issue with hydrogen storage in regards to its use as a motor fuel is the combined weight of the container, safety equipment and any required insulation. Container weights (including fuel) for several hydrogen storage methods are given for an energy equivalent of 7.93 gallons (30 liters) of gasoline in Figure 2.2.

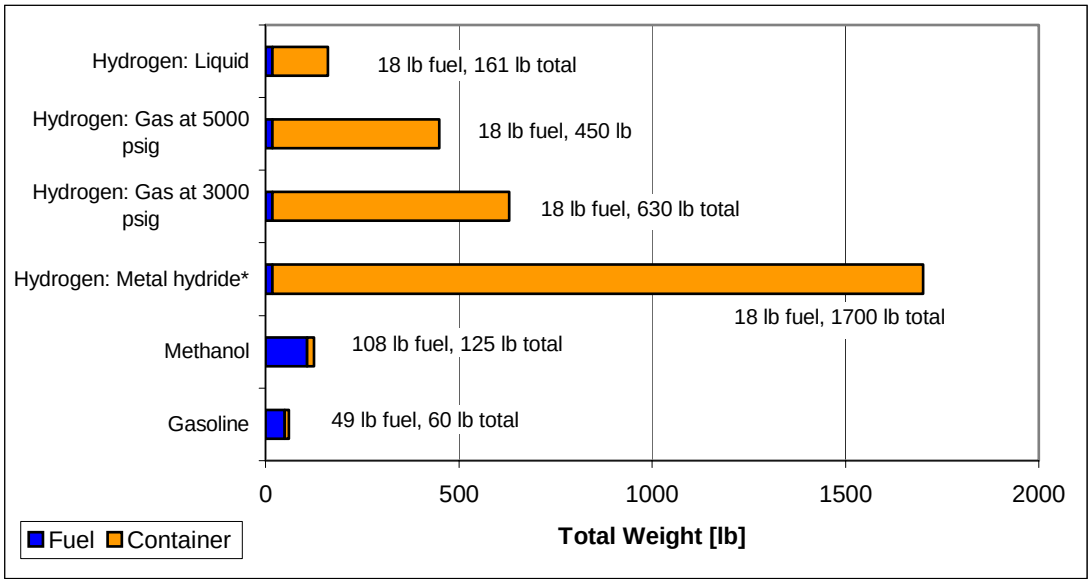

Figure 2.2. Fuel and total weight of several hydrogen storage systems. *Storage capacity by weight approximately 1.1%.

There are several methods of hydrogen storage currently available or being researched. They are summarized as follows:

Metal hydrides. Metal hydrides are specific alloys consisting primarily of granular magnesium, nickel, iron, and/or titanium. These alloys are capable of adsorbing hydrogen (1% - 8% by weight) at high pressure and moderate temperature and releasing it under low pressure and elevated temperature. Metal hydrides are characterized by de-adsorption temperature. Low-temperature (< 200 °F) hydrides operate at higher pressures to prevent hydrogen release at ambient temperatures. These hydrides typically adsorb 1 -

2 percent of their weight in hydrogen. Higher temperature (> 250 °F) hydrides hold 5 – 10 percent hydrogen by weight, but require significant amounts of heat to attain the temperatures required to release the stored hydrogen. (Sunatech Inc., 2001).

Metal hydrides provide the safest means of storing hydrogen. Because the hydrogen is stored in a solid-state media, it cannot be ignited until released. In addition, the hydrogen is released at low pressures and moderate temperatures; therefore, no specialized storage tank is required to deal with high pressures or cryogenic temperatures.

Despite these advantages, metal hydrides are undesirable for use in transportation. Large, heavy, and costly storage units are required to hold equivalent amounts of energy as current gasoline tanks, as shown in Figure 2.2. Common hydrogen impurities such as oxygen and water reduce the ability of the tank to store hydrogen as they bond permanently to the metal. Additionally, vibrations due to typical driving conditions can result in particle attrition that also reduces the tank's useful life.

Compressed hydrogen. Compressed hydrogen is the simplest and one of the most common methods of hydrogen storage and transportation. Even at 10,000 psig, however, compressed hydrogen contains nearly 8 times less energy per unit volume than gasoline (not including the energy expended in compressing the hydrogen). Cylinders tend to be heavy because of the robust construction necessary to withstand the high pressures and impacts. These factors make compressed hydrogen storage suitable for only short ranged applications or as a reserve fuel for liquid hydrogen powered vehicles.

Liquefied hydrogen. Liquid hydrogen is formed by cooling hydrogen gas to -423 °F (-253 °C) at atmospheric pressure. Storage of such low temperature fluids is achieved using a dual-walled cylinder with an evacuated space between the cylinder walls

(Dewer's flask). Due to the relatively high surface to volume ratio typical of the small tanks used in transportation applications, additional multi-layered radiation insulation sheets are also employed (Flynn, 1997).

There are several technological challenges that must be overcome in order for liquefied hydrogen storage to come into widespread use. First is safe tank design to reduce weight and hydrogen boil off due to heat infiltration. The imperfect insulation of the inner tank supports, among other factors, causes a typical boil off rate of 3% per day (Clean Energy Research Center, 2003). Furthermore, improved methods of hydrogen liquefaction must be developed to reduce LH_2 cost. Today, about 30% of the energy contained in LH_2 is consumed by the liquefaction process (Fuel Cell Store, 2003). Lastly, re-filling stations must be developed such that the public can operate them safely.

Liquefied hydrogen (LH_2) is currently the optimum hydrogen storage method for vehicles in terms of tank size/weight and energy density. LH_2 has the highest volumetric energy capacity of any commercially available storage system being only four times less than gasoline; and because hydrogen burns more efficiently than gasoline, LH_2 tanks are not necessarily four times the size of typical gasoline tanks for a given vehicle range. This allows automobile manufactures to continue using current vehicle designs, easing the transition into a hydrogen economy.

Carbon nanotubes and glass microspheres. Carbon nanotubes store hydrogen in microscopic surface pores and within the tube structures via adsorption. The mechanism by which they store and release hydrogen is similar to metal hydrides, however carbon nanotubes are lighter, cheaper, and are capable of storing 4.2 to 65% hydrogen by weight (Fuel Cell Store, 2003). Carbon nanotubes are still under research and development and

currently store between one and ten percent hydrogen by mass (Clean Energy Research Center, 2003).

Glass microspheres are currently being researched as a potential hydrogen storage method. Hydrogen is stored by first warming the tiny glass to increase their surface permeability and then immersing them in high-pressure hydrogen gas. The spheres are then cooled, locking the hydrogen inside of the glass balls. Increasing the temperature of the spheres reverses this process. Experiments to increase hydrogen release rates by crushing the spheres are also being performed. The key advantage of glass microspheres is storage at ambient temperature.

The technology exists today for the introduction of hydrogen-powered vehicles; however, the size, weight, and/or cost limitations imposed on storage systems by the low energy density of hydrogen must first be overcome. Liquid hydrogen holds the greatest promise for hydrogen-powered vehicles. These storage systems have the lowest weight and volume of those commercially available, and with improved tank design and hydrogen liquefaction methods, the relatively high costs will lessen over time.

Electrolysis of Water

English scientists William Nicholson and Sir Anthony Carlisle first discovered that the application of an electric current to water produces hydrogen and oxygen in 1800. The principle of electrolysis was later formulated by Michael Faraday in 1820. Since then electrolysis has played only a minor role in worldwide hydrogen production; recently contributing to only 4% of total global production (National Hydrogen Association, 2004). Current electrolytic hydrogen production is limited to low-cost electricity sources such as hydroelectric or small-scale onsite generation in which purity is essential.

The importance of electrolysis in a future hydrogen economy is two fold: First, as discussed previously, electrolysis powered by wind or the ammonia water combined power/cooling cycle is projected to be the most cost efficient hydrogen production method by 2020. Second, it provides a practical link between hydrogen and renewable resources through electricity generation. In this manner, electrolysis can indirectly utilize any energy source that can be used to produce electricity. Furthermore, when powered by electricity generated from renewable sources of energy, electrolysis does not require fossil fuels and has zero polluting emissions.

Process Description

Electrolysis is defined by McMurray and Fay as the use of an electric current to drive a non-spontaneous chemical reaction (1998). Electrolysis of water consists of a pair of oxidation/reduction reactions driven by a DC voltage applied across two electrodes as described by equations 2.1a – 2.1c.

Cathode: $2H_2O + 2e^- \rightarrow H_2 + 2OH^-$ (2.1a)

Anode: $2OH^- \rightarrow {}^1\!/\!_2 O_2 + H_2O + 2e^-$ (2.1b)

Overall: $H_2O \rightarrow H_2 + {}^1\!/\!_2 O_2$ (2.1c)

Water is reduced at the cathode to form hydrogen gas and hydroxide ions (OH^-). The OH^- ions migrate toward the anode where they are oxidized to form oxygen, water, and two free electrons. The free electrons are then attracted to the positively charged cathode, thus completing the circuit. A schematic of a simple electrolyzer and the overall electrolysis process is given in Figure 2.3.

Each electrode is isolated from the other with an ion-conducting diaphragm to keep the product gases separate; and an electrolyte is used to make the solution conductive.

The electrolyte is chosen such that its reduction and oxidation potentials are less than that of water. In this manner, the electrolyte is conserved because it acts only as an ion-conducting substance.

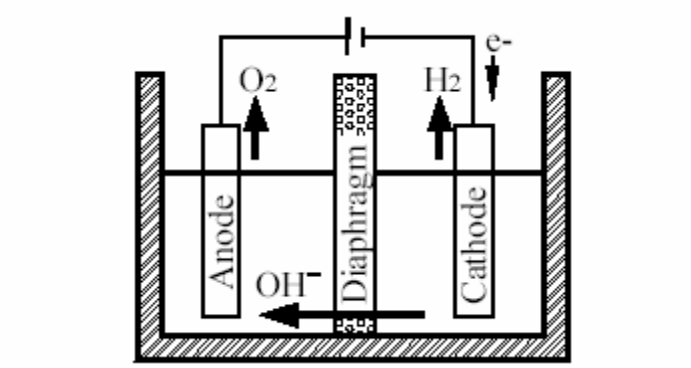

Figure 2.3. Process diagram of a simple alkaline electrolyzer (adapted from Mirabal)

Energy and Efficiency

The voltage required for reversible or isentropic electrolysis is proportional to Gibb's free energy of reaction as defined by Faraday's Law:

$$\Delta G = -nFE \tag{2.2}$$

where ΔG is Gibb's free energy of reaction
n is the number of electrons transferred in the reaction
F is Faraday's constant, 9.648531×10^4 $Coulombs/mol$
E is the cell voltage

A negative sign is included on the right hand side of Equation 2.2 because by convention voltage input is considered negative (McMurray and Fay, 1998). The spontaneity of a given reaction is determined by the sign of the Gibbs free energy of reaction (from hereon referred to as GFR). GFR is positive for non-spontaneous reactions and negative for spontaneous ones. For water at standard temperature and pressure, (25 °C and 1 atm), the GFR is 50,941 Btu/lbm_{H2} (14.93 kW-h/lbm_{H2}) and the corresponding reversible voltage is 1.23 V. The electrical energy required to drive the

electrolysis reaction is equal to the GFR (Casper, 1978). The enthalpy of reaction (higher heating value) of hydrogen, however, is 61,451 Btu/lbm (18.01 kW-h/lbm_{H2}). Conservation of energy dictates that the remaining 10,510 Btu/lbm (48.89 kJ/mol) must be supplied as heat. For a reversible process, this heat would be obtained from the surroundings, and the electrolyzer would double as a refrigeration unit.

The second law of thermodynamics states that entropy always increases for any real process. Entropy production in electrolysis increases the required cell voltage as described by equation 2.3.

$$\Delta H = \Delta G + T\Delta S = -nFE + nFT\left(\frac{\partial E}{\partial T}\right)_P \qquad (2.3)$$

$$\text{where } \Delta S = \left(\frac{\partial \Delta G}{\partial T}\right)_P = nF\left(\frac{\partial E}{\partial T}\right)_p \quad \text{from Faraday's Law}$$

The entropy produced is liberated as heat, which supplies the additional 10,510 Btu/lbm necessary to form hydrogen. The voltage required for isothermal electrolysis (defined as the thermoneutral voltage) is 1.47V. This result is obtained by replacing ΔG in Equation 2.2 by the HHV of hydrogen. In reality, the thermoneutral voltage is the lowest that can possibly be achieved.

Real electrolyzers require greater than the thermoneutral voltage due to additional overvoltages independent of the entropy generation. Overvoltage is defined as the difference between the applied voltage and the reversible 1.23V and is proportional to the amount of current passed through the cell (Casper, 1978). These overvoltages include: ohmic resistance of the electrolyte, concentration polarization (changes in the concentration of H^+ or O^{2+} or water near the electrodes), voltage gradients at the electrode/electrolyte interface due to the slowness of reaction (proportional to cell

operating temperature), and wire and component resistance (typically about 2% of total loss) (Casper, 1978). The primary source of electrolyte resistance is the formation of vapor bubbles on the electrodes (Wendt, 1990). Additional energy losses occur (typically 5% of total energy consumption) within each subsystem including AC to DC rectification, cooling water system, feed water pumps, and electrolyzer pumps (if necessary) (Casper, 1978).

The majority of electrolyzer manufacturers have taken steps to reduce these overvoltages. Concentration polarization can be avoided by adequate mixing of the electrolyte through circulation or by natural gas lift. One method developed to reduce electrolyte resistance is zero gap cell geometry in which porous electrodes are pressed on either side of the diaphragm, forcing the product gases to leave from the rear (Wendt, 1990). Another technique is to increase the cell operating temperature and pressure in order to speed up reaction kinetics and reduce electrolyte resistance. However, this also enhances corrosion of the electrodes and shortens operating lifetime.

The figures of merit measuring electrolyzer performance are current, electrochemical, and thermal efficiencies. Current efficiency measures deviation from the hydrogen yield predicted by Faraday's law at 1.47 V and 1000 A-h due to extraneous electrode reactions (Casper, 1978). For most electrolyzers, this number approaches 100%. Electrochemical efficiency is defined as the reversible voltage divided by the operating voltage. The maximum electrochemical efficiency under isothermal conditions is 83.7%. Thermal (1^{st} law) efficiency is the ratio of the isothermal voltage to the operating voltage or the HHV of hydrogen divided by electricity input as given by Equation 2.4.

$$\eta_{Elec} = \frac{V_{th}}{V_{act}} = \frac{HHV_{H_2}}{E_{Elec}} \tag{2.4}$$

Using this definition of efficiency, ideal electrolysis operates at an apparent 120% efficiency. Thermal efficiency is the most widely used figure of merit by electrolyzer manufactures, therefore any given efficiency will be thermal efficiency. Commercial electrolyzers currently operate at efficiencies (excluding subsystems) of up to 85% (Stuart Energy, 2004)

Electrolyzer Designs

Electrolyzers are typically classified by their electrolyte; the most common of which is alkaline/water (Casper, 1978). Others include solid polymer (SPE), seawater, and solid oxide; descriptions of which are given by Casper (1978).

Alkaline/water electrolyzers typically operate with a 30% potassium hydroxide (KOH) solution at relatively low temperatures of 158 – 212 °F (70 – 100 °C). There are two varieties of alkaline/water electrolyzer: monopolar (tank-type) and bipolar (filter-press). A summary of each type highlighting the unique advantages and drawbacks of each is given below:

Monopolar or tank-type cells are constructed as an alternating set of anodes and cathodes connected electrically in parallel and hung vertically from gas collectors into a tank of electrolyte. Mixing of the electrolyte is achieved through simple gas lift. The cathodes are normally surrounded by a diaphragm to prevent the mixing of gases. This arrangement results in individual tanks operating at low voltages (typically 1.9 – 2.5 V) and high currents (Casper, 1978).

Bi-polar or filter-press electrolyzers are characterized by the stacked design of the cells. In this configuration, one side of an electrode serves as the cathode and the other as

the anode of an adjoining cell. Electrodes are connected in series such that a desired operating voltage is achieved by increasing the total number of cells. The geometries of these cells are relatively thin; therefore, a pump is required to circulate the electrolyte through the cells. Bi-polar cells typically operate at lower current levels due to higher operating voltage. Table 2.4 lists the pros and cons of each alkaline/water electrolyzer design.

Table 2.4. Advantages and disadvantages of monopolar and bipolar electrolyzers

	Advantages	Disadvantages
Monopolar	• Require relatively few, inexpensive parts • Easily maintained – individual cells can be isolated for repair with minimum plant downtime • No pumps required for electrolysis circulation	• Unable to operate at high temperatures because of heat loss from large surface areas • Bulky design requires greater space per unit hydrogen produced • Tanks are difficult to design for pressurized electrolysis • Relatively high voltage losses and non-uniform current density distribution result from long current paths (Wendt)
Bi-polar	• Compact design • Capable of operating at high pressures and temperatures • Lower ohmic resistance and energy losses	• Requires precise fabrication tolerances and additional gaskets due to sealing problems • Maintenance is more difficult – if one cell fails, the entire cell must be shut-down and dismantled

One of the largest electrolytic hydrogen production plants in North America was built by Cominco, Ltd. in British Columbia, Canada. Before being shut down due to high electricity costs, the plant produced 41 tons/day of hydrogen with 3,229 individual tank-

type cells operating at 2.1 V (70% efficient) (Casper, 1978). Since that time, most manufactures have adopted the more efficient bi-polar design (Wendt, 1990).

Hydrogen Liquefaction

Liquid hydrogen was first produced by James Dewar in 1898; however, up until the mid 1940s to mid 1950s it remained nothing more than a laboratory curiosity (Flynn, 1997). In the late 1950s, the US Air Force began producing substantial amounts of LH_2 for its top secret "Bear" Program. Under contract to the Air Force, Air Products and Chemicals, Inc., constructed three production plants code named "Baby Bear," "Mama Bear," and "Papa Bear" to support Air Force aerospace programs. The largest of these was Papa Bear, which produced 30 tons/day in 1959 (Flynn, 1997). Today, total annual production of LH_2 in North America is nearly 300 tons/day (Drnevich, 2003).

Demand for large-scale liquid hydrogen production was initially sparked by the Apollo space program. Liquid hydrogen demand has increased and simultaneously shifted since the 1960s from aerospace to research and industry. Flynn reports that aerospace accounted for only 20% of total liquid hydrogen demand in 1990 (1997). This trend is expected to continue with the onset of a hydrogen economy including the advancement of fuel cell powered vehicles and the development of improved storage systems.

Hydrogen production companies are already taking advantage of the higher energy density of LH_2 vs. gaseous hydrogen to effectively reduce distribution costs. Where a full tube-trailer of gaseous hydrogen contains approximately 300 kg of deliverable gaseous hydrogen, a comparably sized liquid hydrogen trailer carries 4000 kg (Drnevich, 2003). Another benefit of liquefying hydrogen is the ultra high purity that results from the majority of trace impurities condensing out. High energy density and purity make

liquid hydrogen a well-suited fuel for hydrogen fuel cell powered vehicles in an emerging hydrogen economy; giving equivalent performance and driving range as today's gasoline and diesel automobiles.

Process Description

Hydrogen, like all gases, is liquefied by cooling it to its boiling point, -423 °F (-252.8 °C). There are several liquefier designs; all of which are derived from the simple Linde cycle shown in Figure 2.4 and follow the same general process.

The incoming gas is compressed isothermally from 1 to 2 on the diagram to a relatively high pressure. Heat is rejected to a cold return stream and the cooled gas is expanded from 3 to 4 on the diagram to atmospheric pressure and cryogenic temperatures. The two-phase flow that results is separated in a flash tank where the liquid yield is drawn off and collected and the remaining gas absorbs heat from the warmer high-pressure stream before it's recycled back to the compressor. The expansion can be accomplished using either a Joule-Thompson (expansion or throttling) valve or a work-extracting device.

Isenthalpic vs. isentropic expansion

Joule-Thompson expansion is modeled as isenthalpic by neglecting potential and kinetic energy changes as well as heat transfer (insulated valve). The effect that a change in pressure has on the temperature for an isenthalpic process is described by the Joule-Thompson coefficient given by Equation 2.5. A negative value indicates a temperature increase with expansion; a positive value indicates a temperature decrease.

$$\mu_{JT} = \left(\frac{\partial T}{\partial p}\right)_h = -\left(\frac{\partial T}{\partial h}\right)_p \left(\frac{\partial h}{\partial p}\right)_T \tag{2.5}$$

By substituting the definition of specific heat at constant pressure, $c_p = \left(\frac{\partial h}{\partial T}\right)_p$,

$\left(\frac{\partial h}{\partial p}\right)_T = v - T\left(\frac{\partial v}{\partial T}\right)_p$, and the volumetric coefficient of thermal expansion,

$\beta = \frac{1}{v}\left(\frac{\partial v}{\partial T}\right)_p$, the Joule-Thompson coefficient is given in its more useful form:

$$\mu_{JT} = \frac{1}{c_p}\{T\beta - 1\}v \tag{2.6}$$

Equation 2.6 demonstrates that the sign of the Joule-Thompson coefficient depends only on the product of $T\beta$. At a given pressure, the volumetric coefficient of thermal expansion and the specific volume are functions of temperature only. Consequently, a temperature can be identified at which $\mu_{JT} = 0$. This point is known as the inversion temperature; and represents the maximum temperature at which a gas can be cooled by isenthalpic expansion.

Most practical liquefaction systems use an expansion valve to produce low temperatures (Barron, 1985). In the case of hydrogen, however, the maximum inversion temperature at STP is well below ambient (-90.7 °F (-68 °C)). Additional energy is required to pre-cool the hydrogen below its inversion temperature for isenthalpic expansion to be effective.

Expansion in a work-extracting or work-producing device is commonly modeled as adiabatic and reversible (i.e. isentropic). This process is represented by an isentropic expansion coefficient, Equation 2.7.

$$\mu_s = \left(\frac{\partial T}{\partial p}\right)_s \tag{2.7}$$

By substituting the Maxwell relation $\left(\frac{\partial T}{\partial p}\right)_s = \left(\frac{\partial v}{\partial s}\right)_p$, applying the chain rule, and using the definitions defined previously, the isentropic expansion coefficient is given in the same terms as the Joule-Thompson coefficient:

$$\mu_s = \frac{1}{c_p}(\beta v T) \tag{2.8}$$

Equation 2.8 shows that the isentropic expansion coefficient is always positive (the temperature always decreases with pressure) because the coefficient of thermal expansion (β) for gases is always positive (Hands, 1986). This conclusion can also be arrived at intuitively by considering conservation of energy. If work is extracted from a fluid adiabatically, the internal energy and hence temperature must decrease.

Thermodynamically, isentropic expansion is more desirable than isenthalpic expansion. The T-S diagram in Figure 2.5 shows that an isentropic expansion will always result in a lower final temperature than isenthalpic expansion.

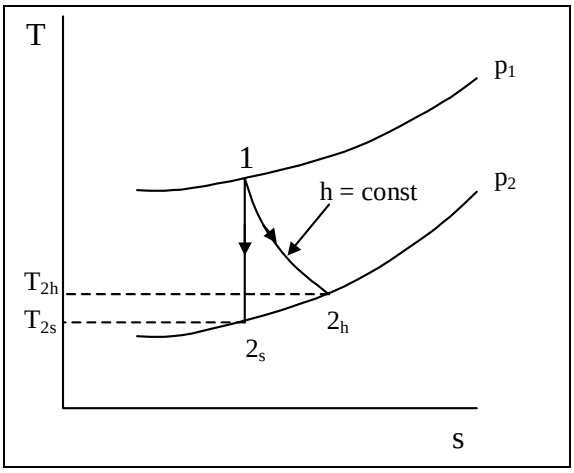

Figure 2.5. T-S diagram comparing isenthalpic and isentropic expansion

Practically, however, expansion devices cannot tolerate an appreciable amount of liquid. For this reason, expansion valves are necessary in all liquefaction systems (Barron, 1985). The Claude cycle discussed later seeks to combine the benefit of isentropic

expansion with the necessity of isenthalpic expansion as an efficient means of liquefying hydrogen.

Ortho/para conversion

Another challenge to simple liquefaction systems is the unique sub-atomic structure of hydrogen. Hydrogen exists in two different molecular forms: ortho-hydrogen and para-hydrogen. Each form is distinguished by the relative spins of its protons. The protons of ortho-hydrogen spin in the same direction whereas the proton spins of para-hydrogen oppose one another. Hydrogen at STP (i.e. normal hydrogen) is composed of 74.928% ortho and 25.072% para hydrogen. At the normal boiling point of hydrogen (-423 °F (-293.4 °C) at 1 atm) the equilibrium ortho/para composition is .21%/99.79% (Flynn, 1997).

Converting from ortho to para hydrogen is an exothermic process, releasing 302.4 Btu/lbm (703.3 kJ/kg) of heat at STP (Barron, 1985). The conversion process is relatively slow and the resident time of the hydrogen within the liquefier is short, so the liquid hydrogen essentially retains its room temperature ortho/para composition. Conversion gradually takes place in the storage tank resulting in boil-off losses because the heat of conversion exceeds the latent heat of vaporization (190.5 Btu/lbm or 443 kJ/kg) (Barron, 1985). The heat liberated during the conversion process is sufficient to evaporate nearly 70% of the original amount of hydrogen liquefied (Flynn, 1997). Storage time is a major issue with regard to liquid hydrogen as a motor fuel so it is important that the boil-off losses due to ortho/para conversion are minimized.

Catalysts are used to speed up the conversion reaction allowing the heat to be absorbed by the liquefier. This alleviates boil-off in storage, but at a penalty to the

overall efficiency of the liquefier. The most efficient method of conversion is to have the process take place simultaneously as the hydrogen is cooled. This is not possible in practice but can be simulated by cooling the hydrogen to liquid nitrogen temperatures (-320.4 °F or –195.6 °C) and passing it through an adiabatic converter then repeating this procedure in a step-wise manner (Flynn, 1997). Common materials proven effective as catalysts are ferric hydroxide gel, chromic oxide on alumina particles, and nickel silicate; all of which provide nearly 100% conversion to para hydrogen within a few minutes (Hands, 1986).

Claude cycle

The Claude cycle is the most commonly used system for large-scale hydrogen liquefaction (Hands, 1986). The performance of the cycle is enhanced by pre-cooling the compressed hydrogen gas to liquid nitrogen (LN_2) temperatures. Adding catalysts in the LN_2 and LH_2 baths provides a convenient and effective means of absorbing the heat of conversion. Figure 2.6 shows a schematic of this variation of the Claude cycle with labeled state points and flow paths.

Hydrogen gas typically enters the cycle at 1 atm and 80.6 °F (27 °C) (state 1). It is compressed isothermally (isothermal compression is achieved through multistage compression with inner-cooling and after-cooling) to state 2, typically 20 to 40 atm (Barron, 1985). The pressurized gas then exchanges heat with the return hydrogen and nitrogen streams (state 2a) before entering the LN_2 bath where it is cooled to -320.4 °F (-195.6 °C) and where the first step of ortho/para conversion occurs (state 2b). At this temperature, the equilibrium concentration of para hydrogen (assuming 100% conversion) is 50%.

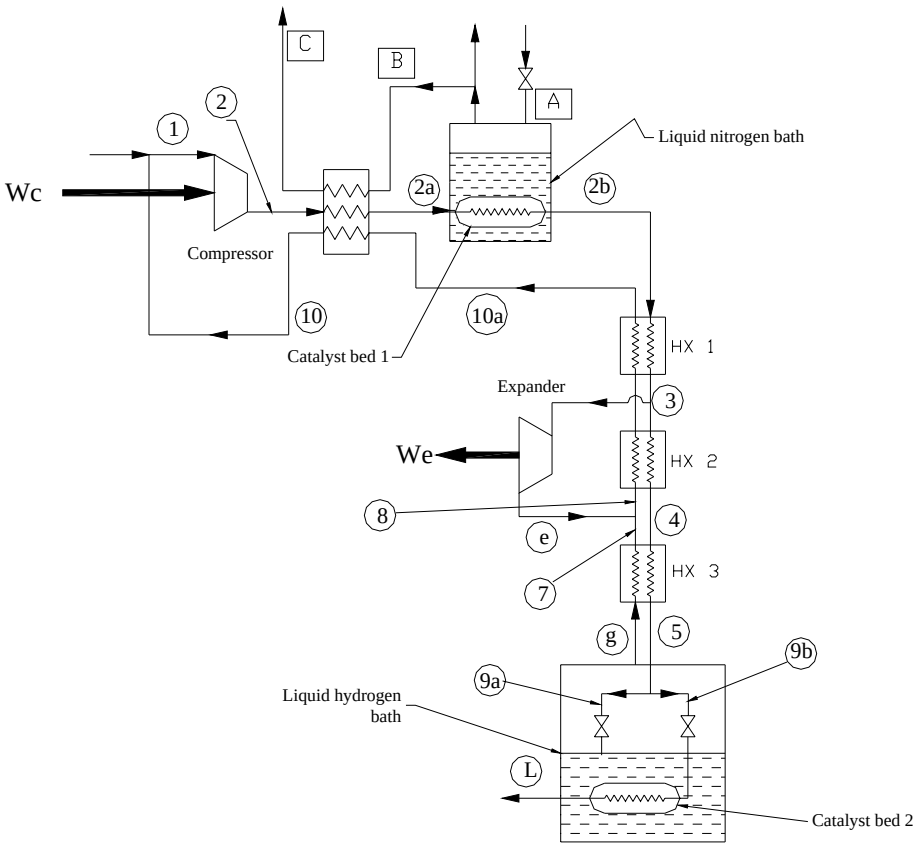

Figure 2.6. Claude cycle with liquid nitrogen pre-cooling and ortho/para catalyzation

It is desirable to perform the maximum amount of conversion at this stage because liquid LN_2 is less expensive to produce then liquid oxygen. The hydrogen is further cooled in the first heat exchanger to state 3. At this point, a portion of the flow (typically 60 to 80%) is diverted and expanded isentropically through a work-extracting device and used to pre-cool the compressed hydrogen. The expander work is used to offset the compressor work requirement, increasing the overall cycle efficiency. The remaining flow continues through the next two heat exchangers and into the liquid receiver. Here the flow streams are halved and throttled through expansion valves. The liquid yield from the first stream (state 9a) is collected in the receiver and used sacrificially to absorb the heat of conversion from the second catalytic bed. The second stream (state 9b) is passed

through the catalytic bed where it is ideally converted to 99.789% para hydrogen and extracted.

Ammonia-Water Combined Power/Cooling Cycle

The ammonia-water combined power/cooling cycle proposed by Goswami (1995) utilizes a binary ammonia/water working fluid to produce both power and refrigeration. The cycle is a combination of an ammonia-water refrigeration system and an ammonia-based Rankine cycle.

An ammonia-water mixture is used because of its desirable thermodynamic properties. Binary mixtures have varying boiling points depending on the concentration of the more volatile species. This characteristic gives a good thermal match with a sensible heat source, thereby reducing the irreversibility associated with heat transfer (Hasan, Goswami, 2003). Additionally, the low boiling point of ammonia allows the utilization of low temperature heat sources such as low-grade waste heat from industrial processes, solar water heaters, and geothermal sources. In a theoretical investigation performed by Tamm et al., the cycle is shown to operate with heat source temperatures as low as 116.6 °F (47 °C) albeit with low first law efficiency (~ 5%). When operating with a heat source temperature of 224.6 °F (107 °C) and idealized parameters, however, second law efficiencies greater than 65% are possible (2003).

The unique ability of this cycle to produce both power and refrigeration gives rise to two advantages for use in a hydrogen economy. First, the cycle can utilize low-grade renewable heat sources such as that available from inexpensive flat plate solar collectors to produce the power needed to drive an electrolyzer and liquefier. Second, the cooling produced by the cycle can be used to pre-cool hydrogen prior to liquefaction, thereby

reducing the power requirement of the compressor. In this manner renewable energy source utilization is improved compared to technologies such as wind or P.V. electrolysis.

Process Description

Figure 2.7 gives a schematic of the cycle showing state points and flow paths.

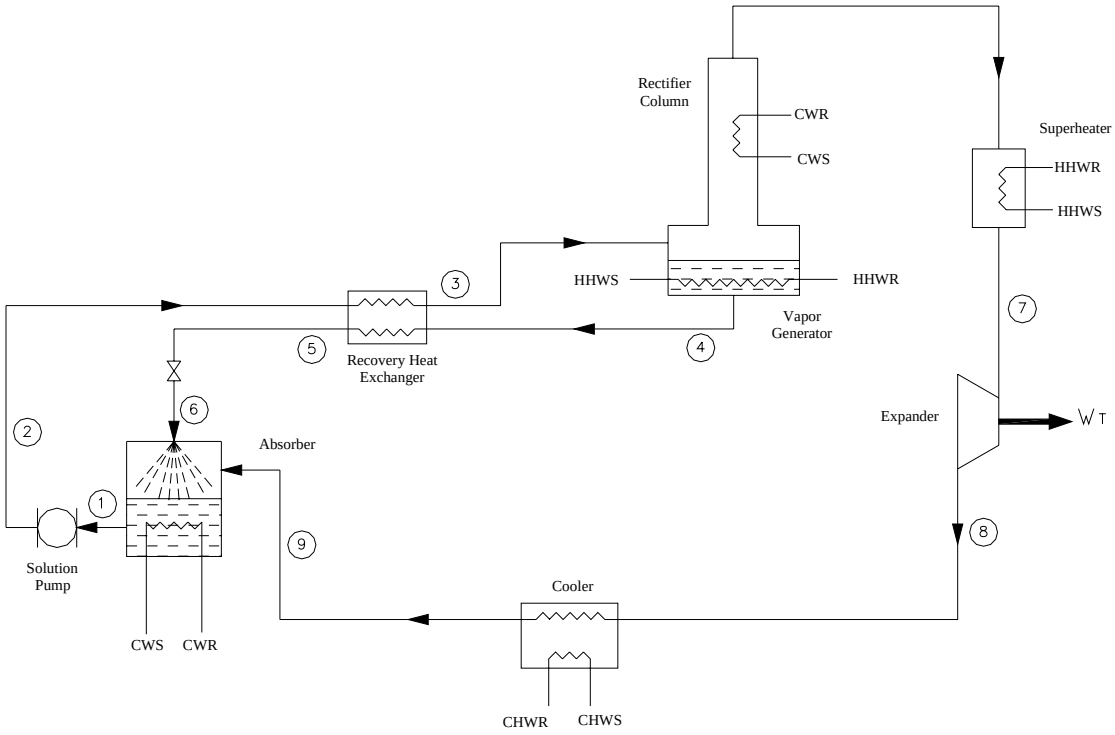

Figure 2.7. Combined cycle flow diagram

The fluid leaves the absorber at state 1 as a saturated solution at the cycle low pressure with a relatively high ammonia concentration. It is pumped to the system high pressure (state 2) before traveling through the recovery heat exchanger where it absorbs heat from the weak solution returning to the absorber. The solution is then partially boiled in the vapor generator by the heat source producing saturated ammonia vapor and relatively weak concentration ammonia-water saturated liquid. The weak solution leaves the vapor generator at state 4 and rejects heat to the high concentration stream before it is throttled

to the system low pressure and sprayed into the absorber. The rectifier cools the saturated ammonia vapor to condense out any remaining water. The vapor is then superheated to state 7 and expanded to produce work. The sub-ambient exhaust vapor (state 8) provides refrigeration before returning to the absorber where it is re-absorbed into the weak solution. The heat of condensation is rejected to the low-temperature source and the cycle repeats.

The power output and cooling capacity of the cycle under given operating parameters is highly dependent on the expander efficiency. Irreversibilties due to friction and leakage decrease the amount of work extracted from the fluid. Because less work is extracted, the expander exhaust temperature is higher and the cooling capacity is reduced. Losses in the expander have the greatest impact on the overall cycle efficiency (Tamm et al., 2003), so it is important to select an optimal design.

The main criteria for expander selection are operating pressures and temperatures, flow rate of ammonia vapor and material compatibility with ammonia. Ammonia is a corrosive substance that reacts with metals such as copper, brass, and bronze, all of which are commonly used as bearing or bushing material. The expander selected for use in the combined cycle must be sized correctly for the flow rate and for the operating pressure ratio for maximum power production and refrigeration capacity. It must also be constructed out of steel, aluminum, or any other material compatible in an ammonia environment.

Expander Design

An expansion device extracts mechanical energy from a fluid by expanding it from a high to a low pressure and converting it into shaft work. Various expander designs using unique expansion methods exist throughout industry. These designs can be

organized into two categories, positive-displacement and turbo-machinery, based on the method of fluid displacement.

Positive-displacement expanders

Positive-displacement machines such as reciprocating and rotary piston, rotary vane, and screw operate by expanding a fixed volume of fluid per oscillation. Torque pulsation is a common phenomenon due to the inherent discontinuity associated with the finite number of pistons or lobes and fixed displacement. Reliability is an issue with positive-displacement machines because of a greater number of moving parts (i.e. piston linkages, sliding vanes); and in the case of pistons, a lubrication system to reduce leakage encountered in the gap between the moving seals and volute.

Turbo-machinery

Turbo-machinery, comprised of axial and radial flow turbines, utilizes the pressure differential across a series of radial blades to provide a “lift” force to turn the rotor, thereby producing shaft work. In this manner, a continuous power output is provided. Reliability is improved over positive-displacement expanders because the rotor is the only moving part.

Turbines are designed with a clearance between the blade tips and the volute to allow free rotation; however, leakage at the tips (windage loss) is the primary cause of irreversibility in the expansion process. Blade tip clearances remain approximately constant for varying turbine size. As turbine size is decreased, the loss due to windage as a percentage of the work output becomes increasingly significant. For this reason, positive-displacement expanders are more suited for small-scale operations.

The amount that the blade tip clearances can be reduced is limited by the centrifugal force and/or thermal expansion of the blade material. Typical turbine

operating speeds range from a few thousand up to tens of thousands RPM. Centrifugal force is dependent on blade tip speed, which is function of the RPM and the rotor diameter. As a result, larger turbines suffer greater radial blade deformation and are less suited for blade tip clearance reduction.

Scroll compressor/expander

The scroll compressor was first invented by Lèon Creux in 1905 (Gravesen and Henriksen, 2001). Commercial interest in the technology wasn't strong until the introduction of computer numerically controlled (CNC) machines in the 1970s. CNC machines provided the basis for machining the precise elements needed for a scroll compressor to operate efficiently and quietly (Copeland corp., 2001).

A scroll compressor consists of two identical spiral elements assembled with a 180° phase difference. During operation, one scroll remains stationary and the other is attached eccentrically to a motor shaft. This configuration allows the scroll to rotate in an orbiting motion within the fixed scroll. The phase difference between the two scrolls is maintained using an anti-rotation device, typically an Oldham coupling (Copeland corp., 2001).

The fluid flow path within a scroll compressor or expander is described by Figure 2.8. As the rotating scroll (green) orbits about the fixed scroll (red), the outer periphery forms a line of contact with the fixed scroll, capturing a crescent shaped volume of gas (step 1). The gas is forced toward the center discharge port in steps 2 thru 5 and compressed due to the decreasing volume of the crescents. This is indicated by the brilliance of the yellow color representing the gas pocket. Because several of these gas pockets are being compressed simultaneously, as depicted in step 6, torque pulsation

common with other positive-displacement machines is low. Scrolls compressors have been widely adopted by the HVAC industry because of the advantages they offer, including: simplistic design (i.e. fewer moving parts), low friction, low torque pulsation, and compliance.

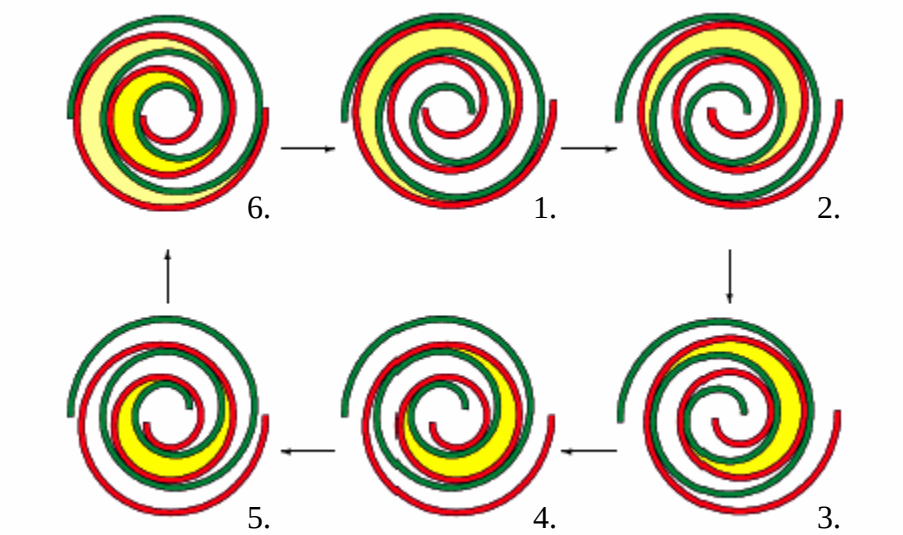

Figure 2.8. Flow path of a single fluid pocket through a scroll compressor (Adapted from Gravesen and Henriksen, 2001)

Because of their unique geometry, scrolls do not require valves or valve actuators; furthermore, there are no linkages or sliding vanes. The relative rolling motion of the contact points offers less resistance than sliding friction. Additionally, the rolling contacts provide a seal such that large volumes of oil used as a sealant are not required and leakage is reduced (Copeland corp., 2001). Continual compression process of the scroll results in a smoother power output and consequently less noise and vibration than piston-type devices. Compliance mechanisms balance the dynamic pressure and centrifugal forces in order to maintain proper sealing. These loading mechanisms correct tolerances as the scroll surfaces wear and allow the scroll elements to separate slightly in the axial or radial directions in response to a sudden pressure spike (axial compliance) or

the presence of small amounts of debris or liquid (radial compliance). Taken together, these attributes contribute to the fact that scroll compressors typically have 10% higher mechanical efficiencies than comparably sized piston compressors (Wells, 2000) and less leakage than other compressors in its class (Schein and Radermacher, 2001).

Literature suggests the potential use of a scroll compressor as a high efficiency expander (Wells, 2000). Copeland® compressors have been used successfully as expanders with R-134A and R-245FA refrigerants as the working fluid. Efficiencies over 70% were demonstrated when operated with pressure ratios between three and five (Warner, Wayne – Copeland Corporation, Personal Conversation, 10 May 2004). Scroll expanders have also been utilized in an organic Rankine micro combined heat and power system patented by Yates et al. in 2002 (US Patent and Trademark Office, 2002).

5 kW Prototype

The applicability of the ammonia-water combined cycle for small scale power generation utilizing low temperature heat sources is currently being studied at the University of Florida's Energy Research Park. A prototype producing 5 kW of electrical power has been designed and is under construction.

Heat source and sink. The low-temperature heat source is simulated using a liquid-propane-fired boiler to heat water to 180 °F. The heat sink for the cycle is cooling water, which is continually circulated through a 500,000 btu/h cooling tower. Temperature control is accomplished using a combination of 3-way automatic control valves and several shell and tube heat exchangers.

Absorber and solution pump. The absorber is a falling-film type. This design offers a combination of sufficiently high heat transfer rates and large surface areas for

absorption. The fluid leaving the absorber is saturated, therefore no net positive suction head (NPSH) is available for the pump, leading to cavitation. For this reason, a roller-type positive-displacement pump is used.

Vapor generator and rectifier. The vapor generator and rectifier are integrated as a single unit such that no separator is required. The vapor generator is a shell and tube heat exchanger with hot water on the tube side; the rectifier is a packed column. As the ammonia bubbles out of solution, it travels through the rectifier and the remaining effluent drips back down into the vapor generator where it is re-boiled.

Electricity production and cooling capacity. The maximum power output of the expander is 5.6kW. This work is used to run an electric generator that produces 200 V_{rms} single phase AC at 400 Hz. A frequency converter switches the frequency from 400 to 60 Hz required by the electrolyzer. The maximum equivalent cooling capacity of the system is 1.25 kW; this is demonstrated by cooling a fixed volume of water.

CHAPTER 3
ANALYSIS METHODOLOGIES

This chapter outlines the analytical procedure developed to find the expected energy requirements for electrolysis and hydrogen liquefaction, as well as the heat and work interactions of the combined cycle at steady state. An analysis on impact of the combined cycle expander efficiency on the cooling capacity and the liquid hydrogen yield is discussed as motivation for an experimental study.

Hydrogen Energy Requirements

Electrolysis of Water

The electrolyzer model used in this study is based on the Stuart Energy Vandenborre IMET® Electrolyzer. The IMET® is selected for two reasons: its relatively simple design due to pump-less electrolyzer circulation, and its high thermal efficiency (operating at a cell voltage of approximately 1.7V) (Stuart Energy, 2004). It utilizes an alkaline electrolyte in a filter-press arrangement and can deliver hydrogen at pressures of up to 363 psi (25 atm), which reduces the compressor power required for liquefaction. The analysis determines the total electrolyzer power consumption per unit mass hydrogen produced including the power required to operate the sub-systems of the electrolyzer, namely the cooling water system, feed water / deionization system, and AC/DC rectifier.

Equation 3.1 defines the thermal efficiency of the electrolyzer, assuming 100% current efficiency (Casper 1978).

$$\eta_{th_{Elec}} = \frac{V_{tn}}{V_{actual}} = \frac{HHV_{H_2}}{E_{Elec}} \tag{3.1}$$

The losses that occur in the electrolysis process are dissipated as heat. A cooling water system is employed to remove this heat and keep the electrolyte temperature relatively low. At temperatures above 302 °F (150 °C), the corrosiveness of the alkaline electrolyte causes significant electrode corrosion (Wendt, 1990). The cooling load is determined using the definition of thermal efficiency and the higher heating value (HHV) of hydrogen as shown in Equation 3.2.

$$Q_{cool_{elec}} = HHV_{H_2}\left(1-\eta_{th_{elec}}\right) \tag{3.2}$$

Using a typical COP value of three for many refrigeration systems, the work required to produce the cooling water is estimated by:

$$W_{CW} = \frac{Q_{cool_{elec}}}{COP} \tag{3.3}$$

The cooling water volumetric flow rate, given by Equation 3.4, is found by applying conservation of energy and specifying a 10 °F (5.56 °C) temperature drop across the electrolyzer.

$$\forall_{cw} = \frac{Q_{cool\ _{elec}}}{\rho_{cw} c_{p,cw}\left(\Delta T\right)} \tag{3.4}$$

Pump work is calculated using Equation 3.5, assuming a pressure drop of 10ft of water and a pump efficiency of 70%.

$$W_P = \frac{\forall_{cw} * \rho_{cw} * \Delta p}{\eta_p} \tag{3.5}$$

The feed water required for electrolysis is obtained by assuming the reaction takes place in stoichiometric proportion. From the overall chemical reaction of Equation (2.1c), one mole of water is required for every mole of hydrogen or 9 lbm of water for every lbm of hydrogen. On a volumetric basis, this equates to 1.0825 gal/lbm H_2. The

maximum energy required for deionization of water is assumed to be 10% of the energy required for electrolysis as suggested in the literature (Casper, 1978).

$$E_{FW} = 0.1 \times \frac{HHV_{H_2}}{\eta_{th_{Elec}}} \tag{3.6}$$

Casper reports the typical efficiency of an AC/DC rectification system to be 95% (1978). The total energy consumed per unit mass of hydrogen by the electrolyzer and sub-systems is given by Equation 3.7.

$$E_{elec} = \frac{HHV_{H_2}}{\eta_{th_{elec}} \eta_{rect}} + W_{CW} + E_{FW} \tag{3.7}$$

Hydrogen Liquefaction

The Claude cycle is analyzed to determine the total liquefaction energy per unit mass hydrogen liquefied. The inlet pressure and temperature, as well as the expander mass flow ratio are varied independently to develop a family of performance curves used to gauge each parameter's effect on liquid yield and the total specific liquefaction energy. Each configuration is then evaluated based on its figure of merit (FOM).

The figure of merit (FOM) is used to measure the performance of liquefaction systems. It is defined as the ratio of the work required by an ideal liquefier to the work of an actual liquefier.

$$FOM = \frac{\dot{W}_{ideal}}{\dot{W}} \tag{3.8}$$

Ideal liquefaction. Ideal liquefaction is described by the first two processes of a reverse Carnot cycle: isothermal compression followed by an isentropic expansion (Barron, 1985). Additionally, all gas that enters the cycle is liquefied. Figure 3.1 shows the T-S diagram of the process.

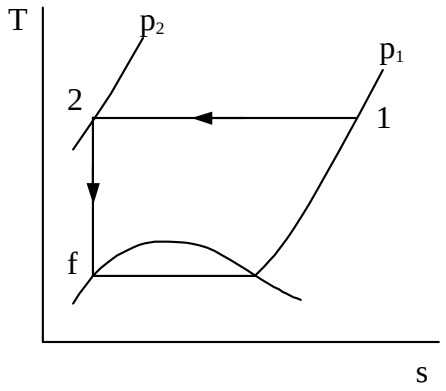

Figure 3.1. T-S diagram of ideal liquefaction process

Applying the First Law to the entire cycle (neglecting changes in potential and kinetic energy) yields:

$$\dot{W}_{net} = \dot{Q}_C + \dot{m}\left(h_f - h_1\right) \tag{3.9}$$

For a reversible isothermal compression process, the heat rejected is given by the Second Law as:

$$\dot{Q}_C = \dot{m}T_1\left(s_1 - s_2\right) = \dot{m}T_1\left(s_1 - s_f\right) \tag{3.10}$$

Substituting this result into Equation 3.9 gives the ideal work requirement per unit mass gas compressed.

$$\frac{\dot{W}_{net_{ideal}}}{\dot{m}} = \frac{\dot{W}_{net_{ideal}}}{\dot{m}_f} = \left(h_f - h_2\right) - T_1\left(s_f - s_1\right) \tag{3.11}$$

Claude cycle. The assumptions for the Claude cycle analysis are listed below:

- Heat transfer from the environment is negligible
- Heat exchangers and liquid baths are 100% effective
- Negligible pressure drop through pipe, fittings, and heat exchangers
- Negligible loss in power transmission from expander to compressor
- $T_{10} = T_1$, $T_{10a} = T_{2b}$
- $T_7 = T_8 = T_e$ to minimize irreversibility upon mixing (Hands, 1986)
- T_3 = -350 °F
- Compressor efficiency, η_c = .75
- Expander efficiency, η_e = .85

- Electrolyzer produces 100% pure normal hydrogen (74.928% ortho, 25.072% para)
- Ortho/para conversion proceeds to equilibrium within the liquid nitrogen (LN_2) bath

In this model, ortho-para conversion takes place in two isothermal stages. First, the gas is cooled to LN_2 temperatures (-320.4 °F, -195.6 °C) and passed over a catalyst bed. Equilibrium concentration of para hydrogen at this temperature is 50.5%. This corresponds to an approximate 25.43% conversion from normal hydrogen, releasing 75.28 btu/lbm (175.1 kJ/kg) of heat (heat of conversion at –320.4 °F is 296.07 btu/lbm_{H2} (688.62 kJ/kg)). The second stage takes place in the liquid hydrogen-receiving tank at liquid hydrogen (LH_2) temperatures (-423 °F, -252.8 °C). The heat of conversion from normal to para hydrogen at -423 °F is 302.38 btu/lbm (703.3 kJ/kg). The heat released in proceeding from 50.5% to 99.789% para hydrogen is 134.56 btu/lbm (312.97 kJ/kg).

The liquid yield of the cycle per unit mass hydrogen compressed is found by applying the First Law to a control volume including the three heat exchangers, Joule-Thompson valve, and liquid hydrogen-receiving tank (subscripts refer to Figure 2.6).

$$\dot{m}_f \Delta H_{C2} + \dot{m} h_{2b} + \dot{m}_e h_e = (\dot{m} - \dot{m}_f) h_{10a} + \dot{m}_e h_e + \dot{m}_f h_f \tag{3.12}$$

where ΔH_{C2} is the heat of conversion in the second stage
$\dot{m}$ is the inlet mass flow rate of hydrogen

Dividing by $\dot{m}$, introducing the liquid yield per unit mass hydrogen compressed, $y = \frac{\dot{m}_f}{\dot{m}}$, and the expander mass flow ratio, $x_e = \frac{\dot{m}_e}{\dot{m}}$, and solving for y gives:

$$y = \frac{h_{10a} - h_{2b}}{h_{10a} - h_f + \Delta H_{C2}} + \frac{\eta_{e_{ad}} x_e (h_3 - h_{e_s})}{h_{10a} - h_f + \Delta H_{C2}} \tag{3.13}$$

The amount of liquid nitrogen required to pre-cool the compressed hydrogen and absorb

a portion of the heat of conversion is determined by applying the First Law to a control volume encompassing the three-stream heat exchanger, liquid nitrogen receiver and the control volume from the previous analysis.

$$\dot{m}\Delta H_{C1} + \dot{m}_f \Delta H_{C2} + \dot{m}h_2 + \dot{m}_e h_e + \dot{m}_{N_2} h_A = (\dot{m} - \dot{m}_f)h_{10} + \dot{m}_{N_2} h_C + \dot{m}_e h_e + \dot{m}_f h_f$$

Dividing by $\dot{m}$, defining the mass ratio of liquid nitrogen to compressed hydrogen as $z = \frac{\dot{m}_{N_2}}{\dot{m}}$, and solving for z yields Equation 3.14

$$z = \frac{\Delta H_{C1}}{h_C - h_A} + \frac{h_2 - h_{10}}{h_C - h_A} - \eta_{e_{ad}} x_e \frac{h_3 - h_{e_s}}{h_C - h_A} + y\frac{h_{10} - h_f + \Delta H_{C2}}{h_C - h_A} \tag{3.14}$$

where ΔH_{C1} is the heat of conversion in the first stage

Dividing Equation 3.14 by the liquid yield, y, gives the hydrogen requirement in terms of unit mass hydrogen liquefied. Based on the literature, the specific energy required to produce liquid nitrogen is assumed 766.82 btu/lbm-N_2 or 0.225 kW-h/lbm-N_2 (Gross et al., 1994).

An energy balance on the compressor, including work contributed from the expander, gives the specific power required per unit mass hydrogen to drive the cycle.

$$\frac{\dot{W}_C}{\dot{m}} = \frac{(h_2 - h_1) - T_1(s_2 - s_1)}{\eta_c} - \eta_e x_e (h_3 - h_{e_s}) \tag{3.15}$$

Dividing this result by the liquid yield ratio gives the compressor work per unit mass hydrogen liquefied. Total liquefaction energy is the summation of compressor work and the liquid nitrogen power requirement.

The expander mass flow ratio, x_e, is varied from 0 to 0.9 with four other independent parameters: expander and compressor isentropic efficiency, and compressor inlet pressure and temperature in individual cases to determine their influence on the

cycle performance. In cases one and two, the expander and compressor isentropic efficiencies are decreased from 1.0 to 0.4 in 0.2 increments to gauge their effect on the cycle performance. Case three looks at a range of compressor inlet pressures (1 to 25 atmospheres in increments of five) at a fixed inlet temperature of 80 °F (26.7 °C) to simulate the operating pressure range of the IMET electrolyzer. In case four, the compressor inlet temperature is varied from 0 to 80 °F (-17.8 to 26.7 °C) in twenty-degree increments; representing the pre-cooling effect of the combined cycle. Plots are created displaying the temperature, pressure, and component efficiency dependence of the key liquefaction parameters: total specific work, liquid yield, liquid nitrogen required, and figure of merit.

The critical state points required to calculate the performance parameters given by Equations 3.13 thru 3.15 are defined based on the inlet temperature and pressure (state 1) as well as the zero pressure drop assumption and the isentropic efficiencies of the compressor and expander. A computer program has been developed to assist in calculating the state properties and performance parameters for each iteration as well as for plotting the data. A detailed description of the program including a portion of the code follows in Appendix A.

Ammonia-Water Combined Power/Cooling Cycle

The ammonia water combined power/cooling cycle of this study is based on the experimental system under construction at the University of Florida's Energy Research Park. This particular system is designed to provide 5kW of electrical power from a heat source temperature of 180 °F in order to simulate temperatures attainable from inexpensive flat-plate solar collectors. Additionally, the maximum pressure is

constrained such that high-pressure fittings are not required, thereby reducing the capital cost. Other assumptions and/or specifications made in the design are listed below:

- Fluid exiting the absorber and vapor generator is saturated liquid/vapor
- Absorber operating temperature is 100 °F
- Vapor generator operates at 170 °F
- Cycle high and low pressures are 110 psia (7.58 bar) and 40 psia (2.76 bar), respectively
- Rectification is 100% efficient (100% pure ammonia vapor at state 7)
- Recovery heat exchanger has a 85% effectiveness, ε
- Weak and strong solution streams have equal specific heats
- 75% electric generator efficiency, η_g
- 5 °F approach temperature in the cooler
- Negligible pressure drop through pipes, fittings, heat exchangers, and other components

Binary mixtures differ from pure substances in that knowledge of three thermodynamic properties is needed to completely define a state (two under saturated conditions). As such, by specifying the operating temperature and pressure of the absorber, and assuming saturated conditions exist at the exit, the mass fraction of ammonia in the strong solution stream is fixed. The mass fraction of ammonia in the weak solution stream leaving the vapor generator at state 4 is determined in a similar matter.

The next step in the analysis is to find the mass flow rate of ammonia vapor through the expander. Equation 3.16 is obtained from an energy balance on the expander including the electric generator efficiency.

$$\dot{m}_{NH_3} = \frac{\dot{W}_e}{\eta_g (h_7 - h_8)} \tag{3.16}$$

The strong and weak solution mass flow rates follow from species and mass balances on the vapor generator as described by Equations 3.16 and 3.17.

$$\dot{m}_{NH_3,weak} = \frac{\dot{m}_{NH_3}\left(X_{NH_3} - X_{NH_3,strong}\right)}{\left(X_{NH_3,strong} - X_{NH_3,weak}\right)} \tag{3.17}$$

where X is the mass fraction of ammonia

$$\dot{m}_{NH_3,strong} = \dot{m}_{NH_3,weak} + \dot{m}_{NH_3} \tag{3.18}$$

The temperatures of the cold (state 3) and hot (state 5) exit stream are found from the definition of heat exchanger effectiveness. Because the specific heats of the two streams are approximated as equal, the equations become a ratio of only temperatures and mass flow rates.

$$T_3 = \frac{\varepsilon \times \dot{m}_{NH_3,weak}\left(T_4 - T_2\right)}{\dot{m}_{NH_3 strong}} + T_2 \tag{3.19}$$

$$T_5 = T_4 - \varepsilon\left(T_4 - T_2\right) \tag{3.21}$$

where ε is the heat exchanger effectiveness

Heat and work interactions of the absorber, pump, and cooler are calculated from energy balances on all inlet and outlet streams. The four equations summarizing this process are given below:

$$\dot{Q}_{ab} = \dot{m}_{NH_3,weak} h_6 + \dot{m}_{NH_3} h_9 - \dot{m}_{NH_3,strong} h_1 \tag{3.21}$$

$$\dot{W}_p = \dot{m}_{NH_3,strong}\left(h_2 - h_1\right) \tag{3.22}$$

Cooling capacity is dependent on the temperature of the cooled fluid. It is assumed that hydrogen at 90 °F is being cooled; therefore, T_9 is 85 °F (assuming a 10° approach temperature).

$$\dot{Q}_c = \dot{m}_{NH_3}\left(h_8 - h_9\right) \tag{3.23}$$

The total heat input to the cycle is determined by “black boxing” the vapor generator, rectifier, and superheater and considering state points 3, 4, and 7.

$$\dot{Q}_{vg} = \dot{m}_{NH_3,weak} h_5 + \dot{m}_{NH_3} h_7 - \dot{m}_{NH_3,strong} h_3 \tag{3.24}$$

Lastly, the cycle thermal efficiency is computed from the work and heat interactions as shown in Equation 3.25. The cooling affect is accounted for by scaling it with the same coefficient of performance used in the electrolyzer analysis.

$$\eta_{th,cycle} = \frac{\dot{W}_e - \dot{W}_p + \dot{Q}_c / COP}{\dot{Q}_{vg}} \tag{3.25}$$

Properties at each state point are estimated using the Gibbs energy method combined with pure fluid correlations as described by Tamm (2003).

This procedure is repeated for a fixed power output and varied expander efficiencies. These data are plotted to study the effect on the cycle cooling capacity, heat input, and pump work and to relate these quantities to the liquid hydrogen yield. Additionally, the effect of trace quantities of water in the expander inlet stream on cycle efficiency and cooling capacity is analyzed.

A MatLAB program is developed to calculate all state points of the combined cycle, equations 3.16 thru 3.24, and the optimum liquid hydrogen yield for each value of expander efficiency. A detailed description of the program and portions of its code are presented in Appendix A.

CHAPTER 4
EXPERIMENTAL SETUP AND DESIGN

The potential application of a scroll compressor as a high-efficiency expander for small-scale power generation (i.e. the 5kW combined cycle) is discussed in this chapter as background for the experimental study. A detailed description of the compressor and testing apparatus is given followed by an outline of the experimental methods.

Scroll Machines as Expanders

Scroll compressors have been proven as viable expansion devices. Copeland has performed limited research on scroll expanders using their refrigeration scroll compressor with R-134A and R-245FA as the working fluid. Results show that efficiencies of greater than 70% are attainable (Warner, Wayne – Copeland Corporation, Personal Conversation, 10 May 2004). Other publications have investigated the use of scroll expanders in small-scale solar driven Rankine cycles (Wells, 2000). To date, however, no known research has been conducted with an ammonia working fluid.

Ammonia offers particular challenges to the design or selection of any expander. One of which is corrosiveness. Ammonia is corrosive to copper and copper-containing alloys present in the bearings and motor stators of hermetically sealed compressors like those manufactured by Copeland. Additionally, ammonia is a small molecule and thus has relatively low density compared to R134-A (0.0433 lbm/ft^3 vs. 0.2622 lbm/ft^3), so leakage losses become more prevalent.

Small-scale, high-efficiency expanders are desired for the 5kW ammonia-water combined power/cooling cycle because its overall performance and cooling capacity is

highly dependent on the expander efficiency as discussed in later sections. For a designed power output, increasing the expander efficiency reduces the required mass flow through the system and hence reduces the total energy consumption. Individual component and pipe size is reduced as well.

At the 5kW size, the scroll design offers several advantages over turbines as explained in the background and theory. Ammonia turbines in the 5kW range are inherently inefficient due primarily to leakage loss at the tips. Tom Revak of Revak Industries reports that the efficiency of a 5kW is likely to be approximately 40% whereas Sam Ni of Scroll Labs predicts an isentropic efficiency of 67% for a comparably sized scroll expander. Custom-design is cost prohibitive however; with the design and fabrication cost of the aforementioned scroll expander being $280,000.

The objective of the experiment is to test an “off-the-shelf” unit with air and predict its performance with ammonia from the data obtained. From these observations, an indication of whether the scroll expander is feasible in the combined cycle is determined and recommendations for design improvements are made. This experiment also lays the foundation for further research of scroll expanders for use in the ammonia-water combined cycle and other small-scale power generation systems.

Testing Apparatus and Instrumentation

The Sanden TRS-90 automotive scroll compressor (shown in Figure 4.1) was selected as the test compressor for three reasons: it operates in the 5kW range, the scroll elements and the housing is constructed of aluminum and the bearings and clutch of steel (ammonia compatible), and it has a pulley and clutch assembly convenient for testing. The only modification necessary to run the compressor in reverse is the removal of a reed-type check valve located beneath the stationary scroll element within the housing.

The compressor is designed to operate at a pressure ratio of approximately six with R-134A refrigerant. Displacement of the compressor is 85.7 cc/rev.

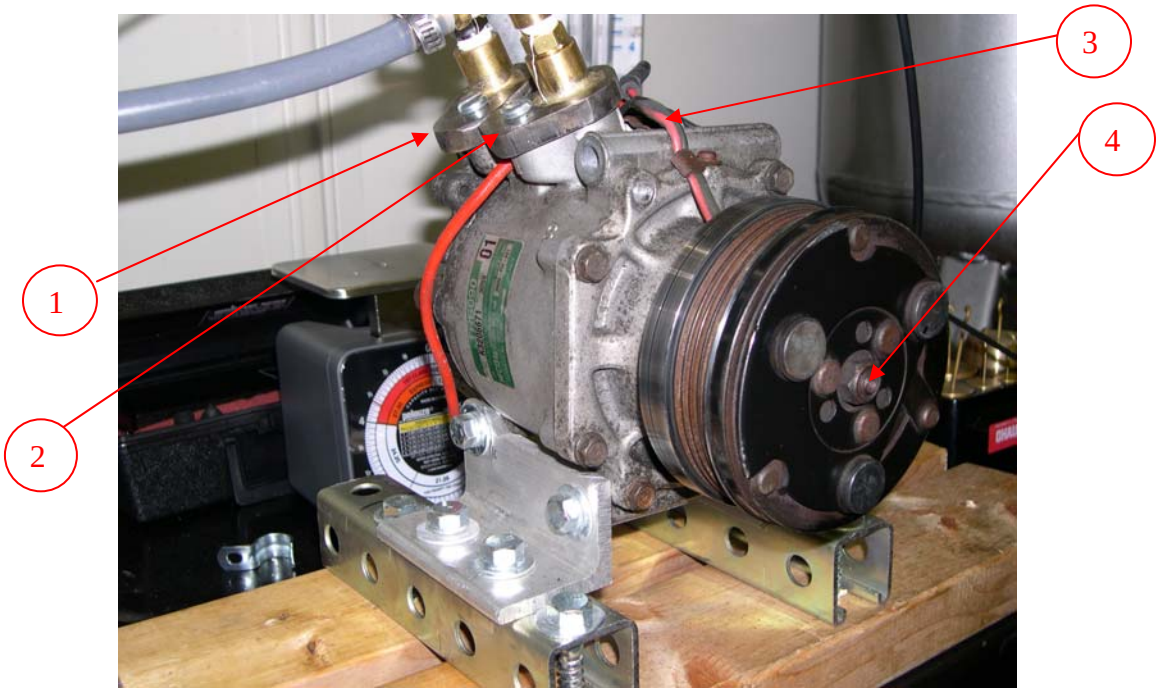

Figure 4.1. Sanden TRS-90 automotive scroll compressor and test stand

The expander is connected to compressed air source at the suction port (1) using ¼" I.D. plastic tubing. The discharge port (2) is ¼" I.D. and is vented to the atmosphere. Also shown in Figure 4.1 is the pulley and clutch assembly (4). The clutch is on/off modulated by applying 12 volts DC at point 3. Figure 4.2 shows the 5-Hp compressor and tank used as the compressed air source. The compressor has a maximum pressure of 125 psig and a pumping capacity of 15.7 scfm at 90 psig. A 110-psig regulator is used to adjust the expander inlet pressure.

Temperatures measurements are taken from thermocouples inserted into the inlet and exit flows at points 1 and 2 as shown in Figure 4.3. The signal from each thermocouple is calibrated and conditioned to 1mV/°F using two thermocouple-to-analog converters (3) and recorded from a pair of multimeters.

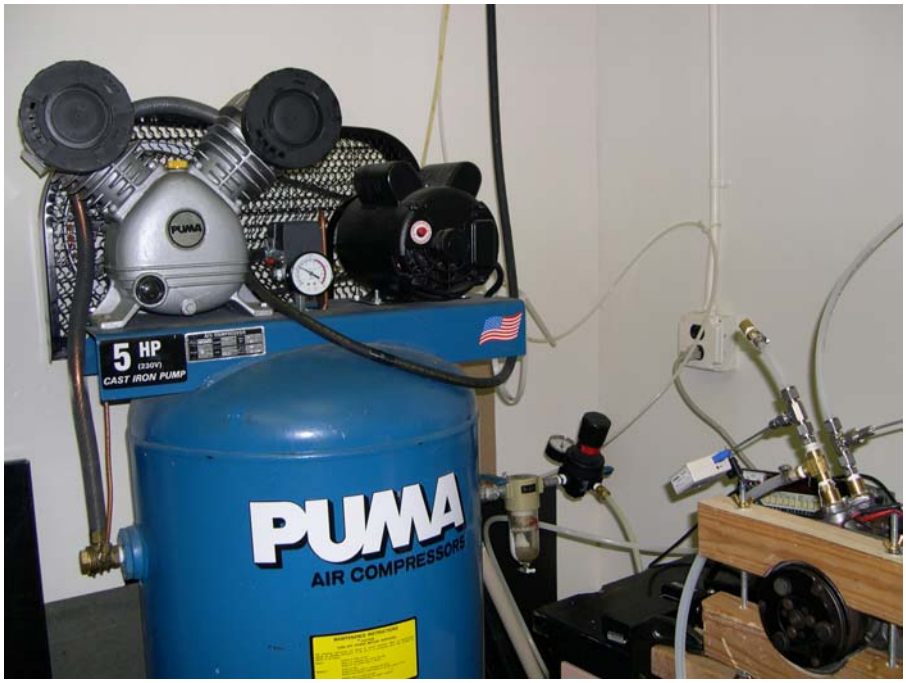

Figure 4.2. Piston compressor with integrated tank and regulator

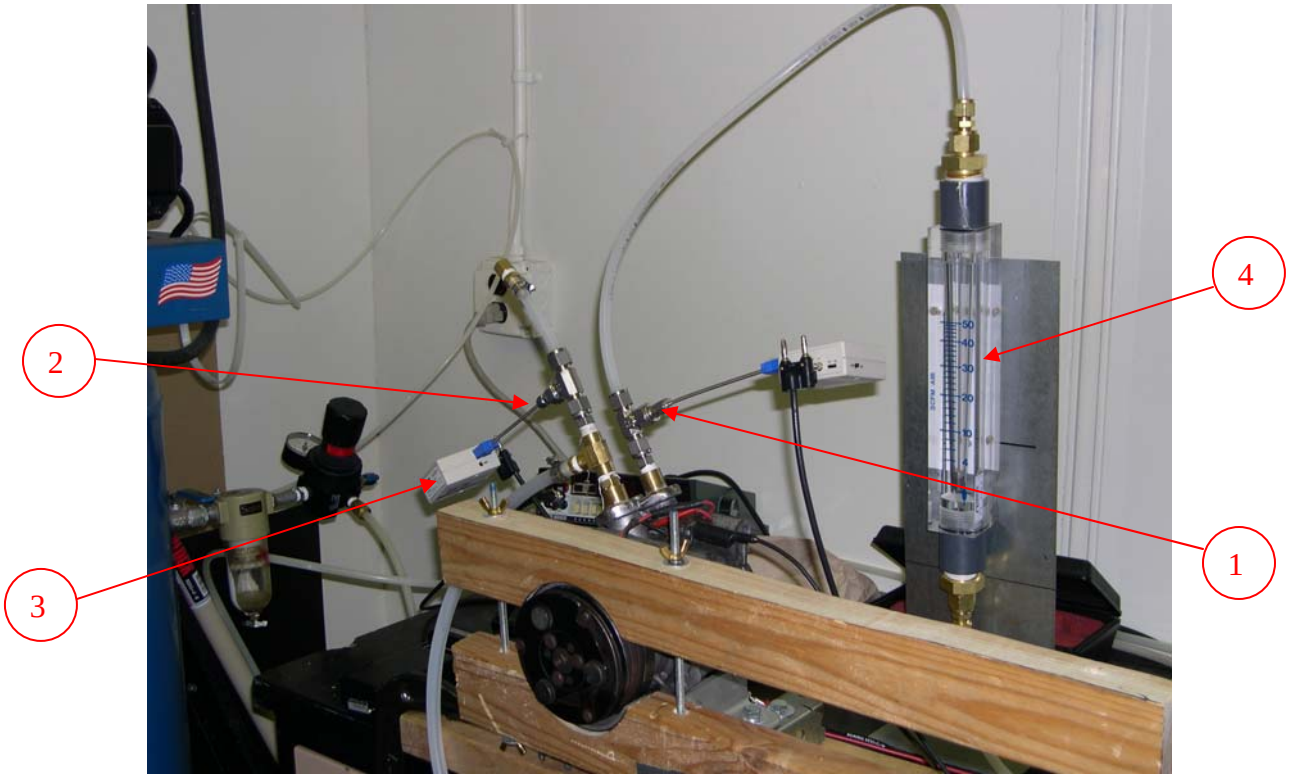

Figure 4.3. Thermocouple locations and flow meter

The volumetric flow rate of compressed air is measured in standard cfm (standard conditions are 1 atm and 70 °F) using an in-line acrylic gas rotameter (number 4). The

reading is adjusted to actual cfm using the ideal gas relation with the observed inlet temperature and pressure as described by Equation 4.1.

Figure 4.4 shows the pony brake used to measure the torque output of the expander and the back pressure gauge (1). The pony brake frame is constructed of wood with ordinary go-cart brake pad material employed as the friction material. An enlarged view of the pulley showing the brake material is seen in Figure 4.5. This material has the added advantage in that it acts as an insulator, protecting the wood from the excessive heat. The frictional force applied to the pulley is varied by adjusting a pair of wing nuts (2). The force exerted by the expander torque is measured 14.125" from the centerline of the expander shaft (3) using a Pelouze 5-pound scale. Rotational speed is measured in RPM from the center of the pulley with a handheld tachometer (not shown).

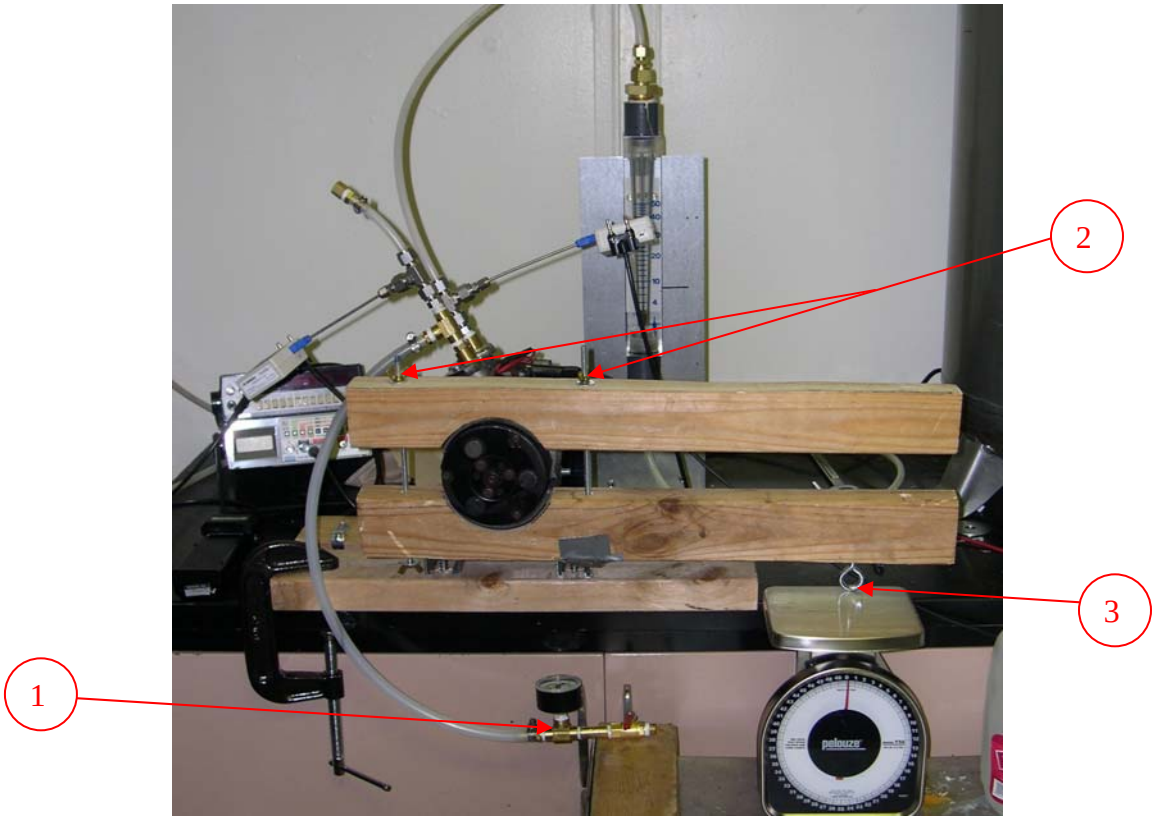

Figure 4.4. Pony brake and back pressure gauge and valve

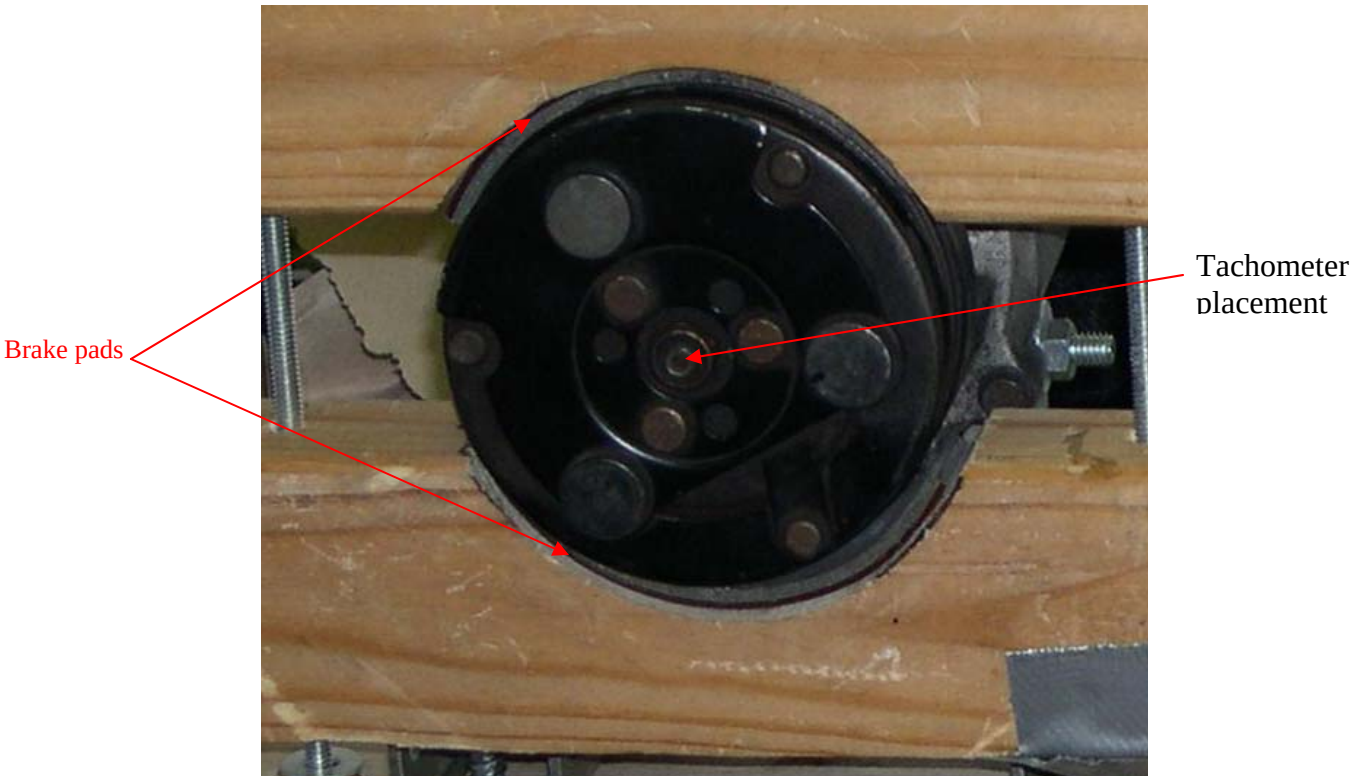

Figure 4.5. View of expander pulley showing the brake pads used as frictional surfaces

A detailed component list of the experimental apparatus including the range and resolution of each instrument (if applicable) follows in Appendix C.

Experimental Methodology

Procedure

Startup:

1. Activate the voltage supply, multimeters, and thermocouple-to-analog converters.
2. Close the compressor valve.
3. Start the compressor and allow it to charge to 125 psig.

Test:

1. Cap the expander exit port.
2. Crack the compressor valve and allow system to charge.
3. Select the desired source pressure by adjusting the tank regulator.
4. Once pressure is selected, close the compressor valve and open the backpressure valve to discharge the system.
5. Close the backpressure valve and remove the expander exit port cap.

6. Loosen the wing nuts on the pony brake to ensure that testing begins with minimum brake force.
7. Initiate the test by fully opening the compressor valve.
8. Record rotational speed (RPM), inlet and exit temperature, flow rate, backpressure and arm force.
9. Tighten the pony brake wing nuts about 1/8 of a turn and repeat step 8 for each trial.
10. Continue until the expander is stalled.
11. Terminate the test by closing the compressor valve.
12. Allow 15-20 minutes between each test for the compressor motor and expander clutch assembly to cool.

Data Analysis

Experimental data is collected in an Excel spreadsheet programmed to perform the conversions and calculations necessary to complete the analysis. Each calculation performed in the spreadsheet and the formulas used for them are explained below.

The corrected volumetric flow rate for the given inlet pressure and temperature is related to the indicated value by treating the air as an ideal gas (Equation 4.1).

$$\dot{V}_{corrected} = \dot{V}_{indicated}\left(\frac{pT_o}{p_oT}\right) \tag{4.1}$$

where p_o, T_o are at standard conditions (1 atm and 70 °F)

The mass flow at standard conditions is found by multiplying the fluid density by the corrected volumetric flow rate as described by Equation 4.2.

$$\dot{m} = \left(\frac{p_o}{RT_o}\right)\dot{V}_{corrected} \tag{4.2}$$

where $\frac{p}{RT}$ is substituted for the density

Mass flow is corrected to the actual inlet conditions using Equation 4.3 (Holman, 2001).

$$\dot{m}_{corrected} = \dot{m}\left(\frac{p_oT}{pT_o}\right)^{1/2} \tag{4.3}$$

Shaft power output is defined by Equation 4.4, the product of the force measurement and the expander rotational speed.

$$\dot{W}_{shaft} = Force \times \varpi \tag{4.4}$$

The volumetric efficiency quantifies the amount of tip leakage encountered during operation. It is defined as the ratio of flow usefully expanded to the total flow through the expander (Equation 4.5).

$$\eta_v = \frac{\varpi d}{\dot{V}} \tag{4.5}$$

where ϖ is the rotational speed (RPM)
d is the expander displacement per revolution

Inlet and exit enthalpies are computed from the measured temperatures and pressures and are used in Equation 4.6 to calculate the isentropic efficiency.

$$\eta_e = \frac{h_{in} - h_{out}}{h_{in} - h_{out_s}} \tag{4.6}$$

CHAPTER 5
RESULTS AND DISCUSSION

The electrolyzer and its sub-systems are analyzed to find the specific energy consumption, thermal efficiency, and cell voltage. Following the electrolyzer investigation, simulations of the Claude cycle are made to determine the effects of component efficiencies and compressor inlet conditions on specific energy consumption. Results of each test are presented in tabular form with several graphs displaying the important trends. The analysis concludes with the selection of the optimum operating parameters.

The ammonia-water combined cycle simulation examines the dependency of the boiler heat input, pump work, and cooling capacity on the expander efficiency for a fixed output and establishes the motivation for the scroll expander performance study. The influence of trace amounts of water in the vapor stream on cycle performance is also investigated. The analytical portion of the results concludes with the calculation of the maximum rate of hydrogen production.

Results of the scroll expander performance study are examined to predict the expander's behavior with ammonia and to determine its feasibility for use in the combined cycle. Several trends are developed to describe the performance of the scroll expander. The data is compared to a performance chart of the same unit operated as a compressor in order to determine if such information can reliably predict expander performance.

Hydrogen Production and Liquefaction

Electrolysis of Water

Specific energy requirements for the electrolysis of water are displayed in Table 5.1. The majority of the electrical energy is required by the electrolyzer itself with the subsystems representing only 16.2% of the total. Cooling water pump work is found to be negligible compared to the energy consumed by the cooler (0.005 kW-h/lbm-H_2 compared to 0.884 kW-h/lbm-H_2). Including all subsystems, the total specific energy required to electrolyze water is 24.839 kW/lbm-H_2 (54.76 kW-h/kg-H_2). Contrasting with the energy requirement of thermoneutral electrolysis (17.865 kW-h/lbm-H_2 (39.385 kW-h/kg-H_2)), the electrolyzer has a thermal efficiency of 85.8%; however, the efficiency drops to 71.9% when all subsystems are considered. At 85.8% electrolyzer efficiency, the cell voltage required to drive the process is 1.713 V.

Table 5.1. Specific energy requirements of the IMET® electrolyzer

	Energy Requirements	
	kW-h/lbm-H_2	kW-h/kg-H_2
Electrolyzer	20.814	45.886
AC/DC Rectifier	1.095	2.415
Cooling Water	0.844	1.860
Feed Water	2.081	4.589
Pump	0.005	0.010
Total	24.839	54.760

The amount of cooling water and feed water corresponding to their energy consumption are 1.726 gpm/lbm-H_2 (6.534 Lpm/lbm-H_2) and 1.085 gal/lbm-H_2 (4.107 Lpm/lbm-H_2), respectively.

Hydrogen Liquefaction

Initial inspection of equations 3.13 and 3.15 indicate that the liquid yield and work per unit mass hydrogen compressed are proportional to the expander mass flow ratio. This is evidenced more clearly by defining the work per unit mass LH_2 (Equation 5.1).

$$\dot{w}_f = \frac{\dot{W}_C / \dot{m}_f}{y} = \frac{\dfrac{(h_2 - h_1) - T_1(s_2 - s_1)}{\eta_c} - \eta_e x_e (h_3 - h_{e_s})}{h_{10a} - h_{2b} + \eta_{e_{ad}} x_e (h_3 - h_{e_s})} (h_{10a} - h_f + \Delta H_{C2}) + \frac{z}{y} \dot{w}_{f,N_2} \quad (5.1)$$

(State points referenced from Figure 2.6).

Equation 5.1 shows that increasing the expander mass flow ratio, x_e, always reduces the specific work for a given set of operating conditions; however, the amount of liquid yield is physically constrained as described by Equation 5.2.

$$x_e + y < 1 \quad (5.2)$$

The liquid yield continues to increase as defined by Equation 3.13 until the constraint is met at which time it becomes a monotonically decreasing function of x_e and T_5. This implies that an optimum value of the expander mass flow ratio exists at which the liquefaction energy is minimized.

The exact form of the constraint is found from an analysis of the third heat exchanger and the expansion valve. Heat exchanger cold side inlet and outlet temperatures T_g = -423 °F (-252.8 °C) and T_7 = -402.32 °F (-241.29 °C) are known from the saturation temperature of hydrogen at atmospheric pressure and by assuming $T_7 = T_e$, respectively. The "hot" side inlet temperature T_4 = -402.32 °F (-241.29 °C) is equal to T_7 because the flow passes through the 100% effective second heat exchanger as the minimum capacity stream. The percent of the mass flow through the J-T valve that is liquefied, k, is initially guessed as 80. T_5 is then calculated from Equation 5.3 and used to find the quality of the expanded stream. The value of k is iterated until convergence is achieved.

$$T_5 = T_4 - (1 - k)(T_7 - T_g) \quad (5.3)$$

Convergence is achieved in only three iterations with k = .725 and T_5 = -408.05 °F (-244.47 °C) because the temperature change of the supply stream is restricted by the lower volume of the return stream. This exactly defines the constraint as:

$$y \le .725(1 - x_e) \tag{5.4}$$

The optimum value of x_e occurs when y exactly equals the constraint; an example of which is seen in Figure 5.1.

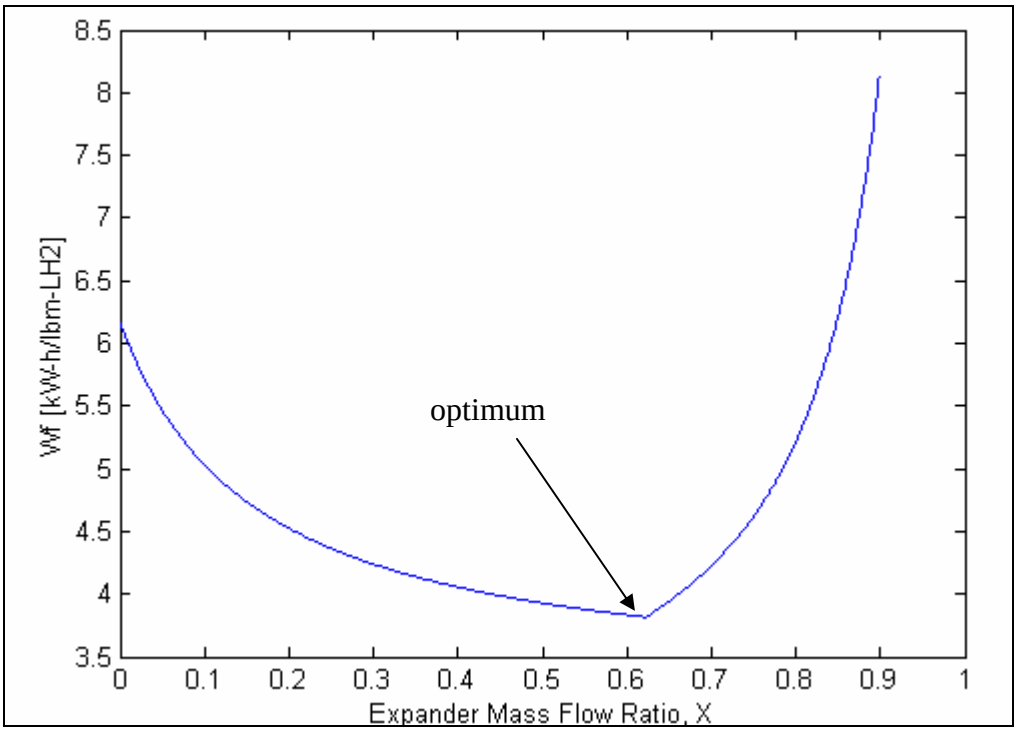

Figure 5.1. Sample output showing the optimum expander mass flow ratio, x_e

Prior to analyzing the effect of compressor inlet temperature and pressure variations on the performance parameters of the Claude cycle, the expander and compressor isentropic efficiencies are studied independently with regard to motivation for further research and development of these components.

Expander efficiency. The effect of the expander isentropic efficiency on the Claude cycle performance is summarized in Table 5.2. As an approximation, the liquid yield constraint is held constant. In reality, however, the liquid yield is further

constrained with decreasing expander efficiency. At $\eta_e = 0.4$, the percent of the source stream liquefied is approximately 48% compared to 72.5% for $\eta_e = 0.85$. The simulation was run with the compressor efficiency fixed as 100% and an inlet temperature and pressure of 80 °F and 25 atm, respectively.

Table 5.2. Claude cycle simulation results for expander isentropic efficiency variation

η_e	$X_{e,opt}$	Y_{max}	$(z/y)_{opt}$	$w_{f,min}$ kW-h/lbm-LH_2	w_{ideal} kW-h/lbm-LH_2	FOM_{max}
1	0.5890	0.2975	15.386	3.684	1.268	0.3444
0.8	0.6350	0.2646	15.485	3.743	1.268	0.3389
0.6	0.6888	0.2256	15.638	3.835	1.268	0.3308
0.4	0.7522	0.1796	15.904	3.995	1.268	0.3175

Table 5.2 shows that an increase in the expander efficiency from 40% to 100% reduces the optimum expander mass flow ratio by 21.7% from 0.7522 to 0.589. This shift in x_e increases the maximum liquid yield by 65.4% since it is related by the constraint of Equation 5.4. The trend between $x_{e,opt}$ and y_{max} for different expander efficiencies is observed in Figure 5.2. Table 5.2 also shows a 3.26% reduction of the cycle liquid nitrogen requirement. The relationship between these two parameters is depicted in Figure 5.3.

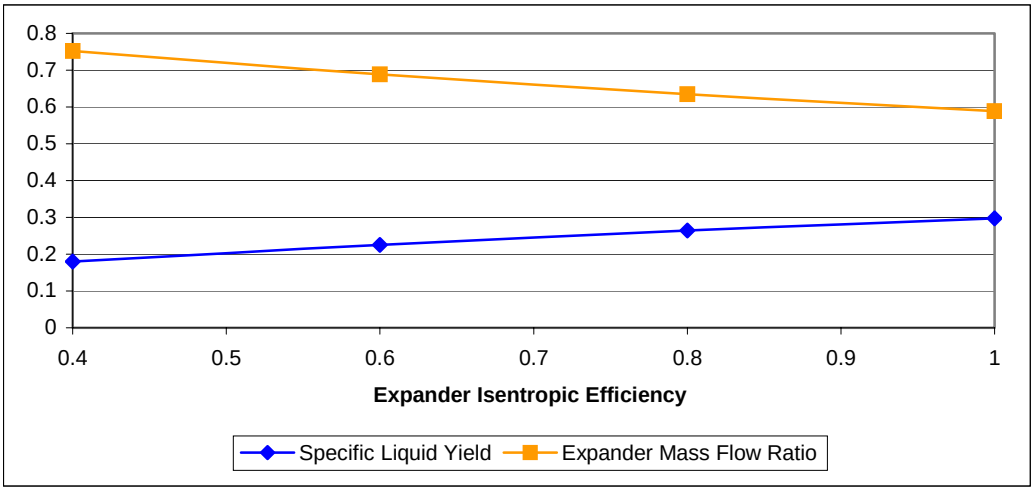

Figure 5.2. Specific liquid yield and expander mass flow ratio as functions of the expander efficiency

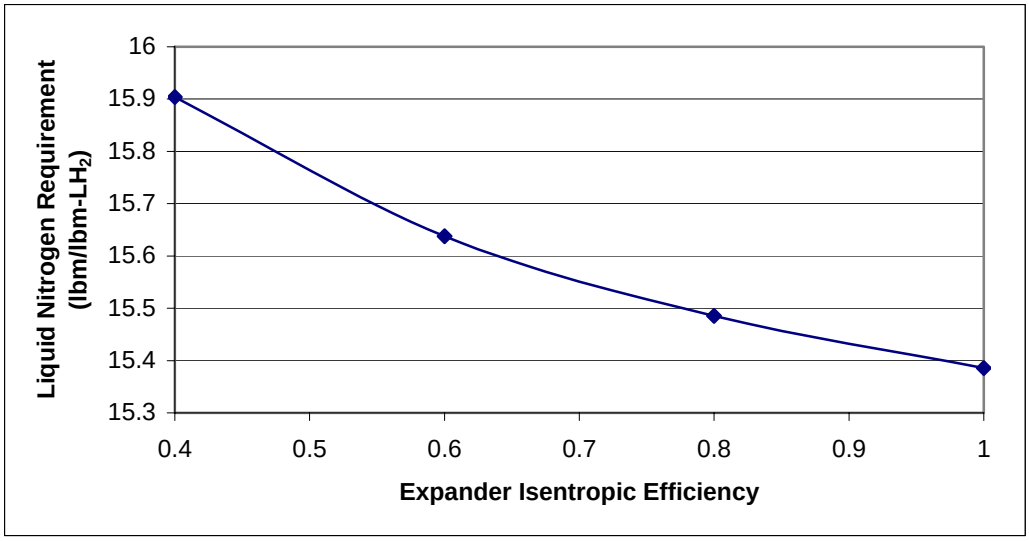

Figure 5.3. Required liquid nitrogen vs. expander efficiency

The combination of these effects results in a 7.78% reduction in specific work as described by equation 5.1. This is shown in Figure 5.4, as well as the shift in x_e that accompanies the decrease in specific work. The ideal work requirement depends only on the inlet and liquid conditions and hence is unchanged; therefore, the FOM scales directly with specific work.

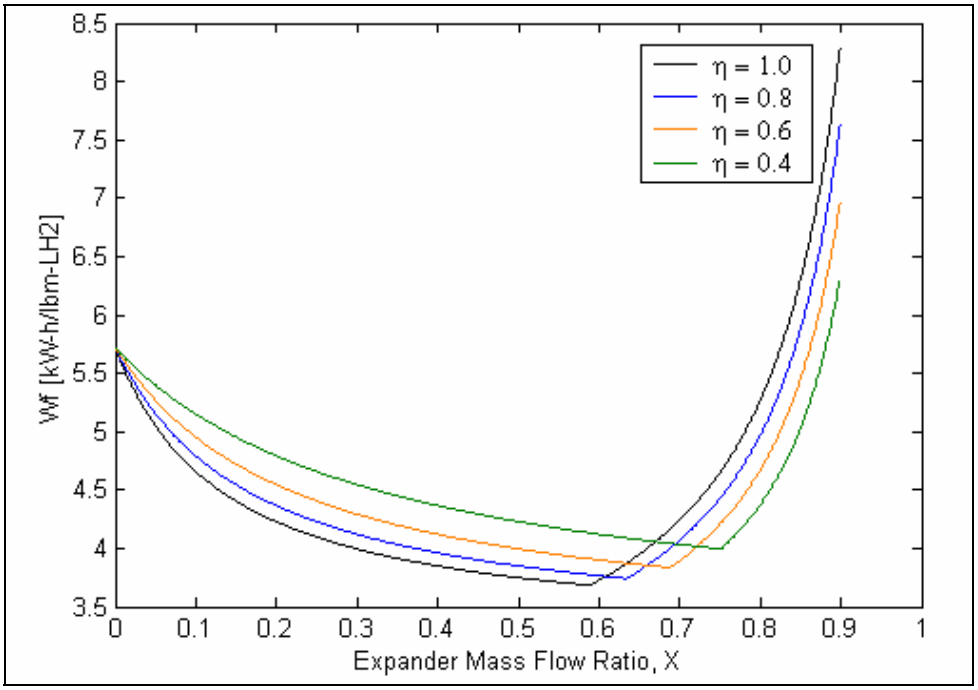

Figure 5.4. Specific work vs. expander mass flow ratio for varied η_e

Compressor efficiency. By inspection of Equations 3.13, 3.14, and 5.1, it is clear that the expander mass flow ratio, liquid yield, and liquid nitrogen requirement are independent of compressor isentropic efficiency for fixed inlet and outlet conditions; provided that the compressor can supply the necessary pressure. The simulation was run with an expander efficiency of 100% and an inlet temperature and pressure of 80 °F and 25 atm, respectively. Results are displayed in Table 5.3.

Table 5.3. Claude cycle simulation results for compressor isentropic efficiency variation

η_c	$X_{e,opt}$	Y_{max}	$(z/y)_{opt}$	$w_{f,min}$ kW-h/lbm-LH_2	w_{ideal} kW-h/lbm-LH_2	FOM_{max}
1	0.5890	0.2975	15.386	3.684	1.268	0.3444
0.8	0.5890	0.2975	15.386	3.746	1.268	0.3386
0.6	0.5890	0.2975	15.386	3.851	1.268	0.3294
0.4	0.5890	0.2975	15.386	4.059	1.268	0.3125

The only effect that increasing the compressor efficiency has is to lower the specific work from 4.059 to 3.684 or 9.2%, as illustrated by Figure 5.5. The ideal work is again independent of component efficiency and thus scales directly with the specific work.

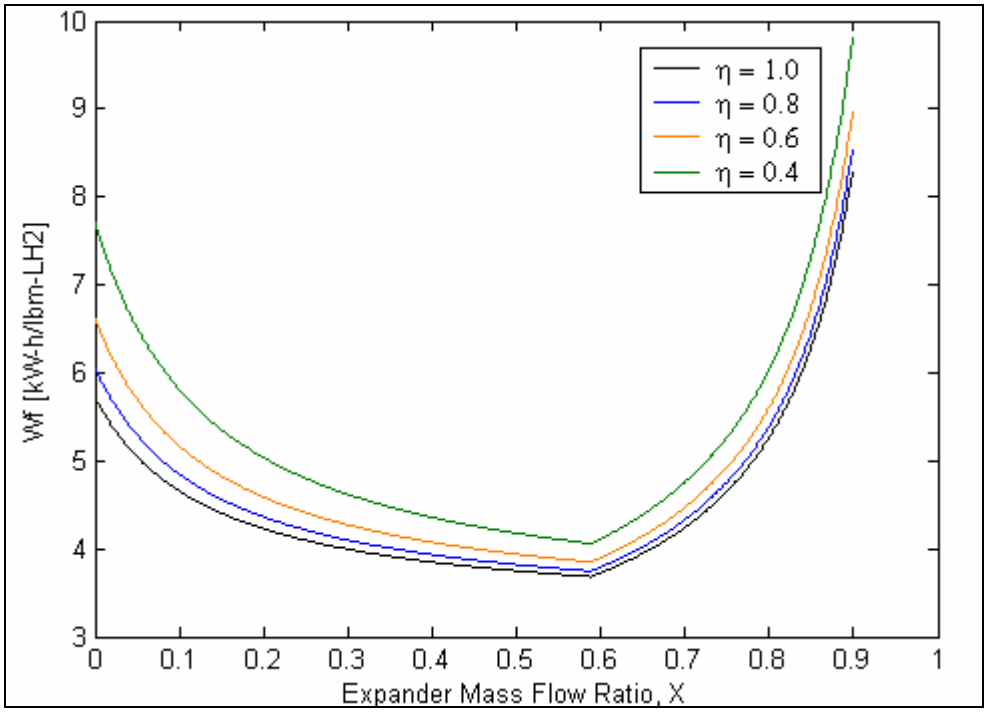

Figure 5.5. Specific work vs. expander mass flow ratio for varied η_c

Comparing the figures of merit for the two cases in Figure 5.6 indicates a more profound impact of the compressor efficiency on the cycle performance. A 60% decrease in efficiency from ideal results in a 9.2% reduction in the FOM for the compressor case compared to 7.8% for the expander. A greater emphasis should therefore be placed on the development of high efficiency hydrogen compressors to minimize liquefaction energy.

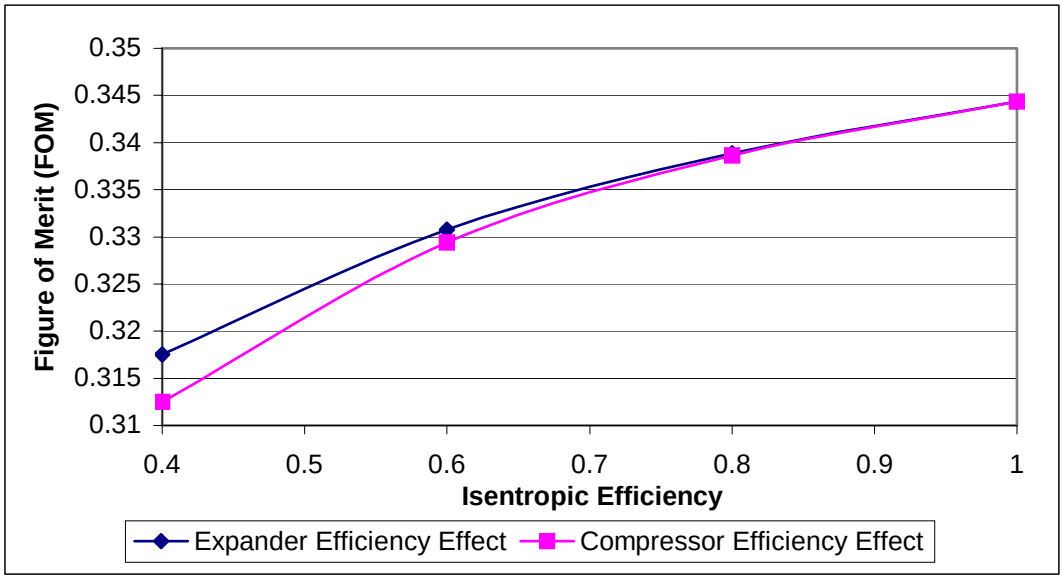

Figure 5.6. Impact of compressor and expander efficiencies on Claude cycle FOM

Compressor inlet pressure. Compressor inlet pressure is varied to determine the advantage of using pressurized electrolysis. A simulation was run for an outlet pressure of 40 atm and compressor and expander efficiencies of 75 and 85%, respectively.

Table 5.4. Claude cycle simulation results for compressor inlet pressure variation

P_1 atm	$X_{e,opt}$	Y_{max}	$(z/y)_{opt}$	$w_{f,min}$ kW-h/lbm-LH_2	w_{ideal} kW-h/lbm-LH_2	FOM_{max}
1	0.6230	0.2733	15.457	6.275	1.772	0.2824
5	0.6230	0.2733	15.457	5.050	1.521	0.3012
10	0.6230	0.2733	15.457	4.521	1.413	0.3125
15	0.6230	0.2733	15.457	4.210	1.349	0.3204
20	0.6230	0.2733	15.457	3.989	1.304	0.3268
25	0.6230	0.2733	15.457	3.817	1.268	0.3357

Table 5.4 shows that the optimum expander mass flow ratio, maximum liquid yield, and minimum liquid nitrogen requirement are independent of the compressor inlet pressure. This is true because the inlet temperature and exit pressure are held constant and the compression process is modeled as isothermal. Furthermore, the liquid yield and expander mass flow ratio are decoupled from the compressor inlet and exit temperatures by the 100% effective cooling bath assumption. The functional relationship between the specific work and inlet pressure is graphically described in Figure 5.7.

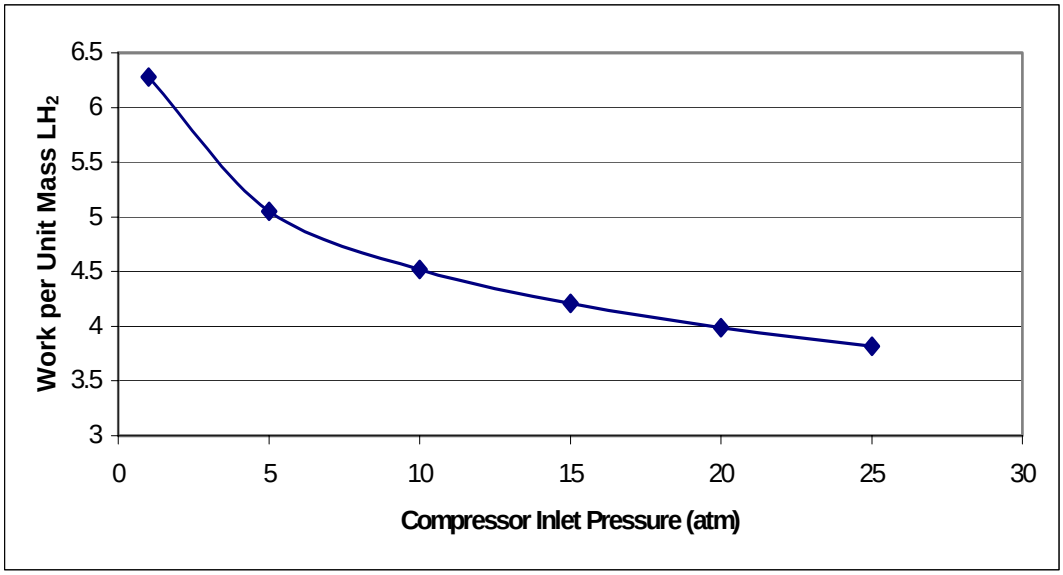

Figure 5.7. Effect of compressor inlet pressure on the specific work

Increasing the pressure from 1 to 25 atmospheres reduces the specific work requirement by 39.2% while also reducing the theoretical work requirement by 28.4%; the net result is an 18.9% increase in the figure of merit.

Compressor inlet temperature. Compressor inlet temperatures ranging from 0 to 80 °F are analyzed to gauge the merits for hydrogen pre-cooling using the combined cycle. A simulation was run for an inlet pressure of 25 atm, exit pressure of 40 atm, and compressor and expander efficiencies of 75 and 85%, respectively.

Results of the simulation are summarized in Table 5.5. An interesting result of this simulation is the reduction in the figure of merit with lower inlet temperatures.

Table 5.5. Claude cycle simulation results for compressor inlet temperature variation

T_1 (F)	$X_{e,opt}$	Y_{max}	$(z/y)_{opt}$	$w_{f,min}$ kW-h/lbm-LH_2	w_{ideal} kW-h/lbm-LH_2	FOM_{max}
0	0.6230	0.2733	15.621	3.802	1.004	0.2639
20	0.6230	0.2733	15.577	3.806	1.069	0.2808
40	0.6230	0.2733	15.535	3.809	1.134	0.2978
60	0.6230	0.2733	15.495	3.813	1.201	0.3150
80	0.6230	0.2733	15.457	3.817	1.268	0.3323

This phenomenon is explained by the increase in the liquid nitrogen requirement due to the assumption that $T_c = T_2$. Reducing the inlet temperature of the compressor effectively decreases T_c and lowers the enthalpy at state C. From Equation 3.14, the denominator $h_c - h_a$ is reduced from 187.2 Btu/lbm (435.5 kJ/kg) to 167.3 (Btu/lbm) 389.2 kJ/kg, thereby increasing the liquid nitrogen requirement from 15.457 to 15.621 lbm-LN_2/lbm-LH_2. This effect partially offsets the benefit of pre-cooling the hydrogen gas resulting in a 0.393% decrease in specific work. The ideal specific work simultaneously decreases by 20.8%. As a result, the FOM actually decreases by 20.6% from 80 to 0 °F. The liquid nitrogen requirement and specific work in relation to the compressor inlet temperature is presented in Figures 5.8 and 5.9.

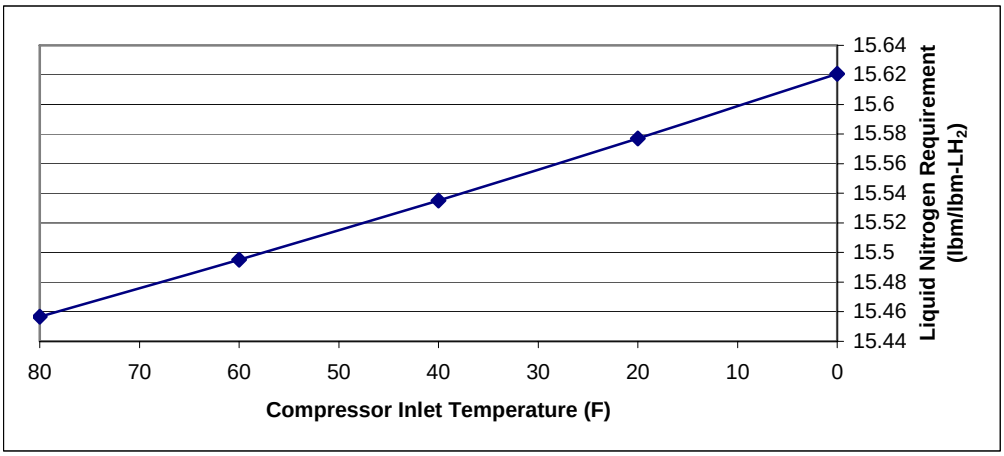

Figure 5.8. Liquid nitrogen requirement vs. compressor inlet temperature

Figure 5.9 concludes that the reduction in specific liquefaction energy due to decreased inlet temperature can be neglected within the specified range. A qualitative comparison of the figures of merit made between cases three and four show that increasing inlet pressure is significantly more effective in reducing the specific liquefaction energy (Figure 5.10).

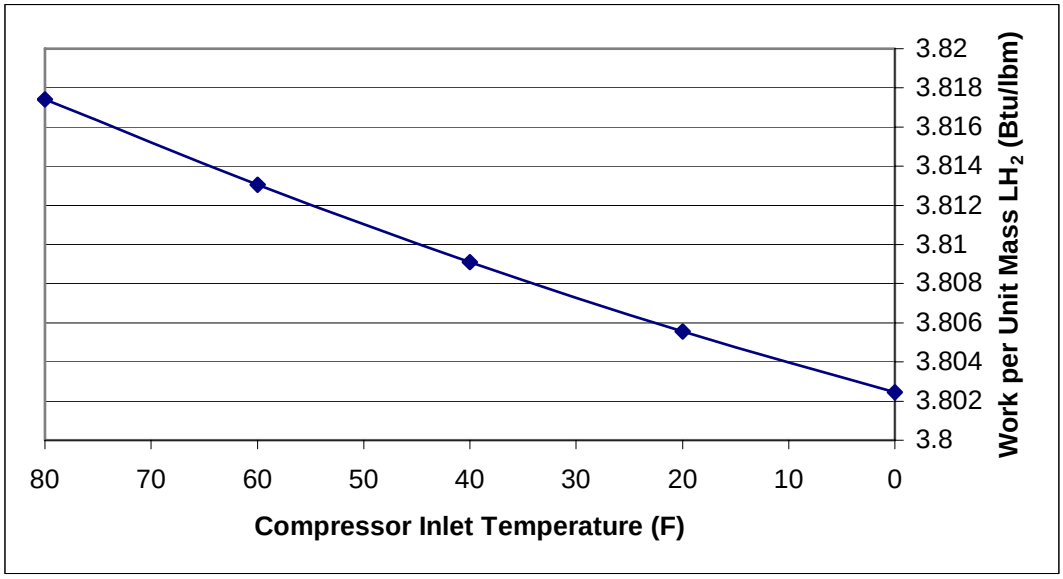

Figure 5.9. Specific work requirement vs. compressor inlet temperature

The analysis concludes that the optimum operating point for the Claude cycle under the assumed component efficiencies ($\eta_e = 0.85$, $\eta_c = 0.75$) is $P_1 = 25$ atm. The cycle parameter values are displayed in Table 5.6 at the optimum design point and at normal operating conditions. The specific work of liquefaction is reduced by 46.7% and the figure of merit is increased 18.9%.

The total energy required to produce and liquefy hydrogen is 28.656 kW-h/lbm-H_2 (63.175 kW-h/kg-H_2). Over 86% of this energy is consumed in electrolysis. Properties at each state point are given for the optimum design condition in Appendix B. Given the conclusion that compressor inlet temperature has little effect on the specific work, the

maximum hydrogen production rate of the combined cycle is 0.1775 lbm/hr or 7.21 gallons/day.

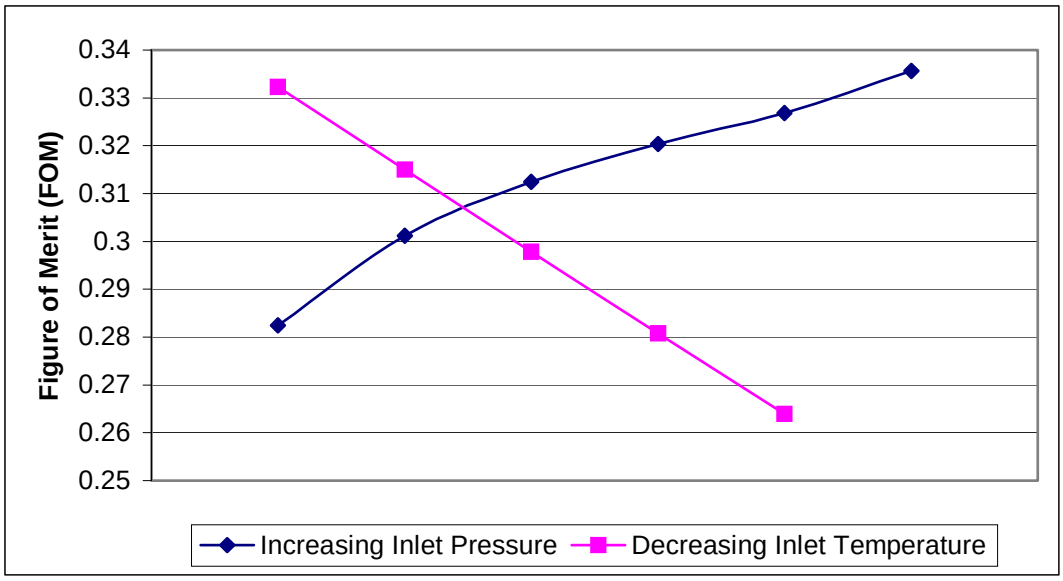

Figure 5.10. Comparison of inlet pressure and temperature affect on the cycle FOM

Table 5.6. Claude cycle performance parameters for normal and optimum configuration

	Normal T_1 = 80F P_1 = 1 atm	**Optimum** T_1 = 80F P_1 = 25 atm
$X_{e,opt}$	0.6230	0.6230
Y_{max}	0.2733	0.2733
$(z/y)_{opt}$	15.457	15.457
$w_{f,min}$		
Btu/lbm-LH_2	21411.70	13025.04
kW-h/lbm-LH_2	6.275	3.817
w_{ideal}		
Btu/lbm-LH_2	6046.88	4327.92
kW-h/lbm-LH_2	1.772	1.268
FOM_{max}	0.2824	0.3357

Ammonia-water Combined Cycle

The ammonia-water combined cycle was analyzed for a fixed power output to observe the impact of expander efficiency on the heat and work requirements as well as the cooling capacity. The simulation was run under the assumptions listed in chapter 3 while varying the expander isentropic efficiency from 10 to 100% in 10% increments.

Results of the simulation are given in Figures 5.11 thru 5.15 and a sample output of the simulation is given in Appendix B.

The ammonia vapor mass flow rate required to drive the expander and produce 5kW of electricity is a function of only the exhaust enthalpy at state 8; since the power output and specified temperatures and pressures are held constant. From the definition of isentropic efficiency, the vapor mass flow scales with $1/\eta_e$. The weak and strong solution flow rates follow a similar trend as shown in Figure 5.11 as they are related to the vapor flow by a constant ratio of the ammonia mass fractions as described by Equations 3.17 and 3.18. The maximum mass flows for the vapor, weak, and strong solutions occur at the lowest efficiency (10%) and are are: 3586.34 lbm/hr (0.4519 kg/s), 72037.7 lbm/hr (9.0767 kg/s), and 75624.1 lbm/hr (9.5286 kg/s), respectively.

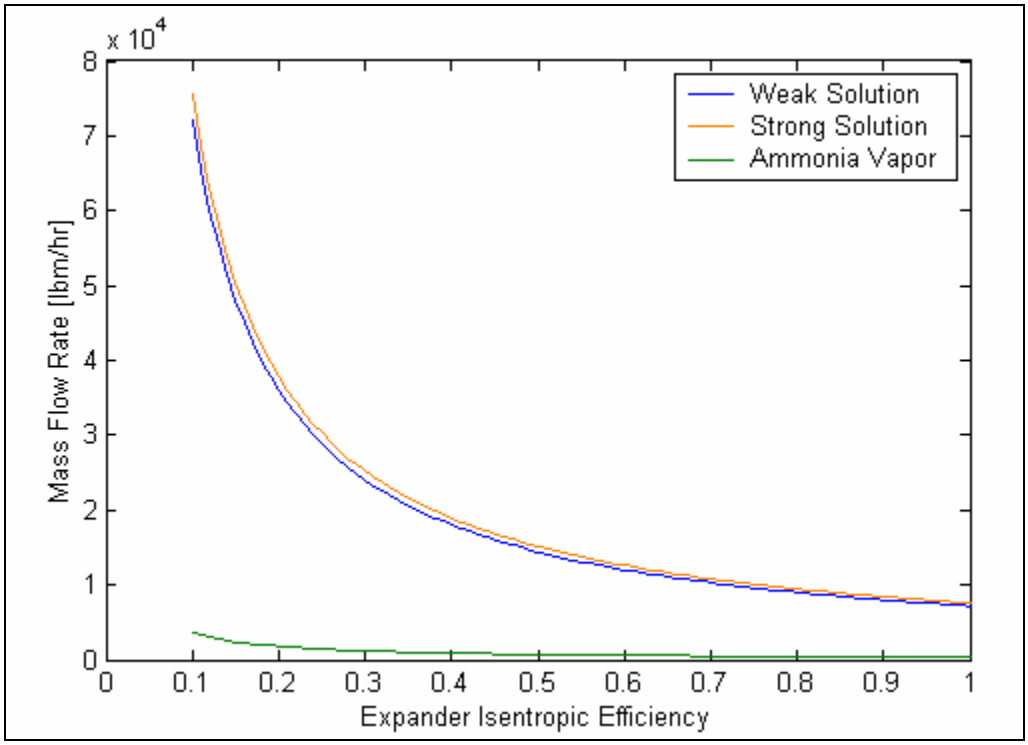

Figure 5.11. Mass flow rate dependence on expander efficiency

Likewise the minimum mass flows are (in the same order): 358.63 lbm/hr (0.0452 kg/s), 7203.77 (0.9077 kg/s), and 7562.41 (0.9529 kg/s). The mass fraction of the strong, weak, and vapor streams are $x_S = 0.3988$, $x_W = 0.3689$, and $x_V = 1.0$ (assumed). A decrease in mass flow through the system manifests itself in the reduction of work and heat interactions of the cycle for a given output as seen in Figures 5.12 and 13.

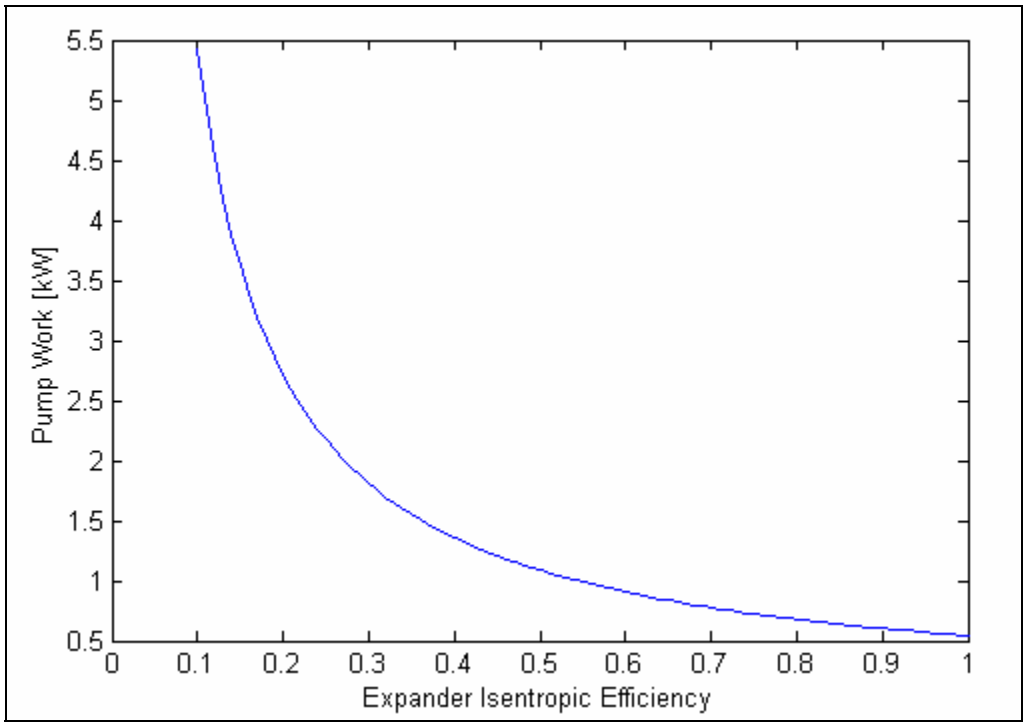

Figure 5.12. Pump work variation with expander efficiency

Minimum pump work, boiler heat input and absorber heat rejection are: 0.724 Hp (0.540 kW), 331,566 Btu/hr (97.18 kW), and 321,117 Btu/hr (94.11 kW). The ideal cooling capacity under these conditions is 9130.26 Btu/hr (2.68 kW). Figure 5.14 concludes that at least 60% efficient expansion is required to obtain any cooling capacity. Below this point, the exhaust temperature of the expander exceeds the assumed temperature of the substance to be cooled (85 °F). This effect is also evidenced in the plot of the expander isentropic efficiency versus the cycle thermal efficiency (Figure 5.15).

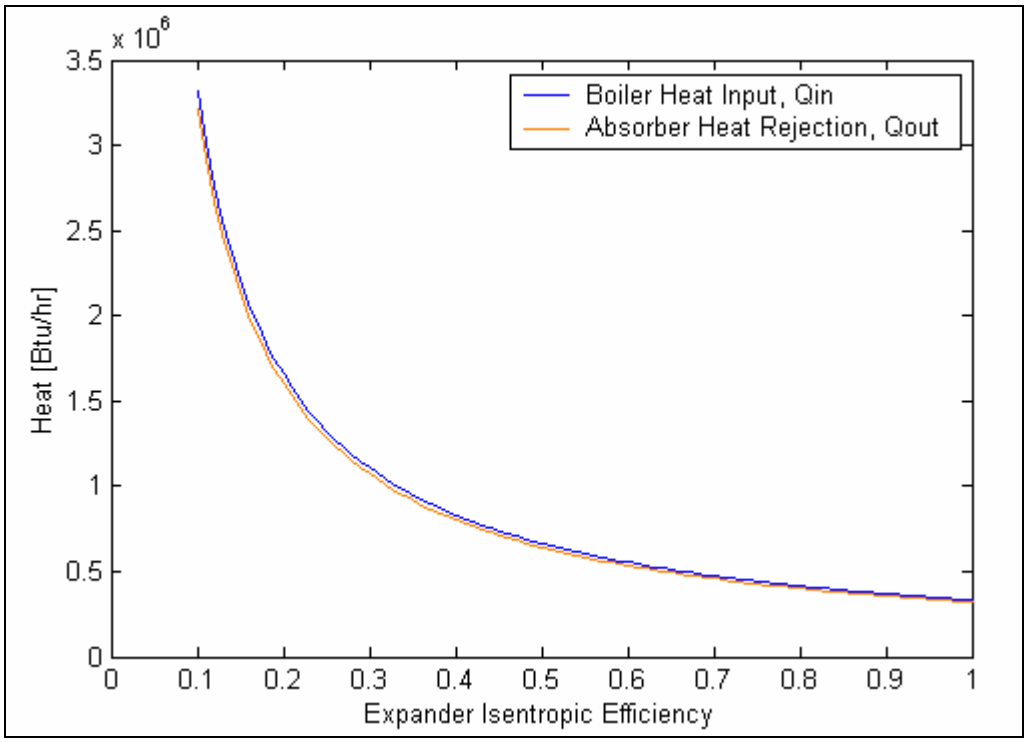

Figure 5.13. Boiler heat input and absorber heat rejection vs. expander efficiency

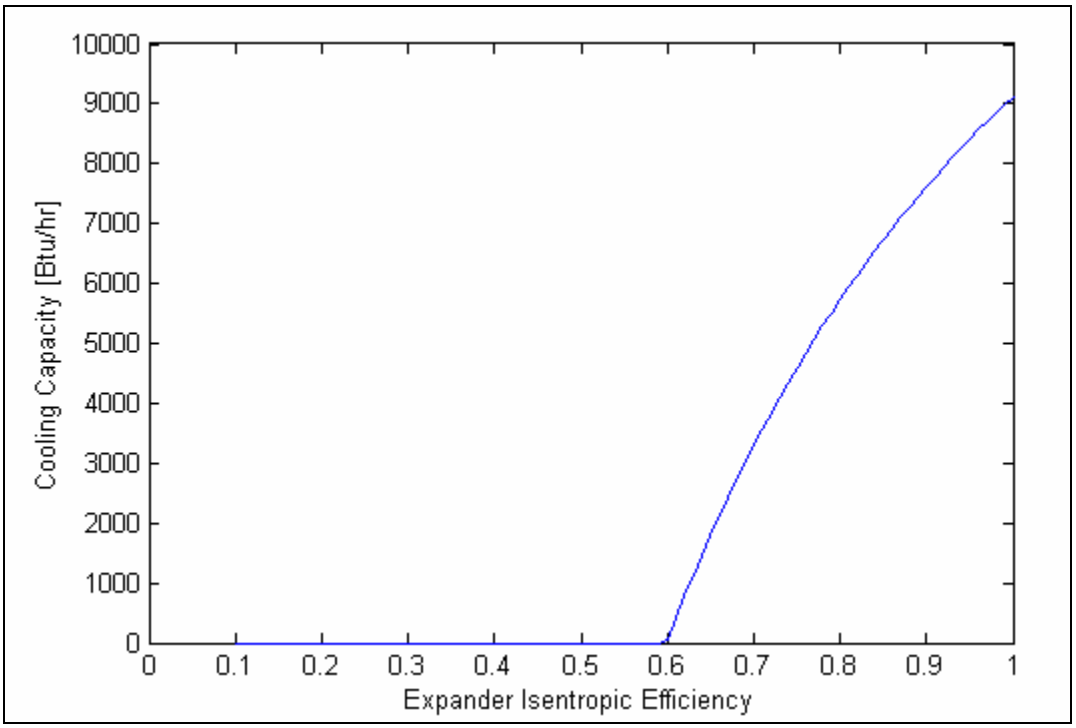

Figure 5.14. Cycle cooling capacity as a function of expander efficiency

Thermal efficiency increases linearly with expander efficiency; however, a sudden increase in slope occurs at approximately $\eta_e = 0.6$ at which point the cooling effect

begins to enhance the thermal efficiency of the cycle. The highest achievable thermal efficiency for the given operating conditions is 7.22%.

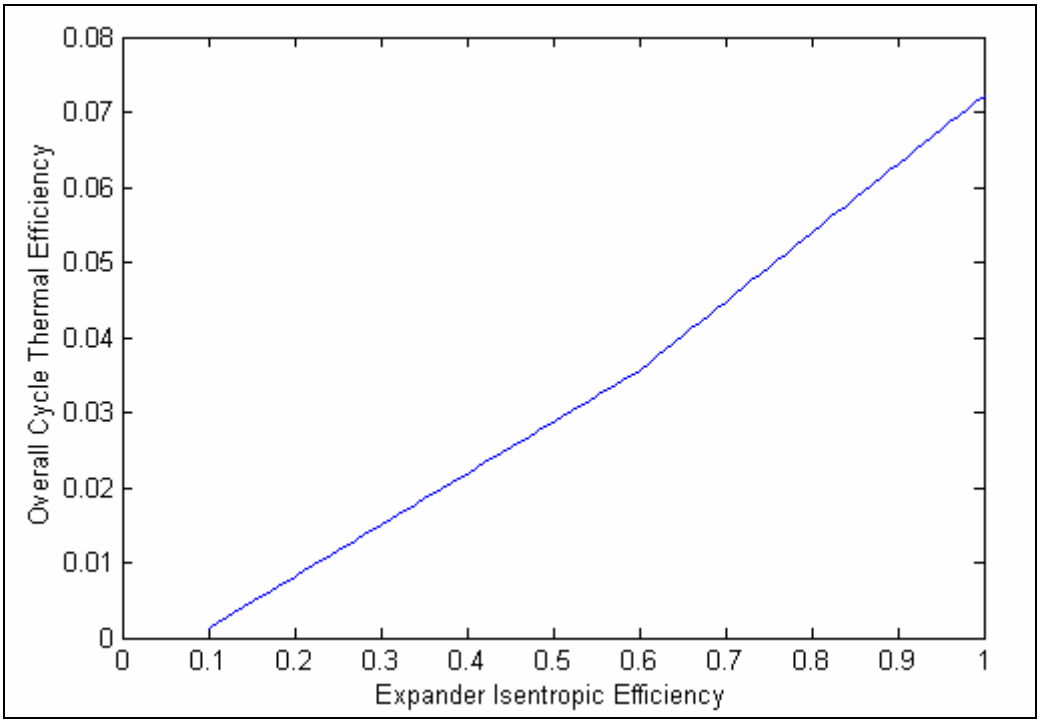

Figure 5.15. Cycle thermal efficiency vs expander efficiency

The mass fraction of ammonia entering the expander was analyzed more closely to judge the assumption of pure vapor leaving the rectifier and to determine the impact that trace quantities of water have on the cycle performance. The analysis was carried out for an ideal expander. Figure 5.16 shows the profound negative effect on cooling capacity. The cooling capacity diminishes to zero rapidly as trace amounts of water are introduced into the expander stream up to only 2.5% by mass. Boiler heat input is reduced from 331,566 Btu/hr (97.18 kW) to 320,934 Btu/hr (94.06); however, thermal efficiency is reduced 9.26% from 7.22% to 6.55% because of the lost cooling benefit. Another concern is that the expander exhaust temperature drops below the mixture dew point as shown in Figure 5.17. At a 2.5% water vapor concentration by mass, the mixture quality is 0.967. This most likely is not an issue for compliant devices such as scrolls in which a

small quantity of liquid can be tolerated, or with high-speed devices such as turbines, in which the residence time of the fluid is shorter than the time required for condensation to occur (metastable condition).

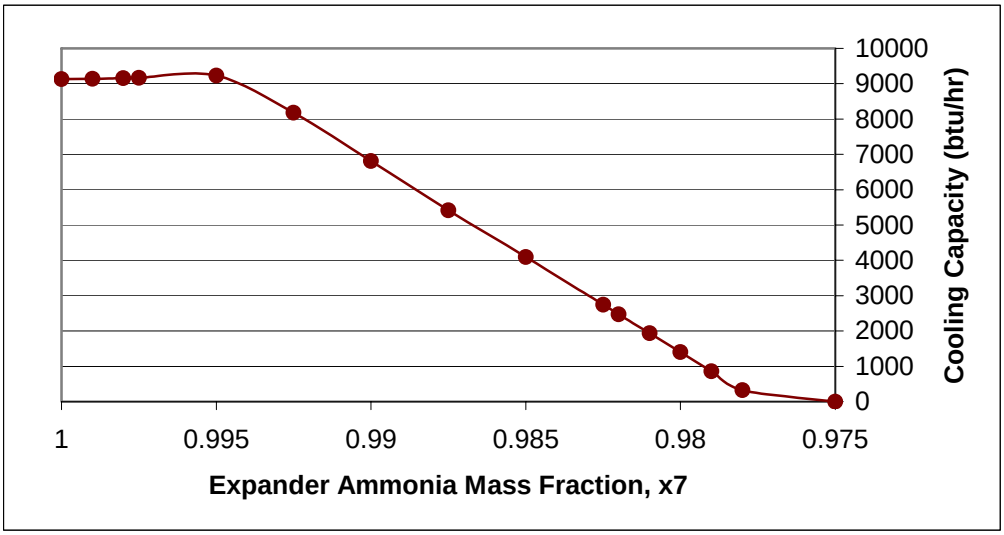

Figure 5.16. Effect of trace amounts of water within in the expander inlet stream on cycle cooling capacity

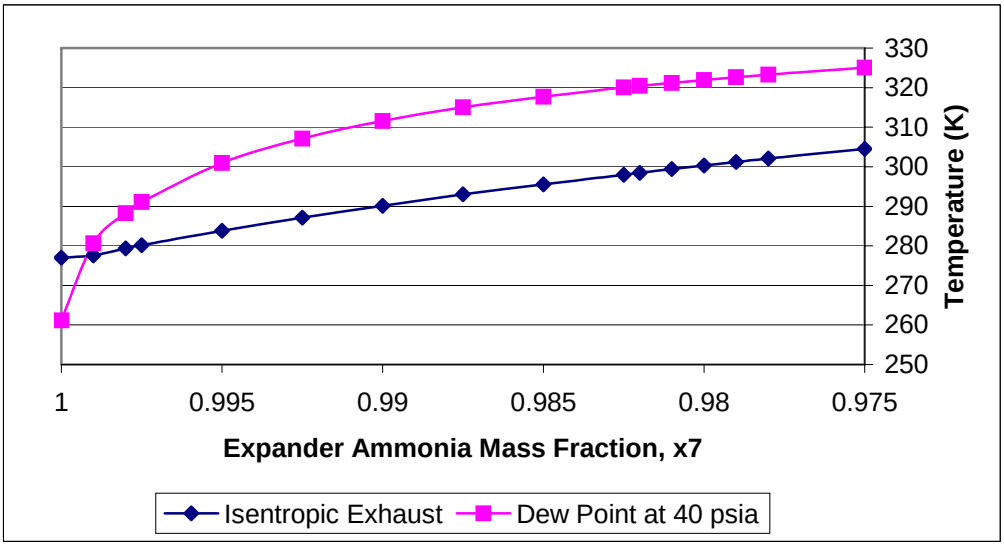

Figure 5.17. Expander exhaust and dew point temperature at several water concentrations

These results show that rectifier design is a crucial element for the success of a small-scale combined cycle in the hydrogen production field in which high efficiency translates into greater liquid yield per unit energy input.

Scroll Expander Performance Study

Scroll expander performance was measured for inlet pressures of 60, 70, and 80 psig; a range suitable for the 5kW combined cycle. Two tests were performed at each pressure to verify repeatability of the results. Tests at pressures over 80 psig were not feasible due to the relatively small tank and the inability of the compressor to supply compressed air at high flow rates (> 60 scfm). Furthermore, the compressor motor is equipped with a high-temperature cut-off switch that disconnects power after approximately 10 minutes of continuous operation. A fan was used to aid in cooling the motor; however periods of lockout continued to occur, limiting the maximum duration of each test.

Figure 5.18 shows the results of the repeatability analysis applied to shaft power measurements at 65 psig. The second set of data indicated by the square points agrees well with the trend line of the initial data.

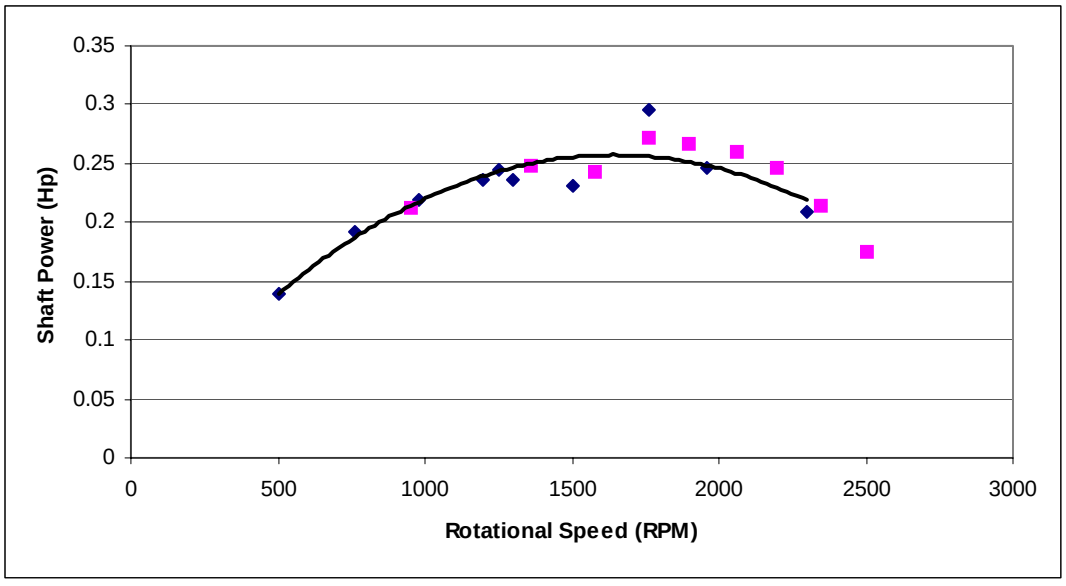

Figure 5.18. Repeatability analysis applied to shaft power output at 65 psig

Results of the study are summarized in Figures 5.19 thru 5.22. Shaft power output is plotted with respected to expander rotational speed in Figure 5.19. Rather than

beginning at a maximum value and decreasing monotonically with RPM as expected, the power output reaches a maximum at approximately 1500 RPM before decreasing toward zero in all three cases. This is thought to occur due to choked conditions at the expander exit. Flow becomes choked when the port to fitting area ratio is smaller than the critical area ratio given by the temperature and pressure of the exiting air. The area of the expander exit port and fitting is 0.375" and 0.25", respectively. Further evidence of choked flow is given by the fact that the maximum attainable rotational speed is only 3000 RPM at source pressures up to 110 psig, whereas the TRS-90 scroll compressor can normally achieve speeds of up to 9000 RPM (Sanden engineer, personal conversation).

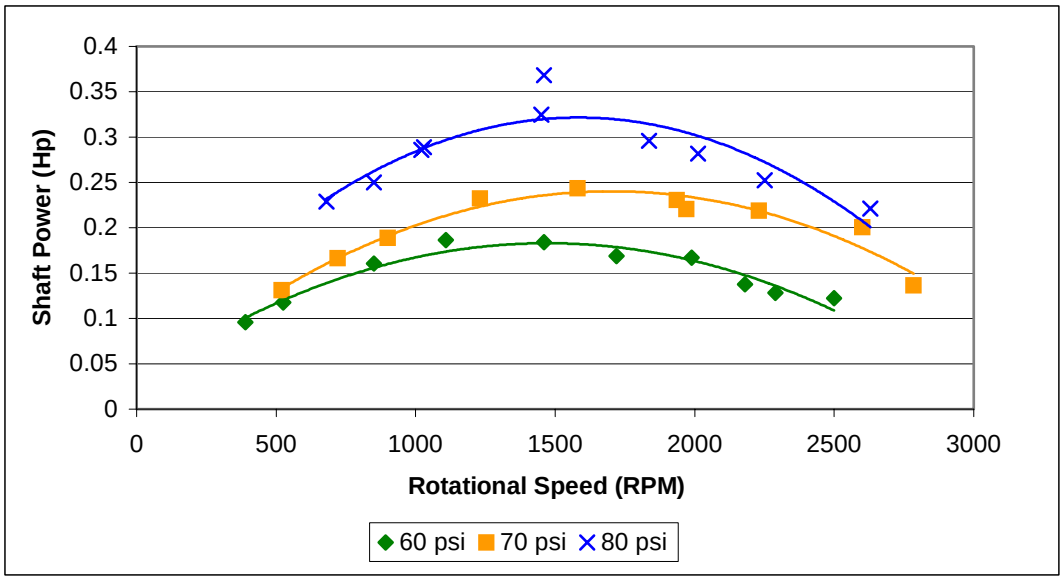

Figure 5.19. Shaft power vs. rotational speed at 60, 70, and 80 psig inlet pressure

A similar trend is witnessed with isentropic efficiency, η_e (Figure 5.20). Low values of η_e are attributed to the poor volumetric efficiency, η_v, of the expander at low RPM and relatively high torsional load. Increased torsional resistance raises the pressure within each pocket of the scroll, enhancing tip leakage and reducing volumetric efficiency. Figure 5.21 illustrates the relationship between volumetric efficiency and

rotational speed. At each pressure, η_v increases asymptotically toward a final value between 0.8 and 0.9.

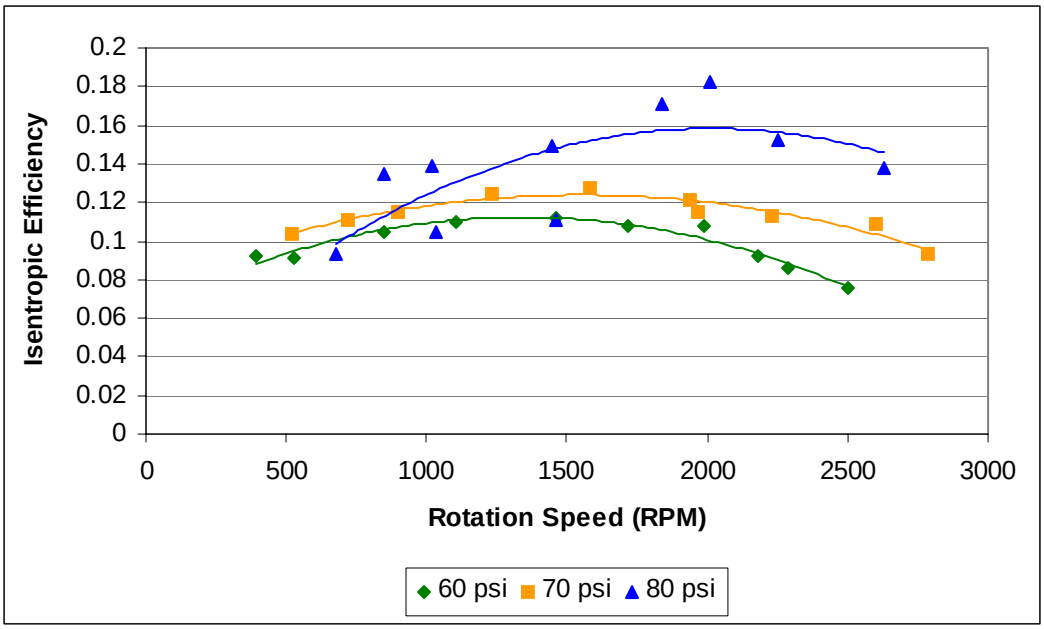

Figure 5.20. Scroll expander isentropic efficiency

The volumetric efficiency indicates the percentage of air that passes through without doing any useful work. This process can be modeled as isenthalpic, with the approximation of constant temperature (ideal gas). The warmer air mixes with the cold air, from which work was extracted, within the scroll housing effectively raising its temperature prior to the measurement location. Furthermore, heat is exchanged from the surroundings to the fluid through the exit port fittings. This temperature rise causes an erroneous calculation of the exit enthalpy and thus the isentropic efficiency. However, trends may still be observed to determine where the point of maximum efficiency occurs.

The exit temperature variation with rotational speed is shown in Figure 5.22. The points of minimum exit temperature coincide with those of maximum power output as expected from the First Law of Thermodynamics.

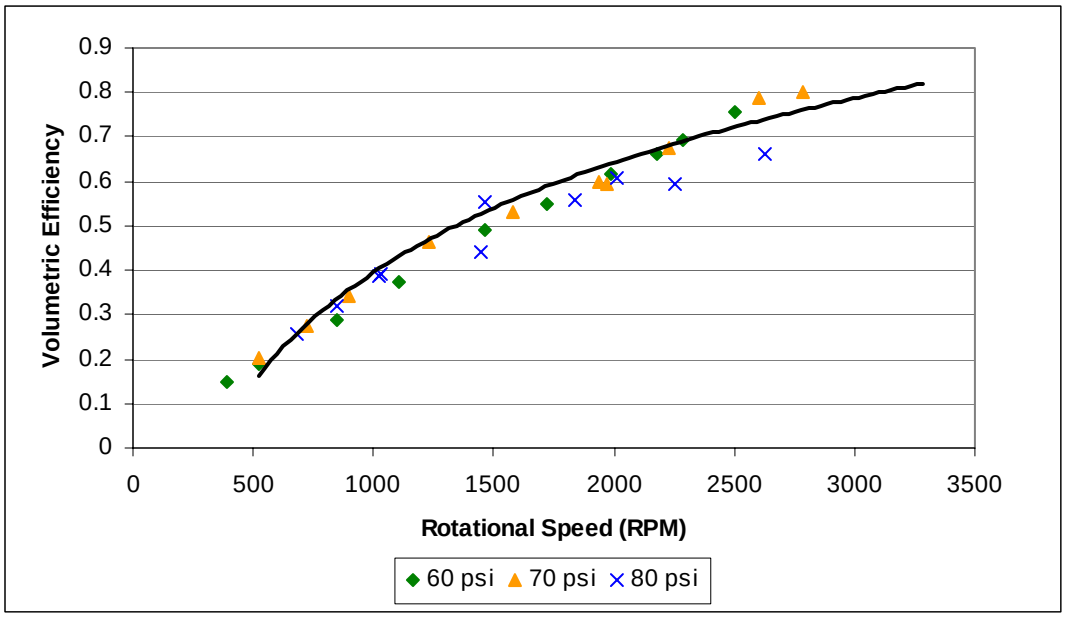

Figure 5.21. Volumetric efficiency variation with expander rotational speed

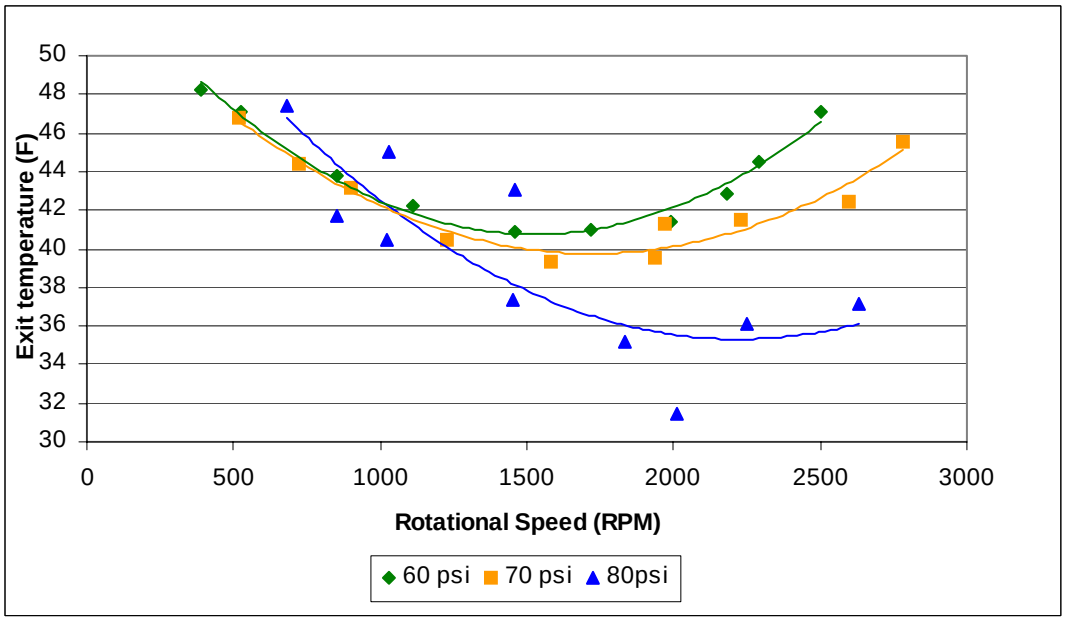

Figure 5.22. Expander exit temperature and rotational speed relationship

The maximum power output of 0.368 Hp (0.274 kW) occurred at 1460 RPM for the 80-psig inlet pressure case. The most efficient operating point is 18.2%. Rotational speed, inlet pressure, and power output at this point is 2000, 80 psig, and 0.282 Hp. The temperature of the working fluid (excluding leakage) is found at any point using the volumetric efficiency and flow rate in Equation 5.5.

$$T_{wf} = \frac{T_{exit} - cfm_{leakage} T_{inlet}}{cfm_{wf}} = \frac{T_{exit} - (1 - \eta_v) T_{inlet}}{\eta_v} \tag{5.5}$$

Therefore, with a volumetric efficiency of 0.6092 and temperatures of 71.6 °F and 31.5 °F at the inlet and exit at this point, the temperature of the working fluid is 4.77 °F.

The low value of isentropic efficiency is due primarily to leakage caused by the density mismatch. The TRS-90 is designed for R-134A with a density of 0.262 lbm/ft^3 at STP whereas the density of air at STP is .07298 lbm/ft^3; nearly 3.6 times lower than R-134A, and the density of ammonia is 0.04333 lbm/ft^3; 1.6 times lower than air. The performance of the expander with ammonia is expected to be worse than with air because higher pressures are required for a unit volume of ammonia to store an equal amount of energy as a unit volume of air at a given temperature. This relationship is arrived at by considering the ideal gas law as a first approximation (Equation 5.6).

$$\left.\frac{p}{mT}\right|_{ammonia} = \left.\frac{p}{mT}\right|_{air} \Rightarrow \frac{p_{air}}{p_{ammonia}} = \frac{m_{ammonia}}{m_{air}} \cong 1.68 \tag{5.6}$$

Higher pressures lead to increased leakage within the scroll and a loss of performance. Additionally, ammonia is a smaller molecule than air and much smaller than R-134A, further facilitating tip leakage and reducing efficiency.

Fundamental design changes are required for the scroll concept to be utilized as an expander. The geometry of each scroll element should be altered such that the total number of chambers is increased as shown in Figure 5.23. This design reduces pressure differences between chambers and hence leakage (Hans-Joachim and Radermacher, 2003).

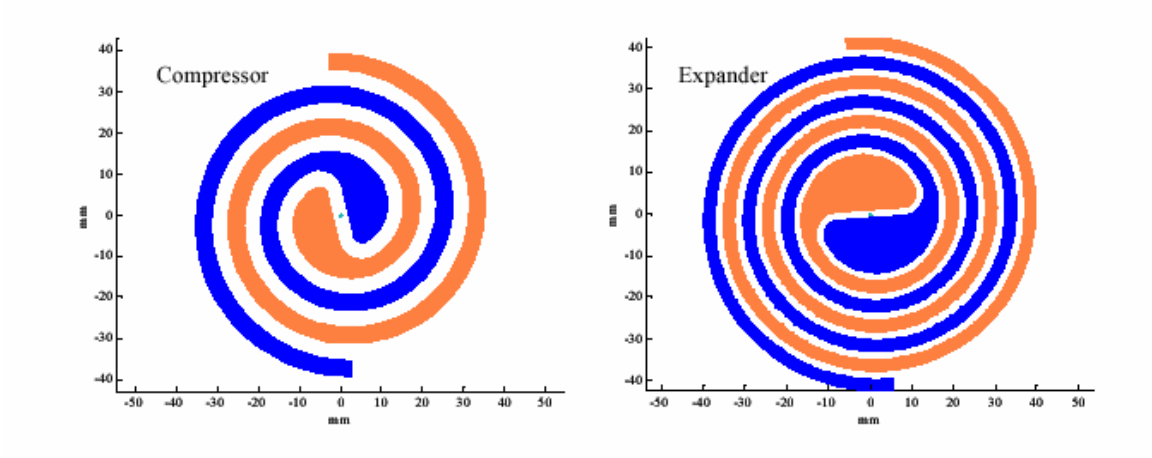

Figure 5.23. Comparison of optimum geometries of a scroll compressor (left) and expander (right) (Adapted from Hans-Joachim and Radermacher, 2003)

CHAPTER 6
RECOMMENDATIONS

Analytical Study

The analytical study of the electrolyzer, Claude cycle, and ammonia-based combined power/cooling cycle examined a limited range of operating parameters. By modeling the overall process with a program such as ASPEN, a greater number of operating configurations could be analyzed.

ASPEN is a chemical processing software package that allows the user design a cycle and specify a set or range of operating and boundary conditions. Using algorithms included in the code for most devices, ASPEN performs a complete thermodynamic analysis and outputs user specified data in an interactive manner.

Additionally, an optimization of the combined cycle for maximum hydrogen production would indicate the operating conditions, power output, and overall system size required to minimize energy cost. The economic viability of a large-scale implementation of this system should be examined through a life-cycle cost analysis.

Scroll Expander Performance Test

The scroll expander used in the performance test was an automotive air-conditioning compressor modified to run in reverse. Recommendations for future scroll expander experimentation are:

13. Test the expander in a closed loop system with ammonia vapor
14. Pre-heat the inlet vapor to simulated the combined cycle operating conditions
15. Re-design the compressor housing to allow higher flow rates and eliminate choking
16. Design an oil injection and separation system to reduce leakage losses
17. Use a dynometer or motor to improve control on the applied torque

Future work should also include improvements to the scroll design. Manufacturing the scroll involute using the optimum expander geometry shown in Figure 5.23 would improve its performance as an expander. Furthermore, the use of low-friction materials such as those under development at the University of Florida would eliminate the need for an oiling system, making the scroll an attractive design for the ammonia based combined power/cooling cycle.

CHAPTER 7
CONCLUSIONS

Global energy consumption is projected to increase 54% over the next 25 years. With proven oil reserves being called into question beyond 2030 it is important to develop renewable technologies to sustain the future global energy demand. By introducing an alternative fuel for transportation only, oil consumption can be reduced by as much as 20%.

Hydrogen has many characteristics that make it a desirable fuel. It has the highest energy content per unit mass of any known fuel – nearly 3 times higher than gasoline, it burns cleanly and efficiently, and it can be produced from water via electrolysis powered by renewable energy. Two major obstacles to the emergence of a hydrogen economy are the limited means available to efficiency produce mass quantities of hydrogen from renewable energy sources and the storage issues related to the low energy density of hydrogen. Liquefying hydrogen provides a solution to its low density; however, the process requires additional energy.

This thesis explored the possibility of using a 5-kW ammonia-based combined power/cooling cycle to produce hydrogen from renewable resources and pre-cool it prior to liquefaction in an effort to reduce the overall energy consumption. The advantage of this cycle is its ability to utilize low temperature heat sources available from solar and geothermal resources.

Simulations of the Claude liquefaction process and the 5-kW ammonia-based combined power/cooling cycle were developed to model the effects of component

efficiencies and operating parameters on the maximum hydrogen production rate and system energy requirement. Additionally, a performance test of a scroll compressor was performed to gauge its effectiveness as an expander for the combined cycle.

Conclusions resulting from tests and analyses are summarized below:

1. Pre-cooling hydrogen has little effect on the specific liquefaction energy and is detrimental to the liquefier efficiency.
2. Pressurized electrolysis is the most effective method of reducing the energy consumed in liquefaction.
3. The total energy required to produce and liquefy hydrogen is 28.656 kW-h/lbm-H_2 (63.175 kW-h/kg-H_2); 86% of which is consumed during electrolysis. A maximum of 7.21 gallons (27.3 liters) per day of liquid hydrogen can be produced from a 5-kW combined cycle.
4. The mass flows as well as the heat and work interactions of the 5-kW combined cycle scale with inverse of expander efficiency ($1/\eta_e$). Sixty percent expansion efficiency is required to extract cooling from the cycle.
5. Cooling capacity of the cycle is extremely sensitive to the vapor mass fraction of the expander inlet stream. At 2.5% water by mass and for perfect expansion, the cooling capacity completely diminishes.
6. Results of the performance test indicate that scroll compressors operate poorly as expanders. Low isentropic efficiencies result from leakage around the scroll tips. Improvements in the scroll design such as increasing the wrap of each scroll element and using low-friction material for oil-less operation would make the scroll an efficient expansion device suitable for the combined cycle.

APPENDIX A
COMPUTER PROGRAM FOR CYCLE SIMULATIONS

Two computer programs were written to assist in the evaluation of thermodynamic properties and to perform cycle analyses of the Claude liquefaction cycle and the ammonia-water combined power/cooling cycle. A description of each program is given below, including portions of the source code.

Claude Cycle Simulation

The program was written to assist in the parametric analysis of the specific work and efficiency of the Claude cycle. A subroutine was included to evaluate the thermodynamic properties at each state point coinciding with Figure 2.6. The code has the flexibility of single point calculations or variable inputs for a parametric analysis.

Thermodynamic Property Evaluation

The property code incorporates portions of RGAS and PSAT, two programs written by Dr. Roger Gater (2001). Property evaluation is carried out as a subroutine of the overall cycle simulation. The properties defined by user input and the listed assumptions are passed into either routine depending on the fluid condition. For saturated conditions, the pressure is defined; for superheated vapor, pressure-temperature, pressure-enthalpy, or pressure-entropy is input. Properties are then evaluated using the Redlich-Kwong gas model and returned to the main program. Critical properties and coefficients required by the Redlich-Kwong model are listed in Table A.1.

Program Description

The Claude cycle simulation program is written in MatLAB. It consists of three sub-routines and a data file: saturation2.m, gas_properties.m, gas_properties_base.m, gas.dat, all of which must be present for the program to operate. The program begins by reading data from the "gas.dat" file. It then asks for user input of compressor inlet temperature and pressure; giving the option of English or SI units. From the user input and given assumptions, the thermodynamic properties at each state point are evaluated by the "gas_properties.m" subroutine. If saturated conditions are known to exist, "saturation2.m is invoked. The key performance parameters of the Claude cycle are then calculated using the equations of Chapter 3. Results are output to the screen in figure form. Additional aspects of the program are described by the imbedded comments.

Main Program - Claude.m

```
[gas_num gas_name R Tc Pc cpoR a b c Zc A w] = textread('GAS.dat','%f %s %f %f %f %f %f %f %f %f
%f %f', 'headerlines',1);

units = input('Select Units: 0 = Metric, 1 = English:  ');
while (units < 0) | (units > 1)
   units = input('\nError, Try again:  ');
end

if units == 0
   T1 = input('\nEnter compressor inlet temperature (K):  ');
   P1 = input('\nEnter compressor inlet pressure (atm):  '); P1 = P1 * 1.0132;
else
   T1 = input('\nEnter compressor inlet temperature (F):  ');
   T1 = (T1 - 32)*5/9 + 273.15;
   P1 = input('\nEnter compressor inlet pressure (atm):  '); P1 = P1 * 1.0132;
end

P2 = input('\nEnter compressor discharge pressure (atm):  '); P2 = P2 * 1.0132;
eta_e = input('\nEnter expander adiabatic efficiency:  ');
%eta_e = .85;
eta_c = input('\nEnter compressor efficiency:  ');
%eta_c = .75;
% properties in J/g or kJ/kg
P_stp = 1.0132; %bar
gas = 10; % selects hydrogen gas from GAS.DAT data file

Pe = P_stp; Pg = P_stp; Pf = P_stp; P7 = P_stp; P8 = P_stp;
```

```
P9 = P_stp; P10 = P_stp; P10a = P_stp; PA = P_stp; PC = P_stp;
P2b = P2; P3 = P2; P4 = P2; P5 = P2;

HC1 = 175.1; HC2 = 312.97;  %Heats of conversion kJ/kg
WN2 = 1783.623; %kJ/kg-N2 Energy of LN2 liquefaction

T2 = T1; T10 = T1; TC = T1;

%State g and f
%call saturation program
routine = 1;
Ps = Pg; P = Pg;
[Ts,Zf,Zg,vf,vg,hfg,ufg,sfg] = saturation2(Ps,R(gas),Tc(gas),Pc(gas),Zc(gas),A(gas),w(gas));
Tg = Ts; Tf = Ts; T = Ts;
gas_properties;
hg = h; sg = s;
hf = hg - hfg; sf = sg - sfg;

%State 1
routine = 1; %pressure and temp specified
T = T1; P = P1;
gas_properties;
h1 = h; s1 = s;

%State 2
routine = 1; %isothermal compression
T = T2; P = P2;
gas_properties;
h2 = h; s2 = s;

%State 2b
Ps = P_stp;
gas = 13; %sets nitrogen properties
Ts = saturation2(Ps,R(gas),Tc(gas),Pc(gas),Zc(gas),A(gas),w(gas)); %calculates temperature of nitrogen
gas = 10; %returns to hydrogen
T2b = Ts; T = T2b; P = P2b;
routine = 1;
gas_properties;
h2b = h; s2b = s;

%State 3
T3 = T2b;
test = 0;
while T3 >= 70 % above critical temperature of hydrogen (asymptotic problems)
   routine = 1;
   T = T3; P = P3;
   gas_properties;
   h3 = h; s3 = s;
%state e_s
   routine = 2; %test to see if saturated conditions exist
   P = Pe; Ps = Pe;
   se = s3; ss = se;
   gas_properties;
   he_s = h; Te_s = T;
   if Te_s <= Tf
      xe = (se - sf)/(sfg);
```

```
      he_s = hf + xe*(hfg);
      Te_s = Tf; %isentropic temperature
   end
   if (h3 - he_s) > test
      T3opt = T3; Te_s_opt = Te_s;
      delta_h_opt = h3 - he_s;
      h3opt = h3; s3opt = s3; he_sopt = he_s;
   end
   test = h3 - he_s;
   T3 = T3 - .1;

   end
%state e
routine = 3; % pressure and enthalpy specified
he = h3opt - eta_e*(delta_h_opt);
hh = he; P = Pe;
gas_properties;
Te = T; se = s;

%state 4
routine = 1;
T = Te; P = P1;
T4 = Te;
gas_properties;
h4 = h; s4 = s;

%state 7 and 8
routine = 1;
T = Te; P = Pe;
T7 = Te; T8 = Te;
gas_properties;
h7 = h; h8 = h;
s7 = s; s8 = s;

%state 10
routine = 1;
T = T10; P = P10;
gas_properties;
h10 = h; s10 = s;

%state 10a
routine = 1;
T = T2b; P = P10;
gas_properties;
h10a = h; s10a = s;

%state A (saturated liquid)
routine = 1;
Ps = PA; P = PA;
gas = 13;
[Ts,Zf,Zg,vf,vg,hfg,ufg,sfg] = saturation2(Ps,R(gas),Tc(gas),Pc(gas),Zc(gas),A(gas),w(gas));
TA = Ts;
gas_properties;
hgA = h; sgA = s;
hA = hgA - hfg; sA = sgA - sfg;
```

```
%state C
routine = 1;
T = TC; P = PC;
gas_properties;
hC = h; sC = s;
gas = 10; %return to hydrogen

%Specific work, liquid yield, liquid nitrogen requirement, and figure of merit calculation
X(1) = 0;
step = .001
for i = 1:1/step
   X(i+1) = X(i) + step;
   y(i) = ((h10a-h2b) + eta_e*X(i)*(delta_h_opt))/(h10a - hf + HC2);
   if y(i) >= .725*(1 - X(i)) %.725 found from iterative procedure on HX 3
      y(i) = .725*(1-X(i));
   end
   z(i) = (HC1 + (h2 - h10) + eta_e*X(i)*(delta_h_opt) + y(i)*(h10 - hf + HC2))/(hC - hA);

   if units == 0
      W(i) = (((h2 - h1) - T1*(s2 - s1))/eta_c - eta_e*X(i)*(delta_h_opt))/3600; %work per unit mass
compressed
      Wf(i) = W(i)/y(i) + z(i)/y(i)*WN2/3600; %work per unit mass liquefied kJ/kg
      W_ideal = ((hf - h1) - T1*(sf - s1))/3600;
   else
      W(i) = (((h2 - h1) - T1*(s2 - s1))/eta_c - eta_e*X(i)*(delta_h_opt))/(2.326*3412);
      Wf(i) = W(i)/y(i) + z(i)/y(i)*WN2/(2.236*3412);
      W_ideal = ((hf - h1) - T1*(sf - s1))/(2.326*3412);
   end

   FOM(i) = W_ideal/Wf(i);
   if X(i+1) >= .9
      break
   end
end

z(i+1) = z(i);
Wf(i+1) = Wf(i);
W(i+1) = W(i);
FOM(i+1) = FOM(i);
y(i+1) = y(i);

Xopt = (1 - max(y)/.725)
Ymax = max(y)
Wfopt = min(Wf)
FOMopt = max(FOM)
zopt = min(z./y)
W_ideal

figure(1)
plot(X,Wf)
title('Work Per Unit Mass LH2 vs. Expander Mass Flow Ratio, X');
xlabel('Expander Mass Flow Ratio, X')
ylabel('Wf [kW-h/lbm-LH2]')
```

Saturation Property Evaluation - Saturation2.m

```
function [Ts,Zf,Zg,vf,vg,hfg,ufg,sfg] = saturation2(Ps,R,Tc,Pc,Zc,A,w)

Psr = Ps/Pc;
Tsr = (A + w*log(Psr))/(A - log(Psr));
Ts = Tsr*Tc;
Zfg = .824*(log(1.3/(Psr + .3)))^.467;
Zf = Zc*Psr*( 1 - Tsr^1.72*(1/Tsr - 1)^.295);
Zg = Zfg + Zf;
vf = Zf*R*Ts/Ps;
vg = Zg*R*Ts/Ps;
hfg = R*Tc*Zfg*(A*Tsr^2*(1 + w) / (Tsr + w)^2);
ufg = hfg - Ps*(vg - vf);
sfg = hfg/Ts;

%need to add warning about pressure and temperature above critical point
```

Gas Thermodynamic Property Evaluation – Gas_properties.m

```
%P & T given
cpo = R(gas)*cpoR(gas); T0 = 300; P0 = 1;

if routine == 1
   [v,u,h,s] = gas_properties_base(T,P,R(gas),cpo,Tc(gas),Pc(gas),a(gas),b(gas),c(gas));
end

if routine == 2
   T = 1.2 * T0*exp(.8*ss/cpo + (R(gas)/cpo)*log(P/P0));
   errorS = 1;
   while errorS > 1E-6
      [v,u,h,s] = gas_properties_base(T,P,R(gas),cpo,Tc(gas),Pc(gas),a(gas),b(gas),c(gas));
      errorS = abs(s - ss)/(abs(s+ss)+1);
      T = T*(.8 + .2*exp((ss - s)/cpo));
      Tr = T/Tc;
   end
end
if routine == 3
   T = 1.2*T0 + hh/cpo;
   errorH = 1;
   while errorH > 1E-6
      [v,u,h,s] = gas_properties_base(T,P,R(gas),cpo,Tc(gas),Pc(gas),a(gas),b(gas),c(gas));
      errorH = abs(h - hh)/(abs(h + hh)+100);
      T = T + .5*(hh-h)/cpo;
      Tr = T/Tc;
   end
end
```

Gas properties base.m

```
function [v,u,h,s] = gas_properties_base(T,P,R,cpo,Tc,Pc,a,b,c)
alpha = .42748; beta=.08664;
T0 = 300; P0 = 1;
```

```
Zp = 1;
errorZ = 1;
Tr = T/Tc;
Pr = P/Pc;
tau = (T/T0) - 1;

while errorZ > 1E-6
   vr = Zp*Tr/Pr;
   Z = 1 + beta/(vr - beta) - alpha/((vr + beta)*Tr^1.5);
   errorZ = abs(Z - Zp)/(Z + Zp);
   Zp = .8*Zp + .2*Z;
end
v = Z*R*T/P;
vr = Z*Tr/Pr;
phi = 1.25*vr^.1;
ud = R*Tc*phi*1.5*(alpha/beta)/Tr^.5*log((vr + beta)/vr);
hd = ud + (1 - Z)*R*T;
sd = R*(ud/(R*Tc*Tr) + log(vr/(vr - beta)) - (alpha/beta)/Tr^1.5*log((vr + beta)/vr) - log(Z));

hig = cpo*T0*(tau + a*tau^2/2 + b*tau^3/3 + c*tau^4/4);
uig = hig - R*T;
sig0 = cpo * ((1 - a + b - c)*log(tau + 1) + (a - b + c)*tau + (b - c)*tau^2/2 + c*tau^3/3);
sig = sig0 - R*log(P/P0);

u = uig - ud;
h = hig - hd;
s = sig - sd;
```

Table A.1. Critical properties and coefficients contained within the “gas.dat” file

	Hydrogen	Nitrogen
R	4.124	0.2968
Tc	33.3	126.2
Pc	13	33.9
Cpo/R	3.47	3.503
a	2.49E-02	2.98E-03
b	-6.75E-03	3.50E-02
c	2.00E-03	-5.86E-03
Zc	0.36	0.291
A	4.925	5.64
w	0.1415	0.0039

Ammonia-Based Combined Power/Cooling Cycle Simulation

The program was written to assist in the parametric analysis of the energy transfer and cooling capacity dependence of the combined cycle on expander isentropic efficiency and ammonia vapor mass fraction.

Thermodynamic Property Evaluation

Thermodynamic properties of the ammonia-water mixture and pure ammonia vapor are evaluated using subroutines adapted from a program developed by Tamm (2003). The evaluation method is based on a Gibbs free energy approach incorporating experimental correlations. A detailed description of the evaluation method and the coefficients used for the calculations are outlined by Tamm (2003).

Program Description

The combined cycle simulation program consists of a main program written in MatLAB, "combined cycle.m" and five property evaluation subroutines: ammonia_water.m, PTX.m, bubble_dew.m, critical_properties.m, and hsv_properties.m. The main program accepts user input values of cycle high and low pressure as well as the absorber and boiler temperatures. Each state point corresponding to Figure 2.7 is defined from these inputs and by the assumptions listed in Chapter 3. The program evaluates the thermodynamic properties at each point and uses these values to calculate the mass flows, mass fractions, energy transfers, and efficiencies given by Equations 3.16 thru 3.25. Results are output to text file named results.txt and displayed in several graphs. A sample output of the program is given in Appendix B. Additional aspects of the program are described by the imbedded comments.

Combined Cycle Main Program – Combined_cycle.m

```
%This program calculates the state points, work and heat exchanges, and flow rates
%of the combined cycle for varied turbine isentropic efficiencies using the user
%inputs of high pressure,low pressure, boiler temperature, and absorber temperature.
%The turbine isentropic efficiency is varied from 10 to 100% to study its effect on
%the overall cycle efficiency.
%
%Results are output to results.txt and graphs
%
%This program can easily be adapted for different operating conditions by
%adjusting values in the assumptions section.
%
```

```
%Sub-programs necessary for operation:  ammonia_water.m, PTx.m, hsv_properties.m,
%critical_props.m, bubble_dew.m, bubble_dew_base.m
clear all;
clc;
cycle = 1; %signifies whether inputs are for cycle or individual states

fprintf('\n**************************************************\n');
fprintf('*          Combined Cycle Analysis          *\n');
fprintf('*    Analysis code written by Robert Reed     *\n');
fprintf('* Property code written in C++ by Gunner Tamm *\n');
fprintf('*       Adapted to MatLAB by Robert Reed      *\n');
fprintf('*             September 12, 2004             *\n');
fprintf('**************************************************\n');
fprintf('IMPORTANT: This program consists of six sub-routines which must be present:\n');
fprintf('\tammonia_water.m, bubble_dew_base.m, bubble_dew.m, critical_props.m,\n\tthsv_properties.m,
and PTx.m\n\n');

P_low = input('Enter the cycle low pressure (psia): '); P_low = P_low/14.504;
P_high = input('Enter the cycle high pressure (psia): '); P_high = P_high/14.504;
while P_high <= P_low
   fprintf('High pressure must be greater than low pressure!!!\n');
   P_high = input('Try again: '); P_high = P_high/14.504;
end

Tabs = input('Enter absorber temperature (F): '); Tabs = (Tabs - 32)/1.8 + 273.15;
Tboil = input('Enter boiler temperature (F): '); Tboil = (Tboil - 32)/1.8 + 273.15;
while Tboil <= Tabs
   fprintf('Boiler temperature must be greater than absorber temperature!!!\n');
   Tboil = input('Try again: '); Tboil = (Tboil - 32)/1.8 + 273.15;
end

%Future additions will include cooling and heating hot water flow rates.
% Tcws = input('Enter cooling water source temperature (F): ');
% Tcwr = input('Enter cooling water return temperature (F): ');
% Thws = input('Enter heating hot water source temperature (F): ');
% Tcwr = input('Enter heating hot water source temperature (F): ');

%assumptions
x7 = 1; %pure ammonia vapor exiting the rectifier
%x7 = input('\nEnter mass fraction ammonia entering turbine:  ');
Elec = 5; %Electrical output of the generator [kW].
etaG = .75; %Generator efficiency
eps = .85; %recovery HE effectiveness

WT = Elec/etaG;

%Define all states by calling ammonia_water.m
%state 1
P = P_low; T = Tabs; option = 8; %option sets the sub-routine used in ammonia_water.m
ammonia_water;
P1 = P; T1 = T; h1 = hL; s1 = sL; v1 = vL; x1 = xb; %return results

%state 2
P = P_high; T2 = T1; x = x1; option = 1;
ammonia_water;
P2 = P; T2 = T; h2 = hm; s2 = sm; v2 = vm; x2 = x;
```

```
%state 4
P = P_high; T = Tboil; option = 8;
ammonia_water;
P4 = P; T4 = T; h4 = hL; s4 = sL; v4 = vL; x4 = xb;
%could also have the actual vapor exit state

%state 5
P = P_high; x = x4; option = 1;
T = T4 - eps*(T4 - T2); %assuming equal specific heats
ammonia_water;
T5 = T; P5 = P; h5 = hm; s5 = sm; v5 = vm; x5 = x;

%state 6
P = P_low; h = h5; x = x4; option = 3;
ammonia_water;
T6 = T; P6 = P; h6 = h; s6 = sm; v6 = vm; x6 = x;

%state 9
T = 302.594444444; %assumed to be 85F for air/hydrogen cooling
P = P_low; x = x7; option = 1;
ammonia_water;
T9 = T; P9 = P; h9 = hm; s9 = sm; v9 = vm; x9 = x;

%state 7
P = P_high; T = Tboil; x = x7; option = 1;
ammonia_water;
P7 = P; T7 = T; h7 = hm; s7 = sm; v7 = vm;

%state 8s Imaginary state obtained from isentropic expansion
P = P_low; s = s7; x = x7; option = 4;
ammonia_water;
P8s = P; T8s = T; h8s = hm; s8s = s; v2s = v2; x8s = x;

%state 8

etaT(1) = .1; %initial value of the turbine efficiency
step = .01; %step change in loop of the turbine efficiency
for n = 1:1/step
   P = P_low; x = x7;
   h = h7 - etaT(n)*(h7 - h8s); option = 3;
   ammonia_water;
   P8 = P8s; T8(n) = T; h8(n) = h; s8(n) = sm; v8(n) = vm; x8 = x;

   %Calculate solution mass flow rates
   mT(n) = WT / (h7 - h8(n)); %Turbine mass flow
   mS(n) = mT(n)*((x7 - x4)/(x1 - x4)); % Strong solution mass flow rate
   mW(n) = mS(n) - mT(n); %Weak solution mass flow rate

   %state 3
   P = P_high; x = x1; option = 1;
   T = eps*mW(n)*(T4 - T2)/mS(n) + T2; %assuming equal specific heats
   ammonia_water;
   T3 = T; P3 = P; h3 = hm; s3 = sm; v3 = vm; x3 = x;

   %Heat and work flows
```

```
    Qin(n) = mW(n)*h4 + mT(n)*h7 - mS(n)*h3; %heat input to vapor generator
    Qout(n) = mW(n)*h6 + mT(n)*h9 - mS(n)*h1; %heat rejected from absorber
    Qc(n) = mT(n)*(h9 - h8(n)); %Cooling capacity
    WP(n) = mS(n)*(h2-h1); %Pump work
    if Qc(n) < 0 % This step disallows negative cooling capacity
       Qc(n) = 0;
    end

    COP = 3; %typical value
    eta_cycle(n) = (WT - WP(n) + Qc(n)/COP) / Qin(n); %cycle efficiency
    etaT(n+1) = etaT(n) + step; %set new value for next loop

end
%Set vector lengths equal, last value is ignored
Qin(n+1) = Qin(n); Qout(n+1) = Qout(n); WP(n+1) = WP(n); Qc(n+1) = Qc(n);
eta_cycle(n+1) = eta_cycle(n); mS(n+1) = mS(n); mW(n+1) = mW(n); mT(n+1) = mT(n);

results = fopen('results.txt','w');
fprintf(results,'*****************************\n');
fprintf(results,'*  Cycle Analysis Results *\t\t Created: %s\n',datestr(now));
fprintf(results,'*****************************\n\n\n');
fprintf(results,'Assumptions:\t Saturated conditions at states 1 and 4.\n');
fprintf(results,'            \t Component pressure losses are negligible.\n');
fprintf(results,'            \t Equal weak and strong solution specific heats.\n');
fprintf(results,'            \t Superheater temperature equal to boiler temperature.\n');
fprintf(results,'            \t Mass fraction of ammonia in the rectifier exit stream, x7 = %g\n',x7);
fprintf(results,'            \t Evaporator exit temperature = %g F (%.2f C)\n',((T9-273.15)*1.8+32),T9-273.15);
fprintf(results,'            \t Electric generator efficiency = %g%%\n',etaG*100);
fprintf(results,'            \t Recovery heat exchanger effectiveness = %g\n',eps);
fprintf(results,'            \t Electric generator output = %g kW\n\n\n',Elec);
fprintf(results,'User Inputs:\t Absorber temperature = %g F (%g C)\n',(Tabs-273.15)*1.8+32,Tabs-273.15);
fprintf(results,'            \t Boiler temperature = %g F (%g C)\n',(Tboil-273.15)*1.8+32,Tboil-273.15);
fprintf(results,'            \t System low pressure = %g psia (%g bar)\n',P_low*14.504,P_low);
fprintf(results,'            \t System high pressure = %g psia (%g bar)\n',P_high*14.504,P_high);
fprintf(results,'_____________________________________________________________________________
_____________________________________\n\n');
fprintf(results,'\t State 1 \t\t\t\t\t\t State 2 \t\t\t\t\t\t State3\n\n');
fprintf(results,' T = %g F (%.2f C) \t\t\t\t T = %g F (%.2f C) \t\t\t\t T = %g F (%.2f C)\n',(T1-
273.15)*1.8+32,T1-273.15,(T2-273.15)*1.8+32,T2-273.15,(T3-273.15)*1.8+32,T3-273.15);
fprintf(results,' P = %g psia (%.2f bar) \t\t\t P = %g psia (%.2f bar) \t\t\t P = %g psia (%.2f
bar)\n',P1*14.504,P1,P2*14.504,P2,P2*14.504,P2);
fprintf(results,' h = %g BTU/lbm (%.2f kJ/kg) \t h = %g BTU/lbm (%.2f kJ/kg) \t h = %g BTU/lbm (%.2f
kJ/kg)\n',h1/2.326,h1,h2/2.326,h2,h3/2.326,h3);
fprintf(results,' s = %g BTU/lbm-R (%.4f kJ/kg-K) \t s = %g BTU/lbm-R (%.4f kJ/kg-K) \t s = %g
BTU/lbm-R (%.4f kJ/kg-K)\n\n',s1/4.1868,s1,s2/4.1868,s2,s3/4.1868,s3);
fprintf(results,'\t State 4 \t\t\t\t\t\t State 5 \t\t\t\t\t\t State6\n\n');
fprintf(results,' T = %g F (%.2f C) \t\t\t\t T = %g F (%.2f C) \t\t\t\t T = %g F (%.2f C)\n',(T4-
273.15)*1.8+32,T4-273.15,(T5-273.15)*1.8+32,T5-273.15,(T6-273.15)*1.8+32,T6-273.15);
fprintf(results,' P = %g psia (%.2f bar) \t\t\t P = %g psia (%.2f bar) \t\t\t P = %g psia (%.2f
bar)\n',P4*14.504,P4,P5*14.504,P5,P6*14.504,P6);
fprintf(results,' h = %g BTU/lbm (%.2f kJ/kg) \t h = %g BTU/lbm (%.2f kJ/kg) \t h = %g BTU/lbm (%.2f
kJ/kg)\n',h4/2.326,h4,h5/2.326,h5,h6/2.326,h6);
fprintf(results,' s = %g BTU/lbm-R (%.4f kJ/kg-K) \t s = %g BTU/lbm-R (%.4f kJ/kg-K) \t s = %g
BTU/lbm-R (%.4f kJ/kg-K)\n\n',s4/4.1868,s4,s5/4.1868,s5,s6/4.1868,s6);
fprintf(results,'\t State 7 \t\t\t\t\t\t State 8s \t\t\t\t\t\t State9\n\n');
```

```
fprintf(results,' T = %g F (%.2f C) \t\t\t\t T = %g F (%.2f C) \t\t\t T = %g F (%.2f C)\n',(T7-
273.15)*1.8+32,T7-273.15,(T8s-273.15)*1.8+32,T8s-273.15,(T9-273.15)*1.8+32,T9-273.15);
fprintf(results,' P = %g psia (%.2f bar) \t\t\t P = %g psia (%.2f bar) \t\t\t P = %g psia (%.2f
bar)\n',P7*14.504,P7,P8*14.504,P8,P9*14.504,P9);
fprintf(results,' h = %g BTU/lbm (%.2f kJ/kg) \t h = %g BTU/lbm (%.2f kJ/kg) \t h = %g BTU/lbm (%.2f
kJ/kg)\n',h7/2.326,h7,h8s/2.326,h8s,h9/2.326,h9);
fprintf(results,' s = %g BTU/lbm-R (%.4f kJ/kg-K) \t s = %g BTU/lbm-R (%.4f kJ/kg-K) \t s = %g
BTU/lbm-R (%.4f kJ/kg-K)\n',s7/4.1868,s7,s8s/4.1868,s8s,s9/4.1868,s9);
fprintf(results,'_____
_____\n\n');
fprintf(results,'Weak solution mass fraction, xW = %g\t Strong solution mass fraction, xS = %g\n',x4,x1);
fprintf(results,'_____
_____\n\n');
fprintf(results,'Turbine shaft work output, WT = %g kW\n\n',WT);
fprintf(results,'Turbine adiabatic efficiency varied from %g%% to %g%% in %g%%
increments\n\n',etaT(1)*100,etaT(n)*100,step*100);
fprintf(results,'                \t\t\t State 8\n\n');
fprintf(results,' Turbine efficiency \t\t T8 \t\t\t\t\t h8 \t\t\t\t\t\t s8\n');
if (1/step) <= 20
   for n = 1:1/step
      fprintf(results,' \t %g \t\t\t %g F (%.2f C) \t %g BTU/lbm (%.2f kJ/kg) \t %g BTU/lbm-R (%.4fkJ/kg-
K)\n',etaT(n),(T8(n)-273.15)*1.8+32,T8(n)-273.15,h8(n)/2.326,h8(n),s8(n)/4.1868,s8(n));
   end
   fprintf(results,'\n\n                \t\t\t Energy transfers and mass flow rates\n\n');
   fprintf(results,' Turbine efficiency \t eta_cycle \t\t\t\t WP \t\t\t\t Qin \t\t\t\t\t Qout \t\t\t\t Qc\n');
   for n = 1:1/step
      fprintf(results,' \t %g \t\t\t %.5f \t\t %g BTU/h (%.2f kW) \t %g BTU/h (%.2f kW) \t %g BTU/h (%.2f
kW)\n',etaT(n),eta_cycle(n),WP(n)*3412,WP(n),Qin(n)*3412,Qin(n),Qout(n)*3412,Qout(n));
   end
   fprintf(results,'\n\n Turbine efficiency \t\t\t Qc \t\t\t mS \t\t\t\t\t mW \t\t\t\t\t mT\n');
   for n = 1:1/step
      fprintf(results,' \t %g \t\t\t %.4f BTU/h (%.2f kW) \t %g lbm/h (%.4f kg/s) \t %g lbm/h (%.4f kg/s) \t
%g lbm/h (%.4f
kg/s)\n',etaT(n),Qc(n)*3412,Qc(n),mS(n)*7936.56,mS(n),mW(n)*7936.56,mW(n),mT(n)*7936.56,mT(n));
   end
else
   fprintf(results,'Too much data to display...see output plots.');
end


fclose(results);
fprintf('\n\nResults of analysis were written to results.txt');

figure(1)
plot(etaT,WP)
title('Pump work')
xlabel('Expander Isentropic Efficiency')
ylabel('Pump Work [kW]')

figure(2)
plot(etaT,Qin.*3412,etaT,Qout.*3412)
title('Qin')
xlabel('Expander Isentropic Efficiency')
ylabel('Heat [Btu/hr]')

figure(3)
```

```
plot(etaT,eta_cycle)
title('cycle efficiency')
xlabel('Expander Isentropic Efficiency')
ylabel('Overall Cycle Thermal Efficiency')

figure(4)
plot(etaT,Qc.*3412)
title('Cooling Capacity')
xlabel('Expander Isentropic Efficiency')
ylabel('Cooling Capacity [Btu/hr]')

figure(5)
plot(etaT,mW.*7936.56,etaT,mS.*7936.56,etaT,mT.*7936.56)
title('Mass flows')
xlabel('Expander Isentropic Efficiency')
ylabel('Mass Flow Rate [lbm/hr]')
```

Ammonia Water Code – Ammonia_water.m

```
format long
global a b Ai Aij Ci Cij
global TB PB R Aa Aw Ba Bw Ca Cw Da Dw E hroaL hrowL hroaG hrowG sroaL srowL sroaG srowG
Troa Trow Proa Prow

%Input constants from data files
[Aa Aw Ba Bw Ca Cw Da Dw E] =
textread('gibbs_coefficients.dat','%f%f%f%f%f%f%f%f%f','headerlines',1);
[hroaL hrowL hroaG hrowG sroaL srowL sroaG srowG Troa Trow Proa Prow] =
textread('reduced_props.dat','%f%f%f%f%f%f%f%f%f%f%f%f','headerlines',1);
[a Ai Aij(:,1) Aij(:,2) Aij(:,3) Aij(:,4) b Ci Cij(:,1) Cij(:,2) Cij(:,3) Cij(:,4) Cij(:,5) Cij(:,6) Cij(:,7) Cij(:,8)
Cij(:,9) Cij(:,10)] =
textread('Bdc_coefficients.dat','%f%f%f%f%f%f%f%f%f%f%f%f%f%f%f%f%f%f%f%f%f%f%f','headerlines',1);
TB = 100; PB = 10; R = 8.314;

global istate %returns mixture condition (superheated vapor, etc.)

if option == 1
   if cycle == 0;
      P = input('Pressure (bar): ');
      T = input('Temperature (K): ');
      x = input('Mass fraction: ');
   end
   [hm,sm,vm] = PTx(P,T,x); %calls PTx.m
elseif option == 2
   x = .5; incr2=.01; limit=.000001;
   if cycle == 0
      P = input('Pressure (bar): ');
      T = input('Temperature (K): ');
      v = input('Specific volume (m^3/kmol): ');
   end
   [hm,sm,vm]= PTx(P,T,x);
   while abs(v - vm)>limit
      n = 1;
      while (vm > v)
         if n >= 11
```

```
            incr2 = incr2*10; n=1;
        end
        x = x - incr2;
        if x < 0
            fprintf('Mixture not possible!!');
            break;
        end
        [hm,sm,vm] = PTx(P,T,x); n = n + 1;
    end
    if x < 0
        break;
    end
    incr2 = incr2/10; n=1;
    while (vm < v)
        if n >= 11
            incr2 = incr2*10; n = 1;
        end
        x = x + incr2;
        if x > 1
            fprintf('Mixture not possible!!');
            break;
        end
        [hm,sm,vm] = PTx(P,T,x); n = n + 1;
    end
    if x > 1
        break;
    end
    incr2 = incr2/10;
  end
elseif option == 3
  T = 400; incr2 = 10;
  if cycle == 0;
    P = input('Pressure (bar): ');
    h = input('Enthalpy (kJ/kg): ');
    x = input('Mass fraction: ');
  end
  [hm,sm,vm] = PTx(P,T,x);
  while (abs(h - hm)) > .01
    while (hm > h)
      T = T - incr2; [hm,sm,vm] = PTx(P,T,x);
    end
    incr2 = incr2/10;
    while (hm < h)
      T = T + incr2; [hm,sm,vm] = PTx(P,T,x);
    end
    incr2 = incr2/10;
  end
elseif option == 4
  T = 400; incr2 = 10;
  if cycle == 0
    P = input('Pressure (bar): ');
    s = input('Entropy (kJ/kg-K): ');
    x = input('Mass fraction: ');
  end
  [hm,sm,vm] = PTx(P,T,x);
  while (abs(s - sm)) > .001
```

```
        while (sm > s)
            T = T - incr2; [hm,sm,vm] = PTx(P,T,x);
        end
        incr2 = incr2/10;
        while (sm < s)
            T = T + incr2; [hm,sm,vm] = PTx(P,T,x);
        end
        incr2 = incr2/10;
    end
elseif option == 5
    T = 300; incr2 = 1; limit = .000001;
    if cycle == 0;
        P = input('Pressure (bar): ');
        v = input('Specific volume (m^3/kmol): ');
        x = input('Mass fraction: ');
    end
    [hm,sm,vm] = PTx(P,T,x);
    while (abs(v - vm)) > limit
        n = 1;
        while (vm > v)
            if n >= 11
                incr2 = incr2*10; n = 1;
            end
            T = T - incr2; [hm,sm,vm] = PTx(P,T,x); n = n + 1;
        end
        incr2 = incr2/10; n = 1;
        while (vm < v)
            if n >= 11
                incr2 = incr2*10; n = 1;
            end
            T = T + incr2; [hm,sm,vm] = PTx(P,T,x); n = n + 1;
        end
        incr2 = incr2/10;
    end
elseif option == 6
    P = 1; incr2 = .01; limit = .000001;
    if cycle == 0
        T = input('Temperature (K): ');
        v = input('Specific volume (m^3/kmol): ');
        x = input('Mass fraction: ');
    end
    [hm,sm,vm] = PTx(P,T,x);
    while (abs(v - vm)) > limit
        while (vm < v)
            P = P - incr2; [hm,sm,vm] = PTx(P,T,x);
        end
        incr2 = incr2/10; n = 1;
        while (vm > v)
            if n >= 11
                incr2 = incr2*10; n = 1;
            end
            P = P + incr2; [hm,sm,vm] = PTx(P,T,x); n = n + 1;
        end
        incr2 = incr2/10;
    end
elseif option == 7
```

```
   if cycle == 0
      P = input('Pressure (bar): ');
      x = input('Mass fraction: ');
   end
   [Tb,Td] = bubble_dew(P,x); Pr = P/PB;
   M = 18.015*17.031/((1-x)*17.031+x*18.015);
   y = x*18.015/(x*18.015 + (1-x)*17.031);
   [hLm, crap, sLm, crap, vLm, crap] = hsv_properties(Tb/TB,Pr,y);
   [crap, hgm, crap, sgm, crap, vgm] = hsv_properties(Td/TB,Pr,y);
   hL = hLm/M; sL = sLm/M; vL = vLm/M;
   hg = hgm/M; sg = sgm/M; vg = vgm/M;
elseif option == 8
   if cycle == 0;
      P = input('Pressure (bar): ');
      T = input('Temperature (K): ');
   end
   Tr = T/TB; Pr = P/PB; choice = 3; bubble_dew_base;
   if xb < 0
      xb = 0; hg = 0; hL = 0; sg = 0; sL = 0; vg = 0; vL = 0;
      fprintf('Not a saturated condition!!');
      break;
   end
   x = xb; M = 18.015*17.031/((1-x)*17.031+x*18.015);
   y = x*18.015/(x*18.015 + (1-x)*17.031);
   if xd > 1
      xd = 1; hg = 0; hL = 0; sg = 0; sL = 0; vg = 0; vL = 0;
      fprintf('Not a saturated condition!!');
   end
   yd = xd*18.015/(xd*18.015 + (1-xd)*17.031);
   Md = 18.015*17.031/((1-xd)*17.031+xd*18.015);
   [hLm, crap, sLm, crap, vLm, crap] = hsv_properties(Tr,Pr,y);
   [crap, hgm, crap, sgm, crap, vgm] = hsv_properties(Tr,Pr,yd);
   hL = hLm/M; sL = sLm/M; vL = vLm/M;
   hg = hgm/Md; sg = sgm/Md; vg = vgm/Md;
elseif option == 9
   if cycle == 0
      T = input('Temperature (K): ');
      x = input('Mass fraction: ');
   end
   Tr = T/TB; M = 18.015*17.031/((1-x)*17.031+x*18.015);
   y = x*18.015/(x*18.015 + (1-x)*17.031);
   choice = 2; bubble_dew_base;
   [hLm, crap, sLm, crap, vLm, crap] = hsv_properties(Tr,Pb/PB,y);
   [crap, hgm, crap, sgm, crap, vgm] = hsv_properties(Tr,Pd/PB,y);
   hL = hLm/M; sL = sLm/M; vL = vLm/M;
   hg = hgm/M; sg = sgm/M; vg = vgm/M;
end

%Enter code to calculate all bubble and dew point properties for display
if istate <= 3
   choice = 1; bubble_dew_base; Tbb = Tb; Tdd = Td;
   choice = 2; bubble_dew_base;
   choice = 3; bubble_dew_base;
end
```

Pressure, Temperature, and Mass Fraction Evaluation – PTX.m

```
%input: Pressure (bar), temperature (K), and mass fraction
%output: enthalpy (kJ/kg), entropy (kJ/kg-K), and specific volume (m^3/kg)

function [hm,sm,vm] = PTx(P,T,x)
global qm istate TB PB Tr Pr M y
Tr = T/TB; Pr = P/PB; M = 18.015*17.031/((1-x)*17.031+x*18.015); %molecular weight
y = x*18.015/(x*18.015 + (1-x)*17.031); %mole fraction
[Tb,Td] = bubble_dew(P,x);

[hLm, hgm, sLm, sgm, vLm, vgm] = hsv_properties(Tr,Pr,y);
if T < Tb %compressed liquid
   istate = 1; %??????
   hm = hLm/M;
   sm = sLm/M;
   vm = vLm/M;
   xNH3v = 0; xH2Ov = 0; xNH3L = x; xH2OL = 1-x;

elseif T > Td %superheated vapor
   istate = 3;%?????
   hm = hgm/M;
   sm = sgm/M;
   vm = vgm/M;
   xNH3v = x; xH2Ov = 1-x; xNH3L = 0; xH2OL = 0;

else %liquid-vapor mixture
   istate = 2; %?????
   choice = 3;
   bubble_dew_base; qm = (x - xb)/(xd - xb); % quality of mixture
   yb = xb*18.015/(xb*18.015 + (1-xb)*17.031); yd = xd*18.015/(xd*18.015 + (1-xd)*17.031);
   Mb = 18.015*17.031/((1-xb)*17.031+xb*18.015);
   Md = 18.015*17.031/((1-xd)*17.031+xd*18.015);

   [hLmb, hgmb, sLmb, sgmb, vLmb, vgmb] = hsv_properties(Tr,Pr,yb);
   [hLmd, hgmd, sLmd, sgmd, vLmd, vgmd] = hsv_properties(Tr,Pr,yd);

   hm = (1-qm)/Mb*hLmb + qm/Md*hgmd;
   sm = (1-qm)/Mb*sLmb + qm/Md*sgmd;
   vm = (1-qm)/Mb*vLmb + qm/Md*vgmd;
   xNH3v = (x - xb)/(xd - xb)*xd; xH20v = (x - xb)/(xd - xb)*(1-xd);
   xNH3L = (1-(x - xb)/(xd - xb))*xb; xH20v = (1-(x - xb)/(xd - xb))*(1-xb);
end
```

Bubble and Dew Point Property Evaluation – Bubble_dew.m

```
%input: pressure (bar) and mass fraction
%output: Bubble and dew point temperatures (K)

function [Tb,Td] = bubble_dew(P,x)
global Ai Aij Ci Cij %empirical constants from ammonia_water.m
[Tc,Pc] = critical_props(x); %calculate critical temperature and pressure
sum2 = 0;
for i = 1:7
   sum1 = 0;
```

```
   for j = 1:10
      sum1 = sum1 + Cij(i,j)*x^j;
   end
   sum2 = sum2 + (Ci(i) + sum1)*(log(Pc/P))^i;
end
Tb = Tc - sum2/1.8; %unit conversion -- bubble point temperature (K)
sum2 = 0;
for i = 1:6
   sum1 = 0;
   for j = 1:4
      sum1 = sum1 + Aij(i,j)*(log(1.0001-x))^j;
   end
   sum2 = sum2 + (Ai(i) + sum1)*(log(Pc/P))^i;
end
Td = Tc - sum2/1.8; %unit conversion -- dew point temperature (K)
```

Critical Property Evaluation – Critical_properties.m

```
%input: mass fraction of ammonia in mixture
%output: critical temperature (K) and pressure (bar)

function [Tc,Pc] = critical_props(x);
Tcw = 1165.14 ; Pcw = 3206.79;  %critical properties of water (R and psia)
global a b Tc Pc

sum1 = 0; i = 1;
while (i <= 4)
   sum1 = sum1 + (a(i)*x^i);
   i = i + 1;
end
Tc = (Tcw - sum1)/1.8; %convert from R to K

sum1 = 0; i = 1;
while (i <= 8)
   sum1 = sum1 + b(i)*x^i;
   i = i + 1;
end
Pc = Pcw*exp(sum1)/14.504; %convert from psia to bar
```

Enthalpy, Entropy, and Specific Volume Evaluation – HSV.m

```
%input: Reduced temperature, reduced pressure, and mole fraction
%output: enthalpy, entropy, and specific volume for liquid and gas mixures

function [hLm, hgm, sLm, sgm, vLm, vgm] = hsv_properties(Tr,Pr,y)
%input empirical constants
global TB PB R Aa Aw Ba Bw Ca Cw Da Dw E hroaL hrowL hroaG hrowG sroaL srowL sroaG srowG
Troa Trow Proa Prow

hLw = -R*TB*(-hrowL + Bw(1)*(Trow - Tr) + Bw(2)/2*(Trow^2 - Tr^2) + Bw(3)/3*(Trow^3 - Tr^3) -
(Aw(1) + Aw(4)*Tr^2)*(Pr-Prow) - Aw(2)/2*(Pr^2 - Prow^2));
hLa = -R*TB*(-hroaL + Ba(1)*(Troa - Tr) + Ba(2)/2*(Troa^2 - Tr^2) + Ba(3)/3*(Troa^3 - Tr^3) - (Aa(1)
+ Aa(4)*Tr^2)*(Pr-Proa) - Aa(2)/2*(Pr^2 - Proa^2));
hgw = -R*TB*(-hrowG + Dw(1)*(Trow - Tr) + Dw(2)/2*(Trow^2 - Tr^2) + Dw(3)/3*(Trow^3 - Tr^3) –
Cw(1)*(Pr - Prow) - 4*Cw(2)*(Pr*Tr^-3 - Prow*Trow^-3) - 12*Cw(3)*(Pr*Tr^-11 - Prow*Trow^-11) –
```

```
4*Cw(4)*(Pr^3*Tr^-11 - Prow^3*Trow^-11));
hga = -R*TB*(-hroaG + Da(1)*(Troa - Tr) + Da(2)/2*(Troa^2 - Tr^2) + Da(3)/3*(Troa^3 - Tr^3) -
Ca(1)*(Pr - Proa) - 4*Ca(2)*(Pr*Tr^-3 - Proa*Troa^-3) - 12*Ca(3)*(Pr*Tr^-11 - Proa*Troa^-11) -
4*Ca(4)*(Pr^3*Tr^-11 - Proa^3*Troa^-11));
hE = -R*TB*y*(1-y)*(-E(1) - E(2)*Pr - 2*E(5)/Tr - 3*E(6)*Tr^-2 + (2*y - 1)*(-E(7) - E(8)*Pr -
2*E(11)/Tr - 3*E(12)*Tr^-2) + (2*y - 1)^2*(-E(13) - E(14)*Pr - 2*E(15)/Tr - 3*E(16)*Tr^-2));

hLm = y*hLa + (1-y)*hLw + hE;
hgm = y*hga + (1-y)*hgw;

sLw = -R*(-srowL - Bw(1)*log(Tr/Trow) + Bw(2)*(Trow - Tr) + Bw(3)/2*(Trow^2 - Tr^2) + (Pr -
Prow)*(Aw(3) + 2*Aw(4)*Tr));
sLa = -R*(-sroaL - Ba(1)*log(Tr/Troa) + Ba(2)*(Troa - Tr) + Ba(3)/2*(Troa^2 - Tr^2) + (Pr - Proa)*(Aa(3)
+ 2*Aa(4)*Tr));
if Pr == 0
   sgw = 0;
   sga = 0;
else
   sgw = -R*(-srowG - Dw(1)*log(Tr/Trow) + Dw(2)*(Trow - Tr) + Dw(3)/2*(Trow^2 - Tr^2) +
log(Pr/Prow) - 3*Cw(2)*(Pr*Tr^-4 - Prow*Trow^-4) - 11*Cw(3)*(Pr*Tr^-12 - Prow*Trow^-12) -
11/3*Cw(4)*(Pr^3*Tr^-12 - Prow^3*Trow^-12));
   sga = -R*(-sroaG - Da(1)*log(Tr/Troa) + Da(2)*(Troa - Tr) + Da(3)/2*(Troa^2 - Tr^2) + log(Pr/Proa) -
3*Ca(2)*(Pr*Tr^-4 - Proa*Troa^-4) - 11*Ca(3)*(Pr*Tr^-12 - Proa*Troa^-12) - 11/3*Ca(4)*(Pr^3*Tr^-12 -
Proa^3*Troa^-12));
end
sE = -R*(1 - y)*y*(E(3) + E(4)*Pr - E(5)*Tr^-2 - 2*E(6)*Tr^-3 + (2*y - 1)*(E(9) + E(10)*Pr - E(11)*Tr^-
2 - 2*E(12)*Tr^-3) + (2*y - 1)^2*(-E(15)*Tr^-2 - 2*E(16)*Tr^-3));
if y==0 | y==1
   smix = 0;
else
   smix = -R*(y*log(y) + (1-y)*log(1-y));
end
sLm = y*sLa + (1-y)*sLw + sE + smix;
sgm = y*sga + (1-y)*sgw + smix;
vLw = R*TB/PB*(Aw(1) + Aw(3)*Tr + Aw(4)*Tr^2 + Aw(2)*Pr); vLw = vLw/100;
vLa = R*TB/PB*(Aa(1) + Aa(3)*Tr + Aa(4)*Tr^2 + Aa(2)*Pr); vLa = vLa/100;
if Pr == 0
   vgw = 0;
   vga = 0;
else
   vgw = R*TB/PB*(Tr/Pr + Cw(1) + Cw(2)*Tr^-3 + Cw(3)*Tr^-11 + Cw(4)*Pr^2*Tr^-11);
   vgw = vgw/100;
   vga = R*TB/PB*(Tr/Pr + Ca(1) + Ca(2)*Tr^-3 + Ca(3)*Tr^-11 + Ca(4)*Pr^2*Tr^-11);
   vga = vga/100;
end
   vE = R*TB/PB*y*(1-y)*(E(2) + E(4)*Tr + (2*y - 1)*(E(8) + E(10)*Tr) + (2*y - 1)^2*E(14));
   vE = vE/100;

   vLm = y*vLa + (1-y)*vLw + vE;
   vgm = y*vga + (1-y)*vgw;
```

APPENDIX B
CYCLE SIMULATION OUTPUT

Claude Cycle Simulation Results

State	Temperature K	Pressure bar	Enthalpy* kJ/kg	Entropy* kJ/kg-K
1	299.80	25.33	7.500069	-13.36727
2	299.80	40.528	14.621	-15.32029
2b	77.60	40.528	-3242.375	-35.44997
3	70.00	40.528	-3368.811	-37.18702
e	31.86	1.0132	-3802.249	-31.92948
4	31.86	40.528	-4341.877	-57.91807
7	31.86	1.0132	-3802.246	-31.92956
8	31.86	1.0132	-3802.246	-31.92956
10a	77.60	1.0132	-3152.423	-19.19284
10	299.80	1.0132	-2.375333	-0.064529
g	20.33	1.0132	-3980.47	-39.02225
L	20.33	1.0132	-4443.23	-61.78849
A	77.60	1.0132	-436.1071	-4.032287
C	299.80	1.0132	-0.603545	-0.005793

*Raw results not adjusted to proper significant figures

****
Analysis Results *
****

Created: 09-Nov-2004 21:39:24

ions: Saturated conditions at states 1 and 4.
Component pressure losses are negligible.
Equal weak and strong solution specific heats.
Superheater temperature equal to boiler temperature.
Mass fraction of ammonia in the rectifier exit stream, x7 = 1
Evaporator exit temperature = 85 F (29.44 C)
Electric generator efficiency = 75%
Recovery heat exchanger effectiveness = 0.85
Electric generator output = 5 kW

uts: Absorber temperature = 100 F (37.7778 C)
Boiler temperature = 170 F (76.6667 C)
System low pressure = 40 psia (2.75786 bar)
System high pressure = 110 psia (7.58411 bar)

State 1	State 2	State 3
F (37.78 C)	T = 100 F (37.78 C)	T = 156.678 F (69.27 C)
sia (2.76 bar)	P = 110 psia (7.58 bar)	P = 110 psia (7.58 bar)
895 BTU/lbm (-61.15 kJ/kg)	h = -26.0447 BTU/lbm (-60.58 kJ/kg)	h = 33.653 BTU/lbm (78.28 kJ/kg)
581 BTU/lbm-R (0.4295 kJ/kg-K)	s = 0.102467 BTU/lbm-R (0.4290 kJ/kg-K)	s = 0.204484 BTU/lbm-R (0.8561 kJ/kg-K)

State 4	State 5	State 6
F (76.67 C)	T = 110.5 F (43.61 C)	T = 109.939 F (43.30 C)
psia (7.58 bar)	P = 110 psia (7.58 bar)	P = 40 psia (2.76 bar)
62 BTU/lbm (117.90 kJ/kg)	h = -11.8009 BTU/lbm (-27.45 kJ/kg)	h = -11.8009 BTU/lbm (-27.45 kJ/kg)
516 BTU/lbm-R (0.9609 kJ/kg-K)	s = 0.124855 BTU/lbm-R (0.5227 kJ/kg-K)	s = 0.125418 BTU/lbm-R (0.5251 kJ/kg-K)

State 7	State 8s	State 9
T = 170 F (76.67 C)	T = 38.93 F (3.85 C)	T = 85 F (29.44 C)
P = 110 psia (7.58 bar)	P = 40 psia (2.76 bar)	P = 40 psia (2.76 bar)
h = 616.066 BTU/lbm (1432.97 kJ/kg)	h = 552.638 BTU/lbm (1285.44 kJ/kg)	h = 578.097 BTU/lbm (1344.65 kJ/kg)
s = 1.17533 BTU/lbm-R (4.9209 kJ/kg-K)	s = 1.17533 BTU/lbm-R (4.9209 kJ/kg-K)	s = 1.22423 BTU/lbm-R (5.1256 kJ/kg-K)

Weak solution mass fraction, xW = 0.368894 **Strong solution mass fraction, xS** = 0.398823

Turbine shaft work output, WT = 6.66667 kW

Turbine adiabatic efficiency varied from 10% to 100% in 10% increments

	State 8		
Turbine efficiency	**T8**	**h8**	**s8**
0.1	143.279 F (61.82 C)	609.723 BTU/lbm (1418.22 kJ/kg)	1.2794 BTU/lbm-R (5.3566kJ/kg-K)
0.2	131.568 F (55.32 C)	603.38 BTU/lbm (1403.46 kJ/kg)	1.26877 BTU/lbm-R (5.3121kJ/kg-K)
0.3	119.858 F (48.81 C)	597.038 BTU/lbm (1388.71 kJ/kg)	1.25794 BTU/lbm-R (5.2667kJ/kg-K)
0.4	108.16 F (42.31 C)	590.695 BTU/lbm (1373.96 kJ/kg)	1.24688 BTU/lbm-R (5.2204kJ/kg-K)
0.5	96.4827 F (35.82 C)	584.352 BTU/lbm (1359.20 kJ/kg)	1.23559 BTU/lbm-R (5.1732kJ/kg-K)
0.6	84.8386 F (29.35 C)	578.009 BTU/lbm (1344.45 kJ/kg)	1.22407 BTU/lbm-R (5.1249kJ/kg-K)
0.7	73.2425 F (22.91 C)	571.667 BTU/lbm (1329.70 kJ/kg)	1.21229 BTU/lbm-R (5.0756kJ/kg-K)
0.8	61.718 F (16.51 C)	565.324 BTU/lbm (1314.94 kJ/kg)	1.20027 BTU/lbm-R (5.0253kJ/kg-K)
0.9	50.27 F (10.15 C)	558.981 BTU/lbm (1300.19 kJ/kg)	1.18796 BTU/lbm-R (4.9738kJ/kg-K)
1	38.93 F (3.85 C)	552.638 BTU/lbm (1285.44 kJ/kg)	1.17538 BTU/lbm-R (4.9211kJ/kg-K)

Energy transfers and mass flow rates

Turbine efficiency	eta_cycle	WP	Qin	Qout
0.1	0.00128	18510.4 BTU/h (5.43 kW)	3.31566e+006 BTU/h (971.77 kW)	3.21117e+006 BTU/h (941.14 kW)
0.2	0.00814	9255.22 BTU/h (2.71 kW)	1.65783e+006 BTU/h (485.88 kW)	1.60559e+006 BTU/h (470.57 kW)
0.3	0.01500	6170.14 BTU/h (1.81 kW)	1.10522e+006 BTU/h (323.92 kW)	1.07039e+006 BTU/h (313.71 kW)
0.4	0.02186	4627.61 BTU/h (1.36 kW)	828916 BTU/h (242.94 kW)	802793 BTU/h (235.29 kW)
0.5	0.02872	3702.09 BTU/h (1.09 kW)	663133 BTU/h (194.35 kW)	642234 BTU/h (188.23 kW)
0.6	0.03561	3085.07 BTU/h (0.90 kW)	552611 BTU/h (161.96 kW)	535195 BTU/h (156.86 kW)
0.7	0.04476	2644.35 BTU/h (0.78 kW)	473666 BTU/h (138.82 kW)	458739 BTU/h (134.45 kW)
0.8	0.05391	2313.8 BTU/h (0.68 kW)	414458 BTU/h (121.47 kW)	401396 BTU/h (117.64 kW)
0.9	0.06305	2056.71 BTU/h (0.60 kW)	368407 BTU/h (107.97 kW)	356797 BTU/h (104.57 kW)
1	0.07220	1851.04 BTU/h (0.54 kW)	331566 BTU/h (97.18 kW)	321117 BTU/h (94.11 kW)

Turbine efficiency	Qc	mS	mW	mT
0.1	0.0000 BTU/h (0.00 kW)	75624.1 lbm/h (9.5286 kg/s)	72037.7 lbm/h (9.0767 kg/s)	3586.35 lbm/h (0.4519 kg/s)
0.2	0.0000 BTU/h (0.00 kW)	37812 lbm/h (4.7643 kg/s)	36018.9 lbm/h (4.5383 kg/s)	1793.18 lbm/h (0.2259 kg/s)
0.3	0.0000 BTU/h (0.00 kW)	25208 lbm/h (3.1762 kg/s)	24012.6 lbm/h (3.0256 kg/s)	1195.45 lbm/h (0.1506 kg/s)
0.4	0.0000 BTU/h (0.00 kW)	18906 lbm/h (2.3821 kg/s)	18009.4 lbm/h (2.2692 kg/s)	896.588 lbm/h (0.1130 kg/s)
0.5	0.0000 BTU/h (0.00 kW)	15124.8 lbm/h (1.9057 kg/s)	14407.5 lbm/h (1.8153 kg/s)	717.27 lbm/h (0.0904 kg/s)
0.6	52.6558 BTU/h (0.02 kW)	12604 lbm/h (1.5881 kg/s)	12006.3 lbm/h (1.5128 kg/s)	597.725 lbm/h (0.0753 kg/s)
0.7	3294.6573 BTU/h (0.97 kW)	10803.4 lbm/h (1.3612 kg/s)	10291.1 lbm/h (1.2967 kg/s)	512.336 lbm/h (0.0646 kg/s)
0.8	5726.1585 BTU/h (1.68 kW)	9453.01 lbm/h (1.1911 kg/s)	9004.72 lbm/h (1.1346 kg/s)	448.294 lbm/h (0.0565 kg/s)
0.9	7617.3261 BTU/h (2.23 kW)	8402.68 lbm/h (1.0587 kg/s)	8004.19 lbm/h (1.0085 kg/s)	398.483 lbm/h (0.0502 kg/s)
1	9130.2601 BTU/h (2.68 kW)	7562.41 lbm/h (0.9529 kg/s)	7203.77 lbm/h (0.9077 kg/s)	358.635 lbm/h (0.0452 kg/s)

APPENDIX C
EXPERIMENTAL COMPONENT LIST

The major components used in the scroll expander performance test are listed with technical specifications where applicable. Basic tubing and fittings are not included.

Scroll compressor
- Description: modified expansion device
- Manufacturer: Sanden International (USA) Inc., Wylie, TX
- Specifications: model TRS-90; displacement 85.7 cc/rev; max speed 9000 RPM

Compressor
- Description: compressed air source
- Manufacturer: Puma Air Compressors
- Specifications: 5 hp; 230 Vac input; tank 60 gallons; capacity 15.7 cfm

Power supply
- Description: DC power supply for expander clutch
- Manufacturer: BK Precision, Yorba Linda, CA
- Specifications: 120 Vac input; 0 – 30 Vdc output

Pony brake
- Description: shaft power measurement
- Specifications: moment arm length 14.125”

Thermocouple
- Description: temperature measurement
- Manufacturer: Omega Engineering, Stamford, CT
- Quantity: 2
- Specifications: T-type copper-constantan; accuracy 2°F; grounded junction

Thermocouple analog converter
- Description: signal conditioner
- Manufacturer: Omega Engineering, Stamford, CT
- Quantity: 2
- Specifications: model TAC80B-T; range -4 – 572 °F

Multimeter
- Description: meter used to read thermocouple voltage
- Manufacturer: Fluke Corporation, Everett, WA
- Quantity: 2
- Specifications: 0.01 mV resolution

Pressure gauge
- Description: pressure measurement
- Manufacturer: Campbell Hausfeld, Harrison, OH
- Quantity: 2
- Specifications: model IFA112; range 0 – 160 psig; resolution 1 psig

Scale
- Description: moment arm force measurement
- Manufacturer: Pelouze, Bridgeview, IL
- Specifications: capacity 5lb; resolution 0.5 ounce; calibrated w/ standard masses

Tachometer
- Description: shaft rotational speed measurement

LIST OF REFERENCES

Barron, R. F., 1985, *Cryogenic Systems*, Oxford University Press, New York.

Casper, M. S., 1978, *Hydrogen Production by Electrolysis, Thermal Decomposition and Unusual Techniques*, Noyer Data Corporation, Park Ridge, NJ

Chevron U.S.A. Inc., 1998, "Diesel Fuel Refining and Chemistry," San Ramon, CA. http://www.chevron.com/prodserv/fuels/bulletin/diesel/L2_4_6_rf.htm, last accessed: 11/2004.

Clean Energy Research Center, 2003, "Journey to Sustainable Energy: The H_2 Solution," University of South Florida, Tampa, FL. http://www.cerc.eng.usf.edu, last accessed: 11/2004.

Copeland Corp., 2001, "Scroll Compressor Technology and Air Conditioning, Heat Pump, and Refrigeration Applications," *Vi Ibero-American Congress of Air Conditioning and Refrigeration*, Available at http://www.copeland-corp.com/americas/news/news004.htm/scroll-english.pdf

Drnevich, R., 2003, "Hydrogen Delivery: Liquefaction and Compression," *Hydrogen Delivery Workshop Proceedings*, U.S. Department of Energy – Energy Efficiency and Renewable Energy, Washington, DC.

Energy Information Administration, 2003, "Annual Energy Review 2003," DOE/EIA – 0384(2003), Washington, DC. http://www.eia.doe.gov/emeu/aer/contents.html, last accessed: 11/2004.

Energy Information Administration, 2004, "International Energy Outlook 2004," Washington, DC. Available at http://www.eia.doe.gov/oiaf/ieo/world.html, last accessed: 11/2004.

Flynn, T. M., 1997, *Cryogenic Engineering*, Marcel Dekker, New York.

Fuel Cell Store, 2003, "Hydrogen Storage," Boulder, CO. http://www.fuelcellstore.com/information/hydrogen_storage.html, last accessed: 11/2004.

Gater, R., 2001, *Engineering Thermodynamics: Advanced Topics*, Course notes, University of Florida, Gainesville, FL.

Goswami, D. Y., 1995, "Solar Thermal Power: Status of Technologies and Opportunities for Research," *Heat and Mass Transfer 95, Proceedings of the 2nd ASME-ISHMT Heat and Mass Transfer Conference*, Tata-McGraw Hill Publishers, New Delhi, India, pp. 57 – 60.

Gravesen, J., Henriksen, C., 2001, "The Geometry of the Scroll Compressor," *SIAM Review*, Vol. 43, No. 1, pp. 113-126.

Gross, R., Otto, W., Patzelt, A., Wanner, M., 1994, "Liquid Hydrogen for Europe – the Linde Plant at Ingolstadt," *Reports on Science and Technology*, Linde, Vol. 54, pp. 37 – 43.

Hands, B. A., ed., 1986, *Cryogenic Engineering*, Academic Press, London.

Hans-Joachim, H., Radermacher, R., 2003, *CO_2 Compressor-Expander Analysis: Final Report*, Air-Conditioning and Refrigeration Technology Institute, Arlington, VA, ARTI-21CR/611-10060-01.

Hasan, A. A., Goswami, D. Y., 2003, " Exergy Analysis of a Combined Power and Refrigeration Thermodynamic Cycle Driven by a Solar Heat Source," ASME *Journal of Solar Energy Engineering*, Vol. 125, No. 1, pp. 55 – 60.

Holman, J. P., *Experimental Methods for Engineers*, McGraw-Hill, New York.

McMurry, J., Fay, R., 1998, *Chemistry*, Prentice Hall Inc., Upper Saddle River, NJ.

Mirabal, S. T., 2003, "An Economic Analysis of Hydrogen Production Technologies Using Renewable Energy Resources," Master's thesis, University of Florida

National Hydrogen Association, 2004, "Hydrogen FAQs," Washington, DC. http://www.hydrogenus.com/h2-FAQ.asp, last accessed: 11/2004.

National Institute of Standards and Technology, 2003, Program: Thermophysical Properties of Fluid Systems, http://webbook.nist.gov/chemistry/fluid/, last accessed: 11/2004.

Ramsay, W. C., 2003, Public-Private Dialogue, *International Partnership for a Hydrogen Economy*, International Energy Agency, Paris.

Schein, C., Radermacher, R., 2001, "Scroll Compressor Simulation Model," ASME *Journal of Engineering for Gas Turbines and Power*, Vol. 123, pp. 217 – 225.

Stuart Energy Systems, 2004, "Stuart Energy Station Product Brochure," Ontario, Canada. http://www.stuartenergy.com/main_our_products.html, last accessed: 11/2004.

Sunatech Inc., 2001, *IEA Agreement on the Production and Utilization of Hydrogen, Task 12: Metal Hydrides and Carbon for Hydrogen Storage, Executive Summary*, edited by Sandrock, U.S. Department of Energy, Washington, DC.

Tamm, G. O., 2003, "Experimental Investigation of an Ammonia-Based Combined Power and Cooling Cycle," Ph.D. dissertation, University of Florida

Tamm, G., Goswami, D. Y., Lu, S., Hasan, A., "A Novel Combined Power and Cooling Thermodynamic Cycle for Low Temperature Heat Sources – Part I: Theoretical Investigation," ASME *Journal of Solar Energy Engineering*, Vol. 125, No. 2, np.

Turns, S. R., 2000, *An Introduction to Combustion: Concepts and Applications*, McGraw-Hill, New York.

Wells, D. N., 2000, "Scroll Expansion Machines for Solar Power and Cooling Systems," *Proceedings of Solar 2000*, American Society of Mechanical Engineers, Madison, WI, np.

Wendt, H., 1990, *Electrochemical Hydrogen Technologies: Electrochemical Production and Combustion of Hydrogen*, Elsevier Science Publishing, New York.

U.S. Department of Energy – Energy Efficiency and Renewable Energy, 2003, "Hydrogen Production," Washington, DC. http://www.eere.energy.gov/RE/hydrogen_production.html, last accessed: 11/2004.

BIOGRAPHICAL SKETCH

Robert Joseph Reed was born in Baltimore, Maryland, in 1980. He graduated summa cum laude from the University of Florida in 2003 with a B.S. degree in mechanical engineering. He will graduate from the University of Florida in May 2005 with an M.S. degree. Robert is currently involved in the design and construction of a 5-kW ammonia-based combined power and cooling cycle at the University of Florida Energy Research Park.